INVESTIGATIONS ON SUBCRITICAL AND SUPERCRITICAL NATURAL CIRCULATION PHENOMENA RELEVANT TO ADVANCED REACTORS

By

SWAPNALEE BARUAH THAKURIA

(Enrollment No: ENGG01200704034)

Bhabha Atomic Research Centre

A thesis submitted to the Board of studies in Engineering Sciences

In partial fulfillment of the requirements

For the degree of

DOCTOR OF PHILOSOPHY

Of

HOMI BHABHA NATIONAL INSTITUTE
MUMBAI

May, 2013

Homi Bhabha National Institute

Recommendations of the Viva Voce Board

As members of the Viva Voce Board, we certify that we have read the dissertation prepared by Swapnalee Baruah Thakuria titled "Investigations on Subcritical and Supercritical Natural Circulation phenomena relevant to advanced reactors" and recommend that it may be accepted as fulfilling the dissertation requirement for the Degree of Doctor of Philosophy.

Chairman:	Dr. V. K. Suri	Date:
Guide:	Dr. P. K. Vijayan	Date:
Member:	Dr. P. Chellapandi	Date:
Member:	Dr. G.R. Reddy	Date: 05/04/13
Member:	Dr. J. Chattopadhyay	Date: 23/5/13
Examiner:	Prof. A. W. Date	Date: 05/04/13
Examiner:	(Dr. A. K. Ghosh)	Date: 05.04.2013

Final approval and acceptance of this dissertation is contingent upon the candidate's submission of the final copies of the dissertation to HBNI.

I hereby certify that I have read this dissertation prepared under my direction and recommend that it may be accepted as fulfilling the dissertation requirement.

Date: 05/04/13

Place: BARC Trombay

Guide: **Dr. P. K. Vijayan**

STATEMENT BY AUTHOR

This dissertation has been submitted in partial fulfillment of the requirements for an advanced degree at Homi Bhabha National Institute (HBNI) and is deposited in the Library to be made available to borrowers under rules of the HBNI.

Brief quotations from this dissertation are allowable without special permission, provided that accurate acknowledgement of source is made. Requests for permission for extended quotation from or reproduction of this manuscript in whole or in part may be granted by the Competent Authority of HBNI when in his or her judgment the proposed use of the material is in the interests of scholarship. In all other instances, however, permission must be obtained from the author.

BThakuria

Swapnalee Baruah Thakuria

DECLARATION

I, hereby declare that the investigation presented in the thesis has been carried out by me. The work is original and has not been submitted earlier as a whole or in part for a degree/diploma at this or any other Institution/University.

BThakuria

Swapnalee Baruah Thakuria

DEDICATIONS

I dedicate this thesis to my family

ACKNOWLEDGEMENTS

I express my sincere gratitude towards my guide **Dr. P. K. Vijayan**, Head-Reactor Engineering Division, Bhabha Atomic Research Center, Trombay, Mumbai-400085, for his valuable guidance, enthusiastic interest and continuous encouragement throughout the course of this work.

I sincerely thank my Doctoral Committee chairman **Dr. V. K. Suri** and members **Dr. P. Chellapandi, Dr. G. R. Reddy**, **Dr. J. Chattopadhyay** for time-to-time evaluation of the research work and useful suggestions, which definitely improved the dissertation. I would like to give special thanks to **Dr. B. K. Dutta,** Dean academic, HBNI for his valuable suggestions during my research work.

My sincere thanks to Shri D. S. Pilkhwal and Shri M. Sharma for their valuable suggestions and cooperation during the experimental study. I would like to take the opportunity to thank with great pleasure for support from the officers working in Reactor Engineering Division Dr. A. K. Nayak, Dr. N. K. Maheswari, Dr. A. M. Vaidya and Shri D. K. Chandraker.

I am extremely grateful to my husband Mintu Thakuria, my lovely daughter Devashree, my little son Krishnayu, my father Shri Girish Baruah, mother Mrs. Anu Baruah, my father-in-law Shri Soneswar Thakuria, mother-in-law Mrs. Girija Das and all my family members for their moral support and blessings.

Swapnalee Baruah Thakuria

CONTENTS

CHAPTER-3: EXPERIMENTAL FACILITY

CHAPTER-4: A GENERALIZED FLOW EQUATION FOR SINGLE-PHASE NATURAL CIRCULATION OBEYING MULTIPLE FRICTION LAWS

CHAPTER-5: STEADY STATE FLOW AND STATIC INSTABILITY OF SUPERCRITICAL NATURAL CIRCULATION LOOPS

CHAPTER-6: CONCLUSIONS AND RECOMMENDATIONS FOR FUTURE WORK

ABSTRACT

Many new generation nuclear reactors incorporate passive safety systems that utilize natural circulation phenomena. These passive safety systems are inherently safe and require no active controls or operator intervention. Natural circulation is the result of buoyancy pressure differential generated by density gradient and hence such systems enhance reliability and safe operational potential compared to systems with pumps. Most applications of natural circulation systems use subcritical fluids. The heat transport capability of natural circulation flow is directly proportional to the flow rate it can generate. Therefore, reliable prediction of flow rate is essential for design and performance evaluation of natural circulation loops. The reported generalized flow equation applicable for single-phase natural circulation is only valid for cases where the entire flow in the loop follows a single friction law. Such a situation arises when the natural circulation loop is either fully laminar or fully turbulent. It is possible that a natural circulation loop can be partly laminar and partly in transition or turbulent flow. In such cases, a single friction law is not applicable throughout the loop.

In the present thesis, a generalized flow equation is proposed for cases where a single friction law is not applicable for the entire loop. The proposed equation is tested with experimental data generated in a uniform diameter rectangular loop and is found to be in good agreement. Subsequently the equation is tested with data reported in the literature.

Stability analysis reported in literature for single-phase loops are either for laminar or turbulent flows. In practice, in natural circulation loops, all the flow regimes like

laminar, transition and turbulent are observed. Therefore, it is required to develop a stability map, which is valid for all the three regions. In the present work, such a stability map is presented.

Another concept of advanced reactor design is the use of fluids at supercritical pressure condition in both forced and natural circulation systems. For thermodynamically supercritical loops, explicit correlation for steady state natural circulation flow is not available. While using the subcritical natural circulation flow equation for supercritical data, it was not able to predict the steady state flow accurately near pseudo critical region. A generalized correlation has been proposed to estimate the steady state flow in supercritical natural circulation loops based on a relationship between dimensionless density and dimensionless enthalpy reported in literature. Experiments have been performed with supercritical CO_2 and water to validate this generalized correlation. The steady state flow rate data with supercritical CO_2 has been found to be in good agreement with the proposed correlation. The correlation has also been validated using limited number of supercritical water data. Subsequently supercritical natural circulation data for different fluids reported in literature has also been compared with the proposed correlation. It is observed that the same generalized correlation is applicable for other fluids also.

Sharp change of fluid properties such as density in the critical region gives rise to instability concerns. The instability could be either density wave type or excursive type (Ledinegg or static instability). Several previous researchers have studied density wave type instability in supercritical natural circulation loops whereas excursive instability is not studied in detail. In the present thesis, therefore, an analysis has been carried out for the present loop to predict the threshold of excursive instability for both supercritical water and supercritical CO_2. Static instability was not found for CO_2 whereas it was found for supercritical water. The effect of pressure is to stabilize the loop.

LIST OF FIGURES

LIST OF TABLES

NOMENCLATURE

a	dimensionless flow area (A/A_r)
A	flow area (m^2)
b	exponent in Eq. (2.2)
C	constant in Eq. (2.3)
Cp	specific heat (J/kg K)
d	dimensionless hydraulic diameter
D	hydraulic diameter (m)
f	Darcy friction factor
g	gravitational acceleration (m/s^2)
Gr_m	modified Grashof number $\left(\frac{D^3 \rho_0^2 \beta\, g\, \Delta T_r}{\mu^2}\right)$
Gr_m^*	modified Grashof number at supercritical pressure $\left(\frac{D_r^3 \rho_{pc}^2 \beta_{pc}\, g\, Q_h \Delta z}{A_r \mu^3}\right)$
h	enthalpy (J/kg)
h^*	dimensionless enthalpy ($h^*=\beta_{pc}(h-h_{pc})$)
$\mathcal{H}$	dimensionless enthalpy $\left(\mathcal{H} = \frac{h-h_r}{\Delta h_{ss}}\right)$
H	loop height (m)
k	thermal conductivity (W/m K)
K	local pressure loss coefficient
l	dimensionless length (L/L_t)
L	length (m)
L_l	laminar region length

L_2	transition region length=$L'_2+L''_2$
L_3	turbulent region length
N	total number of pipe segments
N_G	geometric number defined by Eq. (4.12)
Nu_m	modified Nusselt number (U_iL_t/k)
N_{subpc}	sub-pseudo critical number ($N_{subpc}=\beta_{pc}(h_{pc}-h_{in})$)
Pr	Prandtl number ($C_p\mu/k$)
P	perimeter (m)
p	constant in Eq. (2.2)
q	heat flux (W/m^2)
Q	total heat rate (W)
r	constant in Eq. (2.4)
Re	Reynolds number ($WD/A\mu$)
St_m	modified Stanton number ($4Nu_m/Re_{ss}Pr$)
s	co-ordinate around the loop, m
t	time (s)
T	temperature (^0C)
ΔT_r	reference temperature difference (^0C) $\left(\frac{Q_hH}{A\mu C_p}\right)$
U	overall heat transfer coefficient (W/m^2K)
v	specific volume (m^3/kg)
V_t	total loop volume (m^3)
W	mass flow rate (kg/s)
z	elevation (m)
Δz	centre line elevation difference between cooler and heater (m)
Z	dimensionless elevation (z/H)

Greek Symbols

β	thermal expansion coefficient (1/K)
μ	dynamic viscosity (Pa s)
ρ	density (kg/m^3)
ρ^*	dimensionless density
ρ_0	reference density (kg/m^3)

Subscripts

1	laminar region
2	transition region
3	turbulent region
c	cooler
cl	cold leg
eff	effective
h	heater
hl	hot leg
i	ith segment
l	laminar
pc	pseudo critical
r	reference value
s	secondary side
ss	steady state
t	total
tr	transition
tu	turbulent

CHAPTER-1

INTRODUCTION

Natural circulation is caused by buoyancy pressure differential resulting from density gradient in systems under the influence of a force field like gravitational or centrifugal. The density gradient can be generated diabatically or adiabatically. In case of diabatic natural circulation systems (also known as thermosyphons), the essential hardware includes a heat source and a heat sink connected by pipes (***Figure1.1***).

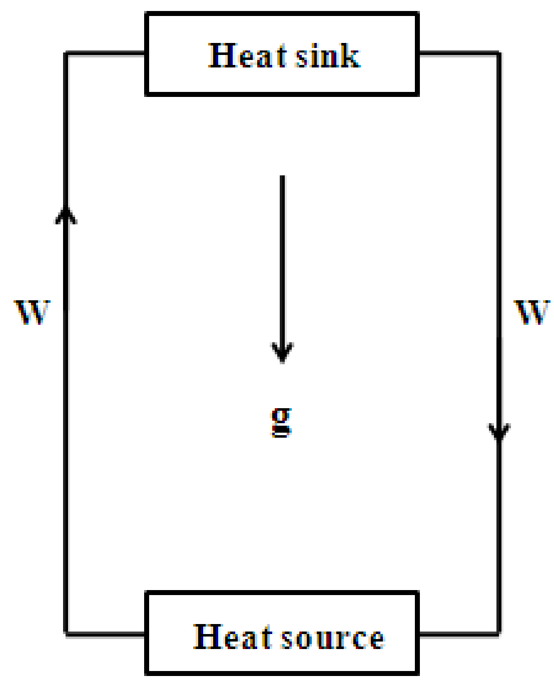

Figure 1.1: A simple natural circulation system

In a natural circulation loop (***Figure 1.1***), the circulating fluid absorbs heat from a source, becomes lighter and rises up and rejects the heat to a sink at a higher elevation. The fluid after rejecting heat at the sink becomes heavier and sinks thus establishing a circulation.

Natural circulation systems do not require a pump to maintain flow in the loop. Pump is an active element and its availability depends on proper functioning of many components and subsystems such as, electrical power supply system, lubrication system, shaft sealing system, motor cooling system, instrumentation system etc. Hence system with pumps is likely to fail more often than the natural circulation system with no active elements. Natural circulation system enhances reliability and safe operational potential compared to systems with pumps. Natural circulation phenomena is utilized for many industrial applications such as solar water heaters, thermosyphon reboilers, natural circulation boilers in fossil-fuelled power plants, transformer cooling and cooling of nuclear reactor core under shutdown condition.

1.1 Importance of natural circulation in nuclear reactors

Nuclear reactors continue to generate heat even after shutdown due to the radioactive decay of fission products. This decay heat is large enough to cause fuel overheating and subsequent melting in case of a Complete Loss Of Power (CLOP) as exemplified by the Fukushima plants which experienced a long term station blackout following a massive earthquake and the resultant tsunami. Natural circulation can be employed to remove decay heat in the event of station black out as it is based on a natural physical law and it is less likely to fail. It will continue to provide adequate cooling as long as the source and the sink are present. Hence almost all nuclear reactors are designed to remove decay heat by natural circulation in the event of CLOP.

1.2 Problem Definition

The available steady state flow correlation for natural circulation systems under subcritical condition is applicable only when the flow in the entire loop follows the same friction law i.e. when flow in the loop is either fully laminar or fully turbulent. However, the equation is not applicable if flow in the loop follows two different friction laws. In many instances, the loop may follow more than one friction law. The simplest example, where a part of the loop follows one friction law and another part follows a different friction law is a natural circulation loop with the cold leg in the laminar and hot leg in the transition or turbulent flow regime. It can also be caused by geometrical variations within the loop even if the flow regime is the same. For example, nuclear fuel bundles follow a different friction law compared to tubes even though both are in the same flow regime. Similar situation can arise for a loop comprising of a combination of circular and non-circular conduits such as annulus, rectangular, trapezoidal, etc. in laminar flow regime. Thus, even though the flow regime is same, the friction laws required can be more than one. Therefore, a generalized flow equation is essential for natural circulation loop obeying multiple friction laws.

Stability analyses reported in the literature for single-phase loops are either for the laminar or for the turbulent flow regime only. These analyses have generated stability maps for laminar and turbulent flows using corresponding friction laws. The stability maps are found to be a strong function of the friction laws employed. Also, the stability map for laminar flow reported earlier shows laminar condition only at low Gr_m values. Similarly, stability map for turbulent flow shows that the flow is actually laminar in the region of low Gr_m values. Hence, there is a need to generate a single stability map valid for laminar, transition and turbulent regions for a single-phase loop.

Another concept of advanced reactor design use fluids at supercritical pressure condition as coolant. Supercritical water has excellent heat transfer characteristics and is a candidate coolant for advanced nuclear reactors. Besides enhancing the thermodynamic efficiency, supercritical fluids do not experience phase change thus eliminating the Critical Heat Flux (CHF) phenomenon which could result in larger power density. Apart from forced circulation, natural circulation could also be a viable option for supercritical water cooled reactors. Due to the large change in fluid properties, the steady state equation for subcritical natural circulation flow is not adequate for supercritical fluids. Traditionally, natural circulation analysis is carried out by 1-dimensional approach based on constant fluid properties assuming Boussinesq approximation to be valid. Such an approach, although well suited for subcritical fluids is not applicable for supercritical fluids where the density change is quite sharp especially in the pseudo critical region. As a result, modeling of the density variation is central to modeling of natural circulation loop with supercritical fluids.

The density change for supercritical systems is comparable to or even more than that of two-phase systems resulting in instability concerns. The instability could be either density wave type or excursive type (Ledinegg or static instability). Although, there is considerable literature on the density wave instability in supercritical fluids, there are not many studies dealing with the static instability of the excursive type. Therefore, an analysis has been carried out to predict the threshold of excursive instability for both supercritical water and CO_2 for the present loop.

1.3 Scope and Objectives of the present study

1.3-1 Natural circulation analysis at subcritical pressure condition

The heat transport capability of natural circulation loops is directly proportional to the flow rate it can generate. Therefore, reliable prediction of flow rate is essential for design and performance evaluation of natural circulation loops. Dimensionless equations which are not loop specific are desirable to compare the performance of different natural circulation loops. The available dimensionless equation [Vijayan (2002)] for steady state flow in both uniform and non-uniform diameter loops is applicable only when the entire loop follows the same friction law i.e. when the loop is fully laminar or fully turbulent. Therefore, a generalized flow equation is necessary for natural circulation loops obeying multiple friction laws.

The generalized flow equation enables us to calculate the steady state flow in a Natural Circulation Loop (NCL). However, it does not tell us whether that particular steady state is stable or unstable. Thus, stability analysis is necessary to ascertain whether a particular steady state is stable. In general, stability of a NCL is analyzed either by linear stability method or by non-linear stability method. Stability analysis using non-linear method involves tedious computations and also is very expensive. Therefore, linear stability analysis provides the best route to generate a stability map. In the linear stability method, the governing equations are perturbed over the steady state and the perturbed governing equations are linearized to obtain a characteristic equation for the stability parameter. If this equation has any root with positive real part then the system is considered to be unstable in accordance with the Nyquist criterion. In most of the published literature, the results of the linear stability analysis have been given in dimensionless form. Usually the stability map in dimensionless form is plotted as a function of the modified Grashof number, modified Stanton number and L_t / D for a specified geometry of the loop. However, for conditions such as high values of the modified Grashof number it becomes difficult to ascertain whether the system remains in single-phase condition or not. Hence, there is a need to generate a single stability map valid for laminar, transition and turbulent regions for a given single-phase loop. Such a stability map was generated as part of the present study.

1.3-2 Natural circulation analysis at supercritical pressure condition

Many new generation reactors use fluids under supercritical condition. Lots of work has already been carried out on subcritical natural circulation, however, limited amount of work has been done on supercritical natural circulation. Supercritical fluids undergo large change in density, specific heat and other thermodynamic and thermo physical properties without the formation of interfaces and separate phases. The elimination of phase change results in elimination of the Critical Heat Flux (CHF) phenomenon. As mentioned earlier, natural circulation analysis for subcritical fluids is based on 1-dimensional approach with constant fluid properties and Boussinesq approximation used to account for density variation [Vijayan (2002)]. However, such an approximation is not valid for supercritical fluids where the density change is quite sharp in the neighborhood of the critical region. Therefore, modeling of the density variation for natural circulation loop with supercritical fluids is a concern. Ambrosini and Sharabi (2008) have found that if dimensionless density is plotted as a function of dimensionless enthalpy then the data for different supercritical fluids, collapse into a unique curve irrespective of the pressure. This relationship is reasonably general and is valid for several fluids. Therefore, a new model has been developed for density variation in supercritical fluids using the dimensionless relationship proposed by Ambrosini and Sharabi (2008). In addition, a generalized correlation has been proposed as part of the present thesis work to estimate the steady state flow in supercritical natural circulation loops based on the relationship between dimensionless density and dimensionless enthalpy proposed by Ambrosini and Sharabi.

Flow and pressure oscillations might occur under supercritical condition when certain operating conditions are reached [Zuber (1966)]. These oscillations were observed in systems with forced flow as well as natural circulation. The occurrence of sustained pressure and flow oscillations are undesirable for reliable operation of a thermal hydraulic system. Furthermore, in nuclear reactor, system flow and pressure oscillations may induce undesirable power excursion. Consequently, there is considerable interest to study the conditions leading to the initiation of these oscillations. At supercritical pressure, a flow system with heat addition could undergo flow excursion. This excursive flow instability at supercritical pressures is equivalent of the 'Ledinegg' excursive instability in boiling systems at subcritical pressure. The flow excursion instability involves a sudden change in the flow rate to a lower value. Although, there is considerable literature on the density wave oscillation in supercritical fluids, there are not many studies dealing with static instability of the excursive type. Therefore, static instability in a closed loop natural circulation system at supercritical condition has been investigated for supercritical water and CO_2 as a part of the present work.

1.4 Organization of the thesis

This thesis is divided into 6 Chapters.

Chapter 1 presents the problems related to subcritical and supercritical natural circulation considered in the present thesis as well as the scope and objectives of the thesis.

Chapter 2 presents literature review of natural circulation under subcritical and supercritical condition.

Chapter 3 presents a description of the experimental facility installed at BARC for carrying out subcritical and supercritical natural circulation tests.

Chapter 4 presents a generalized equation for the steady state flow in single-phase natural circulation loops. The equation was derived based on 1-dimensional theory by assuming the loop to be partly in laminar and partly in transition or turbulent flow. The derived dimensionless flow equation is applicable for any loop obeying multiple friction laws. The generalized flow equation was tested with the experimental data generated in a uniform diameter rectangular loop for all four orientations such as, Horizontal Heater and Horizontal Cooler (HHHC), Horizontal Heater and Vertical Cooler (HHVC), Vertical Heater and Horizontal Cooler (VHHC), Vertical Heater and Vertical Cooler (VHVC). Subsequently, it has been tested with data reported in literature.

A stability code LISA (LInear Stability Analysis) based on linear stability analysis methodology has been developed and validated with previously reported stability map for both laminar and turbulent flows. Subsequently a stability map valid for laminar, transition and turbulent regions has been obtained using the LISA code for the same loop and is presented in chapter 4.

Chapter 5 presents natural circulation analysis at supercritical pressure condition. New studies were conducted to generate the performance of natural circulation loops with supercritical fluids. Present analysis makes use of dimensionless relationship between the density and the enthalpy of supercritical fluids proposed by Ambrosini and Sharabi to develop a new model for density variation in supercritical fluid. This relationship is reasonably general and it is valid for several fluids and therefore enables us to generate a generalized flow correlation valid for different fluids at supercritical pressure. This generalized flow correlation was tested with the experimental data generated with supercritical CO_2 and water in a uniform diameter rectangular loop and also with the data available in the literature.

Chapter 6 presents conclusions and recommendation for future work.

1.5 Closure

Present chapter introduces the natural circulation phenomena under subcritical and supercritical condition. Present thesis is concerned with reliable prediction of the steady state flow rate of natural circulation loops under subcritical and supercritical pressure condition since the heat transport capability of natural circulation loops depend on it. For the first time, a generalized flow equation valid for all regions i.e. laminar, transition and turbulent under subcritical condition has been obtained. In addition, stability analyses reported in the literature for single-phase loops are either for the laminar or for the turbulent flow regime only. These analyses have generated stability maps for laminar and turbulent flows using corresponding friction laws. In the present thesis a single stability map is proposed which is valid for all the three flow regimes.

New studies are being conducted to generate the performance of natural circulation loops with supercritical fluids. Analysis makes use of dimensionless relationship between density and enthalpy of supercritical fluids proposed by Ambrosini and Sharabi to develop a new model for density variation in supercritical fluids. A generalized correlation has been derived for the steady state flow based on the Ambrosini and Sharabi relationship for the density of supercritical fluids. Simple flow equations for supercritical fluids have been provided after subdividing the near critical region into three regions. Experiments have been performed with supercritical CO_2 and water to validate these generalized flow equations. In addition, static instability in a closed loop natural circulation system at supercritical condition has been investigated for supercritical water and CO_2.

CHAPTER-2

LITERATURE SURVEY

2.1 Natural circulation at subcritical pressure condition

Natural circulation is the result of thermally generated buoyancy pressure differential and hence such systems enhance reliability and safe operational potential compared to systems with pumps. Due to this, natural circulation loops are extensively used in several industries. In nuclear industry, some of the innovative reactors like MASLWR [Modro et al. (2002)], CAREM [MAZZI (2005)], LFR [Smith et al. (2008)], ABV [Kostin et al. (2004)], SSTAR and STAR-LM [IAEA No.NP-T-2.2, Annex IX, Vienna (2009)] are designed to remove core heat by single-phase natural circulation, as these designs eliminate the need for recirculation pumps. Literature survey revealed that great deal of work has already been carried out on natural circulation. Reviews are available on single-phase natural circulation [Japikse (1973), Zvirin (1981), Mertol and Greif (1985) and Greif (1988)]. The heat transport capability of natural circulation loops is directly proportional to the flow rate it can generate. Steady state flow prevails in a natural circulation loop when the driving buoyancy pressure differential is balanced by the retarding frictional pressure losses. Based on this, an equation for the flow can be derived. For an incompressible fluid with negligible viscous dissipation and axial conduction effects flowing in a natural circulation loop with a heat source supplied with uniform heat flux and a heat sink supplied with specified coolant flow rate and inlet temperature, a generalized equation for steady state flow (applicable to both uniform and non-uniform diameter loops) has already been derived in [Vijayan (2002)] and can be expressed as:

$$\mathrm{Re} = C\left[\frac{Gr_m}{N_G}\right]^r \tag{2. 1}$$

The above equation is applicable if a friction law of the form

$$f = \frac{p}{\mathrm{Re}^b} \tag{2.2}$$

is valid throughout the loop with the same values of p and b. The constants C and r are related to p and b as follows:

$$C = \left(\frac{2}{p}\right)^{\frac{1}{3-b}} \tag{2. 3}$$

$$r = \frac{1}{3-b} \tag{2. 4}$$

The constants C and r take the values of 0.1768 and 0.5 for a fully laminar loop (p=64 and b=1) and 1.956 and 0.364 for a fully turbulent loop (p=0.316 and b=0.25). The generalized equation given above was previously tested by various authors Vijayan and Austregesilo (1994), Vijayan (2002), Ambrosini et al. (2004), Bodkha

(2009) and Misale and Garibaldi (2010). From these reports, it has been observed that most of the steady state experimental data are in close agreement with the proposed theoretical steady state equation in the fully laminar and fully turbulent regimes. However, in the transition region the agreement is not as good. In addition, the above-mentioned correlation is applicable only when the loop is either fully laminar or fully turbulent. Therefore, it is necessary to develop a generalized equation valid for the case of multiple friction laws.

Stability analyses reported in the literature for single-phase loops are either for the laminar or for the turbulent flow regime only. These analyses have generated stability maps for laminar and turbulent flows using corresponding friction laws. These stability maps primarily depend on the friction laws employed. In addition, the existing stability map for laminar flow shows that the laminar condition prevail only at low Gr_m values. Similarly, existing stability map for turbulent flow reveals that at low Gr_m values the flow condition is actually laminar. Hence, a single stability map which is valid for laminar, transition and turbulent regions for a single-phase loop is required to be generated.

2.2 Natural circulation at supercritical pressure condition

Natural circulation mode of heat transport has considerable applications due to its inherent safety characteristics. Most applications of natural circulation systems use subcritical fluids. Extensive literature exists on the theoretical and experimental investigations on the steady state performance of natural circulation of subcritical fluids [Vijayan and Austregesilo (1994), Vijayan (2002), Ambrosini et al. (2004), Bodkha (2009), Misale and Garibaldi (2010), Swapnalee et al. (2011)]. SuperCritical Water Reactor (SCWR) is currently receiving attention as a promising concept of advanced reactor design. SCWR has many advantages over present generation LWRs. Supercritical fluids are proposed to be used in a few advanced reactor designs like HPLWR [Reiss et al. (2008)], CANDU-X-NC [Torgerson et al. (2006)] and B-500-SKDI [Silin et al. (1993)]. Besides, one of the designs being considered by the Generation IV International Forum (GIF) is a thermodynamically supercritical reactor [GIF-002-00, (2002)]. Some of these concepts use natural circulation as the mode of coolant circulation [Torgerson et al. (2006), Silin et al. (1993)]. The fluids at supercritical pressure undergo large change in density, specific heat and other thermodynamic and thermo physical properties without the formation of interfaces and separate phases. The elimination of phase change results in elimination of the Critical Heat Flux (CHF) phenomenon. In addition, supercritical fluids like water exhibits excellent heat transfer characteristics and high volumetric expansion coefficient (hence capable of high mass flow rates in natural circulation mode) near the pseudo critical temperature. Other than supercritical water, some reactor designs consider supercritical CO_2 as coolant [Driscoll and Hejzlar (2004), Tom and Hauptmann (1979)].

Experiments involving supercritical water are expensive since it involves very high pressure and high temperature equipment. It is possible to overcome this to some extent by using CO_2 (critical point of CO_2 is 31^0C and 7.4MPa whereas for water it is 374^0C and 22.1MPa) which is readily available and inexpensive. Therefore, CO_2 is considered a good simulant fluid for water because of the analogous change in physical properties across the pseudo critical point (see ***Figure 2.1***). In addition, the key advantage of CO_2 is that it is non-toxic and non-explosive.

Typical variation of thermo physical properties of supercritical water and CO_2 are shown in ***Figure 2.1*** where the properties have been taken from the National Institute of Standards and Technology (NIST) database[+1].

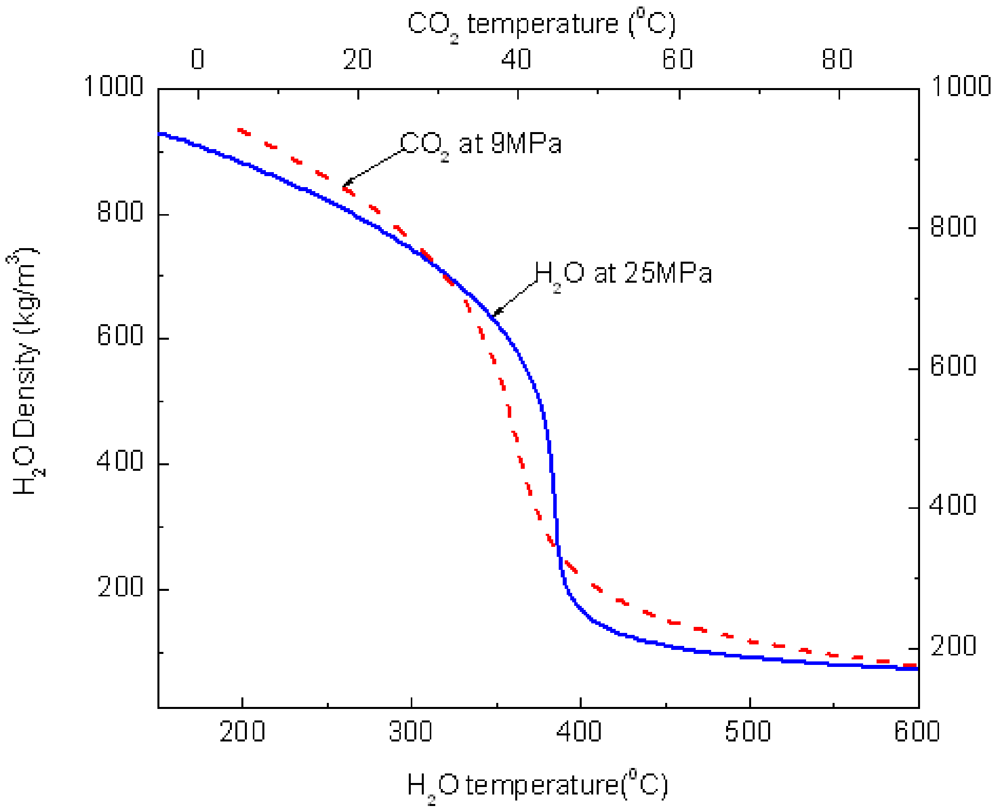

(a) Density variation for supercritical water and supercritical CO_2

[+1] http://webbook.nist.gov/chemistry/fluid/

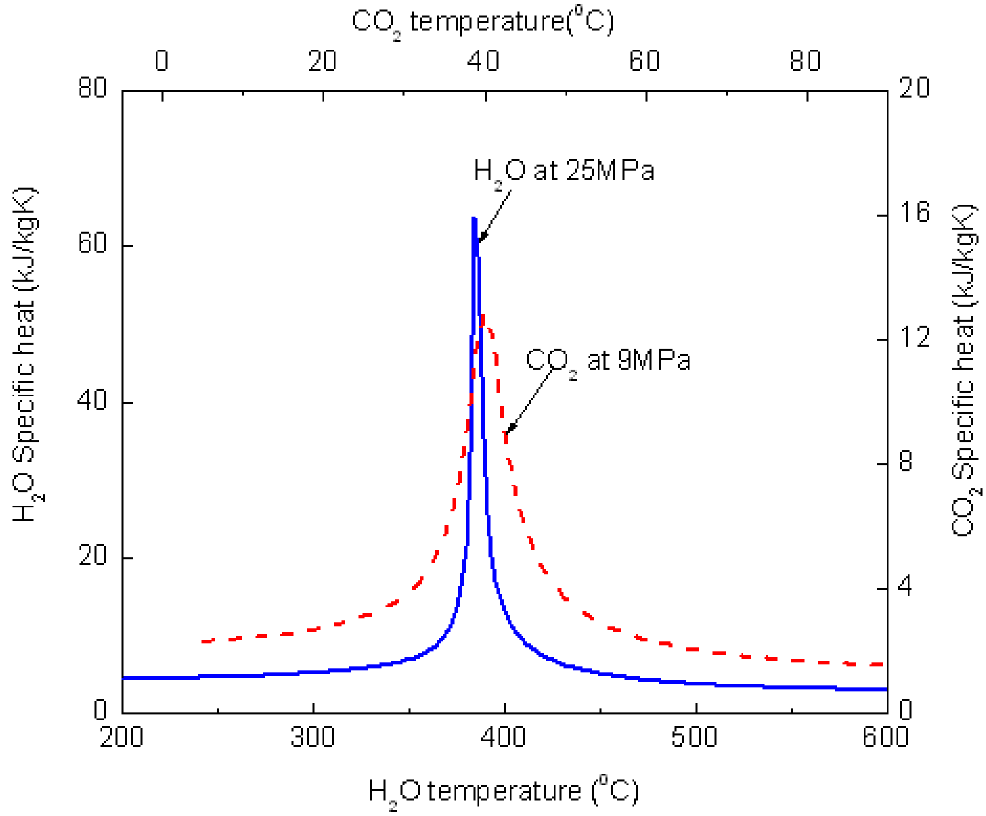

(b) Variation of specific heat for supercritical water and supercritical CO_2

Figure 2.1: Variation of fluid properties under supercritical pressure condition

From ***Figure 2.1*** it has been observed that near the pseudo critical point i.e. where the specific heat is maximum, slight change in temperature will result in sharp variations in properties. Therefore, the large density change that occurs as supercritical fluid is heated through the pseudo critical point can be used to generate a substantial driving head for natural circulation.

Various researchers have already investigated numerically the stability of supercritical natural circulation loops. Chatoorgoon (2001) considered a constant area rectangular open loop with horizontal heater, did the steady state and non-linear stability predictions for the geometry and concluded that the stability threshold power of a natural circulation loop with supercritical fluid is confined to the near peak region of the steady state flow versus power curve. Yi et al. (2004) developed a linear stability analysis code in frequency domain to analyze the stability of high temperature reactor, cooled and moderated by supercritical pressure light water. Zhao et al. (2005) used a three-region model for approximating the variation of density with enthalpy in the subcritical, pseudo critical and supercritical regions for carrying out the stability analysis. Jain and Corradini (2006) has performed linear stability analysis of a supercritical water natural circulation loop and obtained stability maps. Their results suggest that the instability threshold of supercritical natural circulation loops is not strictly related to the peak of the steady-state flow versus power curve. Manish et al. (2010) performed both linear and nonlinear stability analysis of a supercritical water loop. Reviews on heat transfer of fluids at supercritical pressure [Pioro and Duffey, Pioro and Duffey (2005), Pioro et al. (2004)] are available in open literature. In the above studies, however, the emphasis was on heat transfer and stability. There are very few experimental studies of natural circulation loops with supercritical fluids. Holman and Boggs (1960) studied the heat transfer characteristics of Freon-12 in its critical region in a closed natural circulation loop. Harden (1963) studied the transient behavior of a natural circulation loop operating near the thermodynamic critical point. Lomperski and Cho (2004) at Argonne National Laboratory (ANL) performed experiments in a rectangular test loop with supercritical CO_2 to study the stability behavior. Yoshikawa et al. (2005) have studied the performance of a natural circulation system for supercritical CO_2.

Assumption of constant fluid property with Boussinesq approximation [Vijayan (2002)] used in natural circulation analysis under subcritical flow condition is not applicable for supercritical fluid due to large change in fluid properties such as density near the pseudo critical region. Therefore, there is a need to develop model equivalent to Boussinesq approximation for reliable prediction of flow rate under supercritical condition.

Literature review revealed that the flow and pressure oscillations might occur under supercritical condition when certain operating conditions are reached [Zuber (1966)]. These oscillations were observed in systems with forced flow as well as natural circulation. The occurrence of sustained pressure and flow oscillations are undesirable for reliable operation of a thermal hydraulic system. Furthermore, in nuclear reactor, system flow and pressure oscillations may induce undesirable power excursion. Consequently, there is considerable interest to investigate the conditions leading to the initiation of these oscillations. Literature review revealed that at supercritical pressure, a flow system with heat addition could undergo flow excursion. This excursive flow instability at supercritical pressures is equivalent of the 'Ledinegg' excursive instability in boiling systems at subcritical pressure. The flow excursion instability involves a sudden change in the flow rate to a lower value. Zuber (1966) first did an extensive review and in-depth analytical study of various instability modes of supercritical fluid flow. He concluded that supercritical flow instability would be similar to two-phase instability possessing both the excursive and oscillatory nature. Ambrosini (2007) also observed the existence of Ledinegg instability in heated channels with supercritical fluids. He concluded that in order to achieve excursive behavior, it was needed to adopt very low values of inlet channel temperatures resulting in a sufficiently large value of dimensionless number known as sub-pseudo-critical number, N_{subpc} (up to about 3.4). Although, there is considerable work on the density wave oscillation in supercritical fluids, there are not many studies dealing with static instability of the excursive type. In this context static instability in a closed loop natural circulation system at supercritical condition has been investigated for supercritical water and CO_2 in the present thesis.

2.3 Closure

Literature review on the natural circulation phenomena under subcritical and supercritical condition has been presented. It is observed from the review on natural circulation under subcritical condition that for reliable prediction of flow rate it is necessary to develop a generalized flow equation obeying multiple friction laws.

Also explicit correlation for steady state flow is not available for supercritical fluid. Due to large change in fluid properties near the pseudo critical region Boussinesq approximation is not valid. Therefore, there is a need to develop model equivalent to Boussinesq approximation.

CHAPTER-3

EXPERIMENTAL FACILITY

The experimental facility of BARC (Bhabha Atomic Research Centre, Mumbai, India) is described in this chapter which is used to perform experiments on subcritical water. In addition, experiments on near critical and supercritical regions of water and CO_2 were also performed. These experiments were performed for the following orientations of the heater and the cooler:

a. Horizontal Heater and Horizontal Cooler (HHHC)

b. Horizontal Heater and Vertical Cooler (HHVC)

c. Vertical Heater and Horizontal Cooler (VHHC)

d. Vertical Heater and Vertical Cooler (VHVC)

However, with supercritical water, experiments were conducted only for Horizontal Heater and Horizontal Cooler (HHHC) orientation.

3.1 Experimental Facility for subcritical water

A rectangular natural circulation test facility as shown in ***Figure 3.1a*** has been constructed and installed at BARC with the length scale of the different components as shown in ***Figure 3.1b***. It is a uniform diameter rectangular loop of inside diameter

13.88 mm made of stainless steel (SS-347). The loop pressure is maintained with the help of a pressurizer. The loop fluid fills the pressurizer up to a certain level. Beyond this level, a cover gas (Nitrogen) is filled. The loop had two heaters and two coolers. The heater was made of nichrome wire wound uniformly on the outside surface. The cooler was tube-in-tube type with secondary coolant flowing through the annulus. The outside diameter of the inner tube is 21.34 mm and the inside diameter of the outer tube is 73.7 mm. Any of the heater (either horizontal or vertical) and cooler (either horizontal or vertical) combination can be used for the experiments. The unused cooler secondary side was drained. The entire loop was insulated with ceramic mat. The loop was extensively instrumented with K-type thermocouples to measure loop fluid temperature, heater surface temperature as well as primary and secondary side coolant inlet and outlet temperatures. The loop had 44 thermocouples in all, 24 of which were used to measure the outside wall temperature in the heater sections. 16 thermocouples (2 at each location) at each of the eight locations in the primary side of the loop to measure fluid temperature. In addition, 2 thermocouples were used to measure the inlet and outlet temperature of the secondary side coolant. Since the secondary side coolant flow was forced, this was adequate to measure the average temperature. The heater power was measured using a Wattmeter. The overall heat transfer coefficient of the cooler is estimated from the measured power and fluid temperatures at inlet and outlet of primary and secondary side [Ref.Appendix-1]. The secondary side flow rate was measured with the help of a turbine flow meter. The accuracy of temperature readings were within $\pm 1^0$C. Similarly, the accuracy of the primary and secondary flow measurements was within ±1%. The output of all instruments was recorded on a PC based datalogger with a scanning speed of 100 milliseconds.

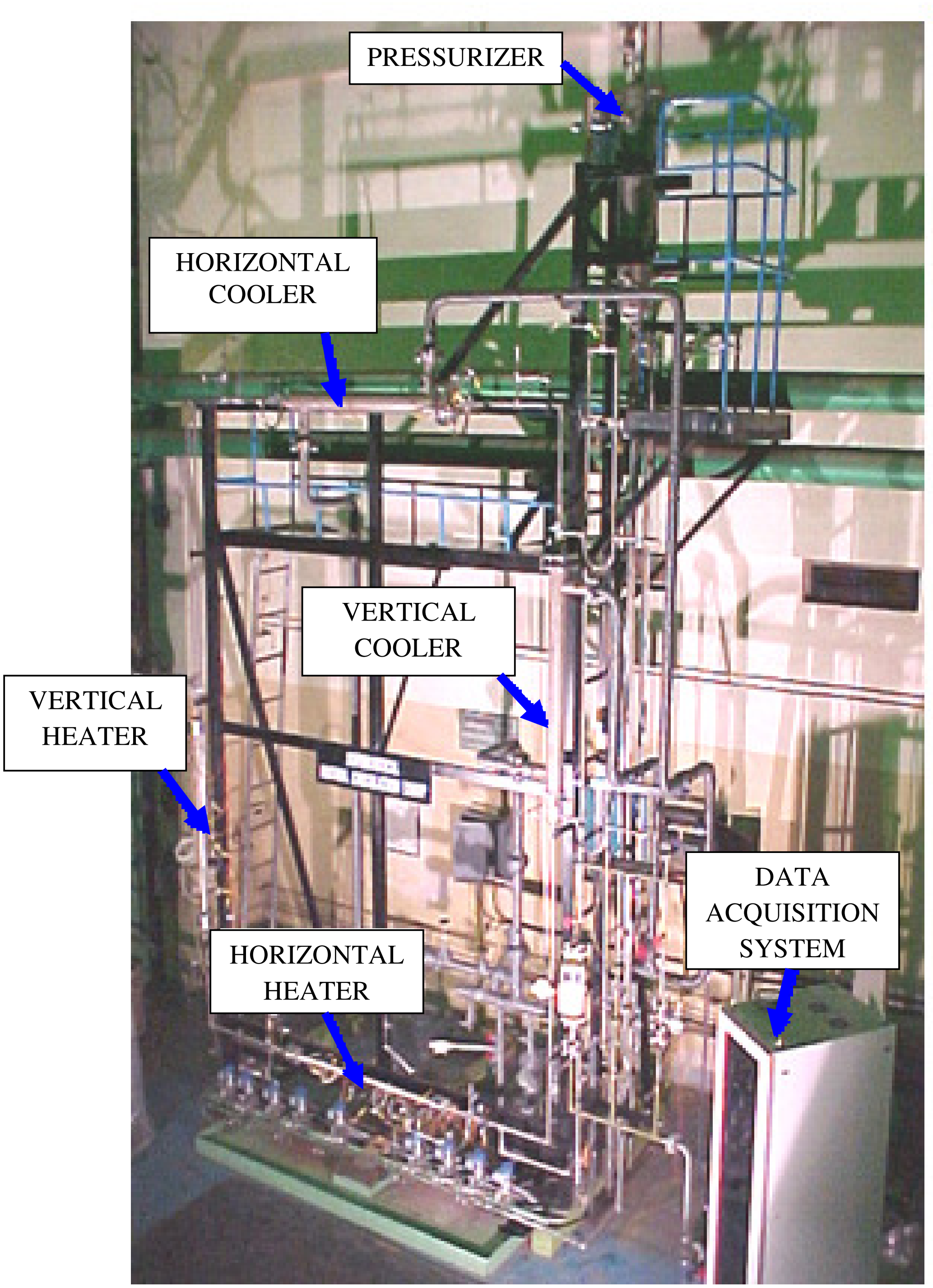

Figure 3.1a: Photograph of the subcritical water test facility

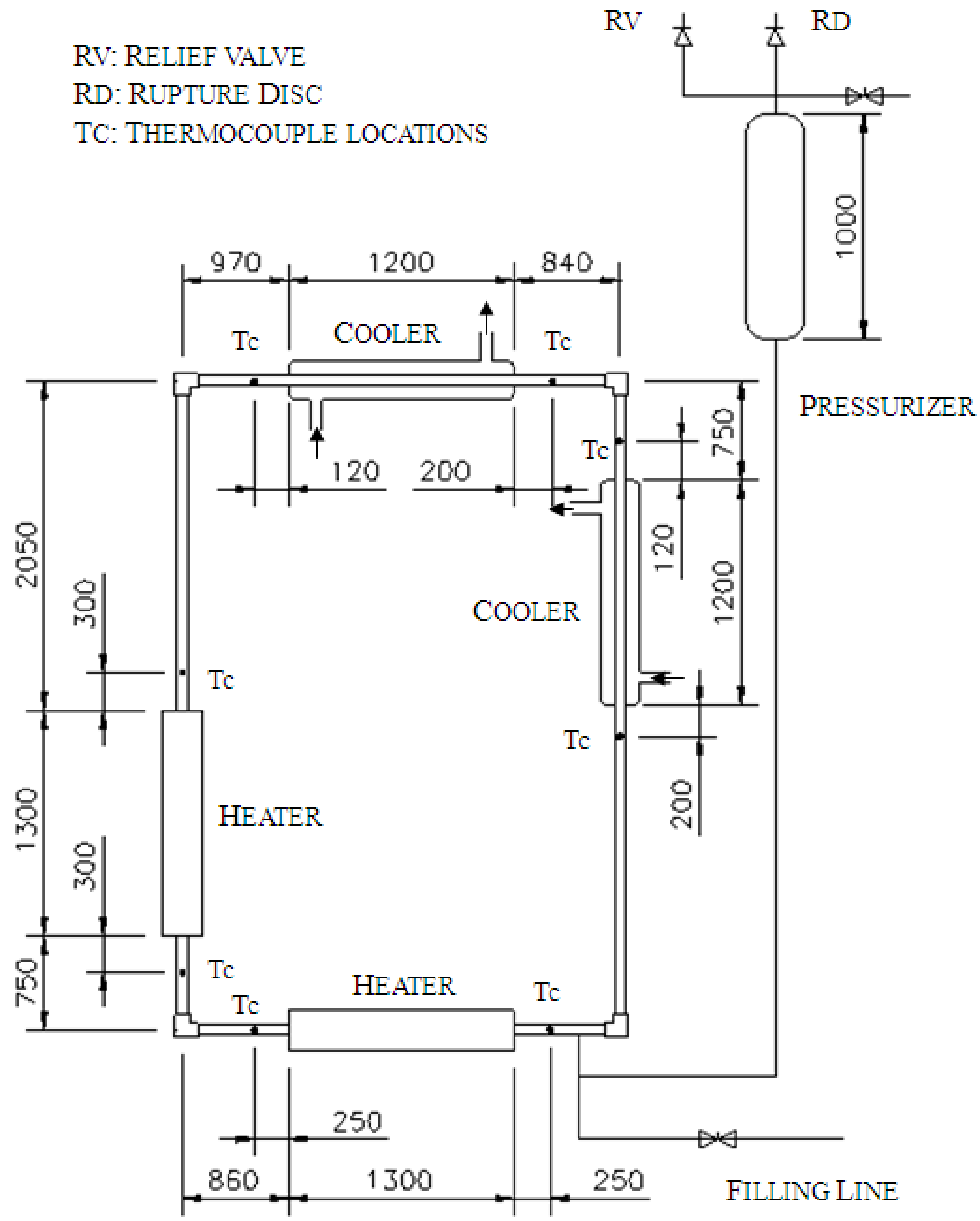

Note: All dimensions are in mm

Figure 3.1b: Schematic of the subcritical water test facility

3.1.1 Experimental data generated

Experiments were carried out with water at 30-bar pressure. The secondary side coolant was chilled water. Steady state observations were taken for the four orientations of the heater and the cooler. The range of parameters of steady state data for water is given in Table-3.1.

Table-3.1: Range of parameters for the test data

Orientation	Centre line elevation difference between cooler and heater, m	Range of Parameters for the data							
		Power, W		Re		Gr_m		Secondary flow at 10 ^{0}C, lpm*	
		Min.	Max.	Min.	Max.	Min.	Max.	Min.	Max.
HHHC	4.10	225.4	3507.1	4.82E+2	1.02E+4	2.11E+10	1.55E+13	7.95	8.2
HHVC	2.75	504.4	3522.5	1.29E+3	1.01E+4	9.06E+10	2.27E+13	7.95	8.6
VHHC	2.70	244.9	3067.2	5.81E+2	5.91E+3	1.72E+10	5.87E+12	7.6	8.4
VHVC	1.35	249.5	2996.0	5.01E+2	6.58E+3	1.54E+10	6.35E+12	6.8	8.6

* lpm: liters per minute

3.2 Experimental facility for operation with supercritical CO_2

A rectangular natural circulation test facility as shown in ***Figure 3.2a*** with a design pressure of 30 MPa and design temperature of 550 ^{0}C has been constructed at BARC with the length scale of the different components as shown in ***Figure 3.2b***. It is a uniform diameter rectangular loop of inside diameter 13.88 mm made of stainless steel (SS-347). The loop has two heater and two cooler sections so that it can be operated with different orientations of heater and cooler. The heater was made by uniformly winding nichrome wire over a layer of fiberglass insulation. The cooler was tube-in-tube type with chilled water as the secondary coolant flowing in the annulus. The outer tube forming the annulus had 77.9 mm ID and 88.9 mm OD. The loop had a pressuriser located at the highest elevation, which takes care of the thermal expansion besides accommodating the cover gas helium above the CO_2. The safety devices of the loop i.e. rupture discs (RD) were installed on the top of the pressuriser which had also the provision for CO_2 and He filling. The entire loop was insulated with ceramic mat.

The loop was extensively instrumented with 44 calibrated K-type thermocouples (1 mm diameter) to measure temperatures of loop fluid, heater surface as well as secondary side coolant inlet and outlet. Primary fluid temperatures at each location was measured as the average value indicated by two thermocouples inserted diametrically opposite at r/2 from the inside wall whereas secondary fluid temperatures were measured by a single thermocouple located at the tube centre. The heater power was measured using a Wattmeter. The secondary side flow rate was measured with the help of a turbine flow meter. All instruments were connected to a data logger with a user selectable scanning rate. The accuracy of the thermocouples was within $\pm 1.5^0$C. Similarly, the accuracy of the primary and secondary flow as well as power measurements was within ±0.5% of the reading [Vijayan et al. (2010)].

3.2.1 Experiments with supercritical CO_2

Before operation with supercritical CO_2, the loop was flushed repeatedly with CO_2 at low pressure including all impulse, drain and vent lines. Subsequently the loop was filled with CO_2 up to 50 bar pressure and the chilled water coolant was valved in. This caused condensation of CO_2 and hence a decrease in loop pressure. The pressure decrease was compensated by admitting additional CO_2 from the cylinder and again allowed sufficient time for condensation. The process of filling and condensation was continued till there was no decrease in pressure. At this point the loop pressure was increased to the required value with the help of helium gas cylinder. Once the required supercritical pressure was achieved the helium cylinder was isolated from the pressurizer. Sufficient time was allowed to reach steady state. However it was found difficult to attain completely stagnant conditions with uniform temperature throughout the loop as the higher ambient temperature allowed small amount of heat absorption through the insulation into the loop which was rejected at the cooler causing a small circulation rate. Once the steady state was achieved, the heater power was switched on and adjusted to the required value. Sufficient time was allowed to reach the steady state. Once the steady state is achieved the power was increased and again sufficient time was provided to achieve the steady state. If the system pressure increases beyond the set value by 1 bar, a little helium was vented out to bring the system pressure back to the original value. Similarly, during the power decrease, if the system pressure decreases below the set point by 1 bar, then the loop was pressurized by introducing additional helium into the pressurizer. The experiments were repeated for different pressure and for different chilled water flow rates. Subsequently the experiments were performed for different orientations of the heater and the cooler.

Figure 3.2a: Photograph of the supercritical CO_2 test facility

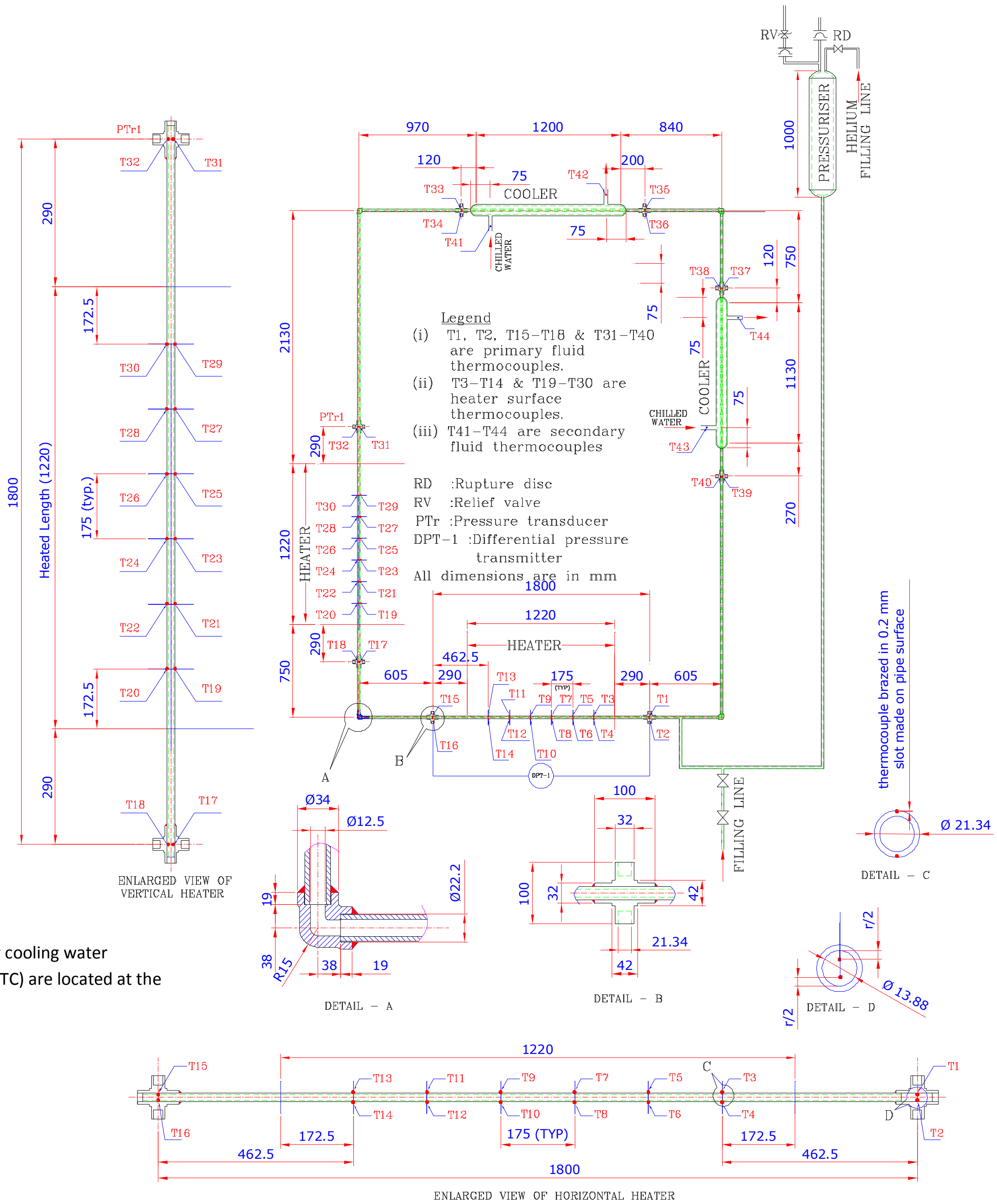

Note: Secondary cooling water thermocouples (TC) are located at the centre.

Note: All dimensions are in mm

Figure 3.2b: Schematic of the supercritical CO_2 test facility

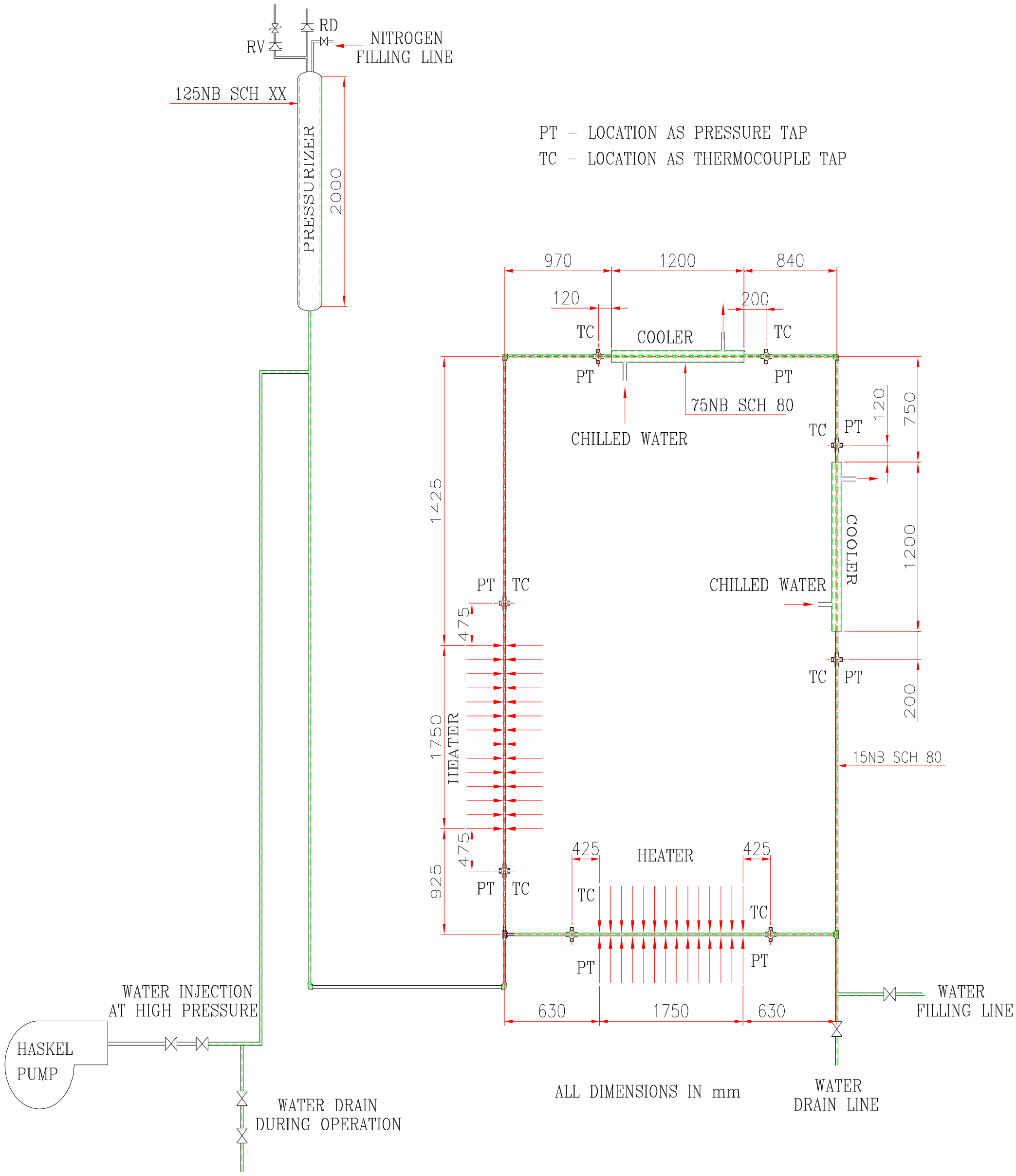

Figure 3.2c: Schematic of the modified test facility for operation with supercritical water

3.3 Experimental facility for operation with supercritical water

After completion of experiments with supercritical CO_2, the supercritical pressure natural circulation loop was modified by installing new test sections, pressurizer, Haskel pump and a low voltage high current power supply (25V and 8000A rated 200 kW) so that uniform heat generation occurs in the heater wall material. The loop has two heater and two cooler sections, so that any of the heater (either horizontal or vertical) and cooler (either horizontal or vertical) combination for the experiments can be used. However, at present experiments were conducted only for Horizontal Heater and Horizontal Cooler (HHHC) orientation. The modified test facility is shown in ***Figure 3.2c***.

3.3.1 Experiments with supercritical water

For experiments under supercritical pressure conditions with water the following operating procedure is followed:

i) The loop is filled up with demineralized water to the required level in the pressurizer.

ii) Nitrogen is filled at the top of the pressurizer and the loop pressure is increased to 11MPa.

iii) Further pressurization to 22MPa and beyond is achieved by injecting more water at the bottom of the pressurizer with the Haskel pump which increases the water level in the pressurizer. Then the Haskel pump is isolated.

iv) Now power is switched on and due to thermal expansion of water, the loop gets pressurized above the supercritical pressure.

v) To get desired pressure at an operating power, water inventory in the pressurizer is changed either injecting water with Haskel pump or draining water from drain line near the outlet of Haskel pump ***(Figure 3.2c)***.

3.4 Steady state data

Steady state data on natural circulation flow were generated with supercritical CO_2 for various orientations of the heater and cooler whereas data with supercritical water was generated only for the orientation with both heater and cooler horizontal. The range of parameters of all steady state data for CO_2 and water is given in Table-3.2 and Table-3.3.

Table-3.2: Range of parameters for the test with CO_2 fluid

Orientation	Centre line elevation difference between cooler and heater, m	Range of Parameters for the data						
		Pressure (MPa)	Power, W		Re		Gr_m	
			Min.	Max.	Min.	Max.	Min.	Max.
HHHC	4.10	8.6	203.7	2391.7	2.2E+04	1.23E+05	6.23E+14	3.01E+16
HHVC	2.75	8.5 to 9.0	101.5	2200.5	1.38E+04	1.23E+05	1.6E+14	3.12E+16
VHHC	2.70	8.7 to9.1	248.9	2012.0	2.86E+04	1.04E+05	5.55E+14	2.6E+16
VHVC	1.35	8.5 to 8.7	205.8	1999.6	1.65E+04	9.43E+04	2.29E+14	1.62E+16

Table-3.3: Range of parameters for steady state natural circulation data with water

Variables		Range
Orientation		HHHC (Clockwise flow)
Pressure		22.5-24.1MPa
Power		4.5-8.0 kW
Cold leg temperature		264.9-389.8^{0}C
Hot leg temperature		292.4-411.2^{0}C
Re	Min.	3.31E+04
	Max.	1.22E+05
Gr_m	Min.	8.33E+14
	Max.	5.84E+15

3.5 Closure

Natural circulation experiments were carried out in a uniform diameter rectangular loop using subcritical water and supercritical CO_2 and water. Steady state data were generated with subcritical water and supercritical CO_2 with four different orientations of the heater and cooler. However, with supercritical water, experiments were conducted only for Horizontal Heater and Horizontal Cooler (HHHC) orientation.

CHAPTER-4

A GENERALIZED FLOW EQUATION FOR SINGLE-PHASE NATURAL CIRCULATION LOOPS OBEYING MULTIPLE FRICTION LAWS

4.1 Introduction

Heat transport capability of natural circulation loops depend on the flow rate generated and therefore reliable prediction of flow rate is essential. Dimensionless equations which are independent of loop geometry are useful in comparing the performances of different natural circulation loops. The reported dimensionless equation [Vijayan (2002)] for steady state flow (in both uniform and non-uniform diameter loops) is applicable only when the loop is obeying a single friction law throughout. However, it is not always essential that a single friction law is applicable throughout the loop. In many situations it is possible that, the loop may follow more than one friction law. For example, the simplest natural circulation loop conceivable is with a point heat source and a point heat sink, connected by adiabatic vertical pipes [as considered by Welander (1967)]. Such a loop has essentially two parts, i.e. a hot leg and a cold leg (see ***Figure 4.1***).

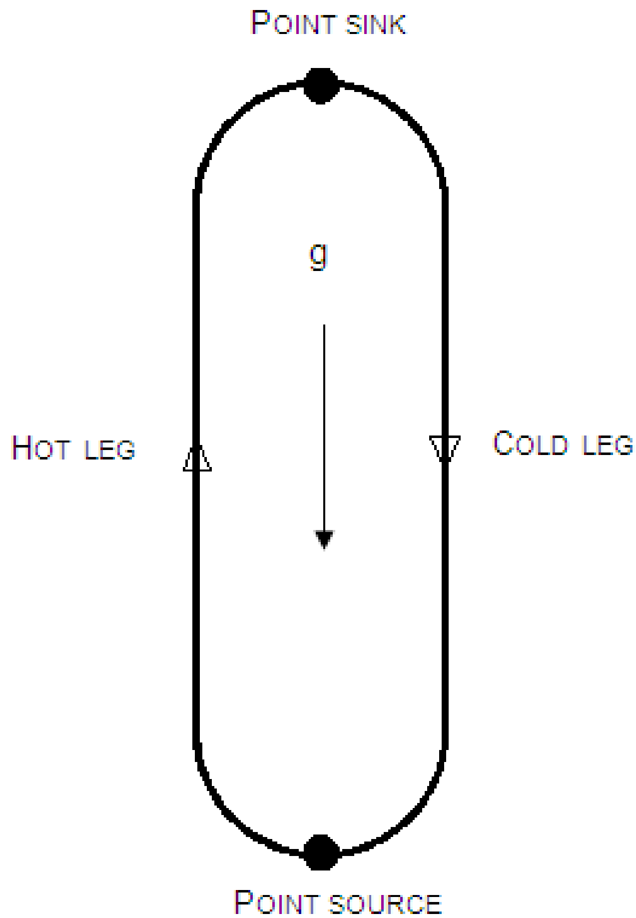

Figure 4.1: Schematic of a loop with point source and sink

Table- 4.1: Flow regimes in natural circulation loop

Flow regime	
Cold leg	**Hot leg**
Laminar	Laminar
Turbulent	Turbulent
Transition	Transition
Laminar	Turbulent
Laminar	Transition
Transition	Turbulent

As shown in Table-4.1, several flow regimes are possible even in such a simple natural circulation loop. As seen from the table, the assumption of a single friction law is valid for the first three cases only. For practical loops with finite lengths of heater and cooler, the number of regions and the possible combination of flow regimes become much larger than that in Table-4.1. Even for a uniform diameter loop, the hot leg can be in transition/turbulent flow with the cold leg in laminar /transition flow regime. Further, consider the case of a non-uniform diameter loop in which it is possible that some pipe sections are in turbulent flow and some in laminar and still others in transition flow. Therefore, the assumption that the same friction law is applicable throughout the loop is not valid always even in the simplest of natural circulation loops. Besides, due to geometric variations in the loop such as presence of rod bundle and noncircular conduits influences the friction law. Thus to cater to these situations, it is necessary to develop a generalized equation valid for the case of multiple friction laws, which is done in the present chapter.

Besides the above, better accuracy in flow rate estimation can be obtained even in case of single friction law if the viscosity variation in the cold and hot legs of the loop are accounted as it is the property which changes significantly with temperature. Large viscosity variations occur in liquid metal systems due to the large temperature difference (between hot and cold legs of the loop) caused by the very low specific heat of liquid metals. It is usual to have a temperature difference of the order of 200^0C or more in liquid metal natural circulation systems using lead or lead–bismuth eutectic as coolant [Smith et al. (2008), Sienicki et al. (2002), Dulera et al. (2005)]. In the present chapter therefore, the generalized flow equation has been extended to cases where the loop follows multiple friction laws. The proposed equation has been tested with experimental data generated in a uniform diameter loop and is found to be in good agreement. Subsequently, it has been tested with data reported in literature.

Stability of single-phase loops has been the subject of investigation for many years. Stability analyses reported in the literature for single-phase loops are either for the laminar or for the turbulent flow regime only. These analyses have generated stability maps for laminar and turbulent flows using corresponding friction laws. The stability maps are found to be a strong function of the friction laws employed. In addition, the stability map for laminar flow reported earlier shows laminar condition only at low Gr_m values. Similarly, stability map for turbulent flow shows that the flow is actually laminar in the region of low Gr_m values. Hence, there is a need to generate a single stability map valid for laminar, transition and turbulent regions for a single-phase loop. An attempt is made in this chapter to generate a single stability map valid for all three-flow regimes.

4.2 Derivation of the generalized equation for a loop obeying multiple friction laws

For this development, consider the uniform diameter rectangular closed loop shown in ***Figure 4.2.*** Assuming 1-dimensional incompressible fully developed flow with negligible viscous dissipation and axial conduction effects, the mass conservation equation for a closed loop can be written in terms of the mass flow rate W as

$$\frac{\partial W}{\partial s} = 0 \tag{4.1}$$

This means that the mass flow rate is independent of the location in the loop, and is a function of time only. The integral momentum equation [Ref.Appendix-2] can be written as

$$\frac{L_t}{A}\frac{dW}{dt} - g\rho_0\beta\oint T dz + \sum_{i=1}^{N_t}\left(\frac{f_i L_i}{D}\right)\frac{W^2}{2\rho_0 A^2} = 0 \tag{4.2}$$

In writing the above equation, it has been assumed that the local pressure losses are negligible+ and Boussinesq approximation is valid to account for the density variation. The energy equation [Ref.Appendix-2] can be written for the loop as

$$\frac{\partial T}{\partial t} + \frac{W}{\rho_0 A}\frac{\partial T}{\partial s} = \begin{cases} \dfrac{q_h P}{ACp\rho_0} & \text{for heater} \\ \dfrac{-UP(T - T_s)}{ACp\rho_0} & \text{for cooler} \\ 0 & \text{for pipes} \end{cases} \tag{4.3}$$

The steady state equations are obtained by dropping the temporal derivatives. At steady state the momentum equation reduces to

$$g\rho_0\beta\oint T dz = \sum_{i=1}^{N_t}\left(\frac{f_i L_i}{D}\right)\frac{W_{ss}^2}{2\rho_0 A^2} \tag{4.4}$$

+The assumption of negligible local pressure losses is justified for uniform diameter loops. In a uniform diameter loop the contribution of local pressure losses is negligible under laminar and transition condition where the friction factor is reasonably high. Under turbulent conditions, the contribution of local pressure losses is comparatively higher but is still less than 10% of the total pressure losses.

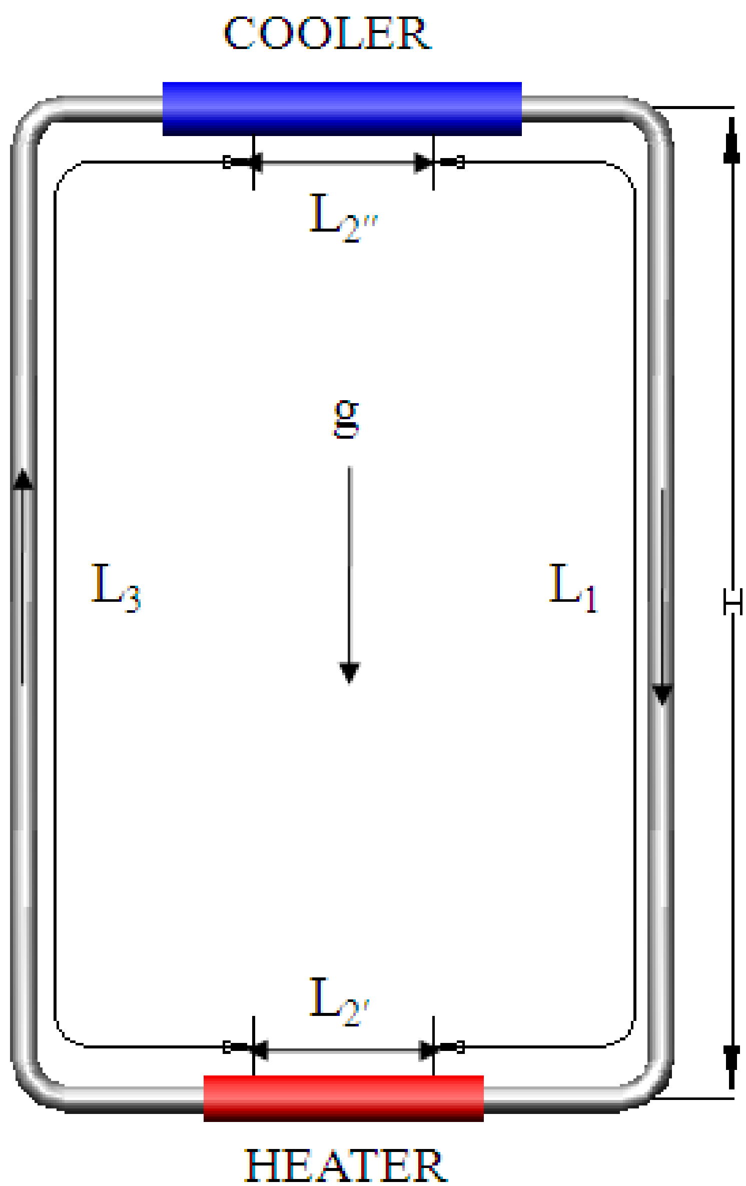

$L_2 = L'_2 + L''_2$

Figure 4.2: Rectangular loop considered for analysis

The energy equation at steady state is

$$\frac{W_{ss}}{\rho_0 A}\frac{dT}{ds}=\begin{cases}\dfrac{q_h P}{ACp\rho_0}\\ \dfrac{-UP(T-T_s)}{ACp\rho_0}\\ 0\end{cases} \tag{4.5}$$

The energy equation for the heater can be integrated with the boundary condition that at s=0, T=T_{cl} to obtain

$$(T_h)_{ss}=\frac{q_h P}{W_{ss}Cp}s+(T_{cl})_{ss} \tag{4.6}$$

Similarly, the equation for the steady state temperature in the cooler can be obtained as

$$(T_c)_{ss}=T_s+\left[(T_{hl})_{ss}-T_s\right]e^{\frac{UP(s_{hl}-s)}{W_{ss}Cp}} \tag{4.7}$$

Where the boundary condition, at s=s_{hl}, T=T_{hl} has been used. Using these equations, the integral in equation (4.4) can be calculated as

$$\oint Tdz=\left((T_{hl})_{ss}-(T_{cl})_{ss}\right)H=\frac{Q_h H}{W_{ss}Cp} \tag{4.8}$$

Assuming the loop lengths in laminar, transition and turbulent flow to be L_1, L_2 and L_3 (see ***Figure 4.2***) respectively, we can rewrite the steady state momentum equation as

$$g\rho_0\beta\left(\frac{Q_h H}{W_{ss}Cp}\right)=\left[\frac{f_1L_1}{D}+\frac{f_2L_2}{D}+\frac{f_3L_3}{D}\right]\frac{W_{ss}^2}{2\rho_0A^2} \tag{4.9}$$

Such that L_t=L_1+L_2+L_3 where L_t is the total circulation length of the loop. Alternatively, one can consider three regions in which the friction laws followed are different but has a general form of $f_i=\frac{p_i}{\mathrm{Re}_i^{bi}}$. In all the previous investigations, the fluid viscosity is assumed to be a constant throughout the loop. In the present investigation, the viscosity is assumed to be constant in each region with μ_1, μ_2 and μ_3 being the viscosities in region L_1, L_2 and L_3 respectively. Hence, the Reynolds number in each region is different due to the difference in the viscosity value. With this, the steady state momentum equation can be expressed as

$$g\rho_0\beta\left(\frac{Q_h H}{W_{ss}Cp}\right)=\sum_{i=1}^{3}\left(\frac{p_iL_i}{\mathrm{Re}_i^{b_i}}\right)\frac{W_{ss}^2}{2D\rho_0A^2}=\left[\frac{p_1L_1}{\left(\frac{DW_{ss}}{A\mu_1}\right)^{b_1}}+\frac{p_2L_2}{\left(\frac{DW_{ss}}{A\mu_2}\right)^{b_2}}+\frac{p_3L_3}{\left(\frac{DW_{ss}}{A\mu_3}\right)^{b_3}}\right]\frac{W_{ss}^2}{2D\rho_0A^2} \tag{4.10}$$

Taking region 3 as reference, the above equation can be expressed in dimensionless form as

$$\mathrm{Re}_3 = C\left[\frac{Gr_m}{N_G}\right]^r \tag{4.11}$$

Where $N_G = \frac{L_t}{D}\left[\frac{p_1}{p_3} l_1 \frac{\mathrm{Re}_3^{b_3}}{\mathrm{Re}_1^{b_1}} + \frac{p_2}{p_3} l_2 \frac{\mathrm{Re}_3^{b_3}}{\mathrm{Re}_2^{b_2}} + l_3\right]$ (4.12)

$$C = \left(\frac{2}{p_3}\right)^{\frac{1}{3-b_3}} \tag{4.13}$$

$$r = \frac{1}{3-b_3} \tag{4.14}$$

Special cases:

(a) Same friction law is applicable for all the three regions such that $p_1 = p_2 = p_3 = p$ and $b_1 = b_2 = b_3 = b$

$$N_G = \frac{L_t}{D}\left[l_1\left(\frac{\mathrm{Re}_3}{\mathrm{Re}_1}\right)^b + l_2\left(\frac{\mathrm{Re}_3}{\mathrm{Re}_2}\right)^b + l_3\right] = \frac{L_t}{D}\left[l_1\left(\frac{\mu_1}{\mu_3}\right)^b + l_2\left(\frac{\mu_2}{\mu_3}\right)^b + l_3\right] \tag{4.15}$$

(b) Same friction law is applicable and viscosity variation is negligible so that $\mu_1 = \mu_2 = \mu_3$ and $Re_1 = Re_2 = Re_3$

$$N_G = \frac{L_t}{D}\left[l_1 + l_2 + l_3\right] = \frac{L_t}{D} \tag{4.16}$$

Since $l_1 + l_2 + l_3 = 1$. This is same as that reported in Vijayan (2002).

(c) Length of transition region is negligible compared to the length of laminar and turbulent regions (two-region model)

$$N_G = \frac{L_t}{D}\left[\frac{p_1}{p_3} l_1 \frac{\mathrm{Re}_3^{b_3}}{\mathrm{Re}_1^{b_1}} + l_3\right] \tag{4.17}$$

(d) In many instances it can so happen that the same friction correlation is applicable i.e. $p_1 = p_3$ and $b_1 = b_3 = b$

$$N_G = \frac{L_t}{D}\left[l_1\left(\frac{\mu_1}{\mu_3}\right)^b + l_3\right] \tag{4.18}$$

If the viscosity variation is neglected, then this correlation becomes same as the one that was given in equation (4.16) above. The above equation has been derived for a rectangular loop with horizontal heater and horizontal cooler. For other orientations of the heater and cooler, the same result can be used by taking centre line elevation difference between the cooler and heater instead of the loop height. When the loop is fully laminar i.e. $p_1 = p_3 = 64$ and $b_1 = b_3 = 1$, equation (4.11) reduces to

$$\mathrm{Re}_3 = 0.1768\left[\frac{Gr_m}{\left(\frac{L_t}{D}\right)\left(l_1\left(\frac{\mu_1}{\mu_3}\right)^b + l_3\right)}\right]^{\frac{1}{2}} \tag{4.19}$$

When the loop is fully turbulent i.e. $p_1 = p_3 = 0.316$ and $b_1 = b_3 = b = 0.25$, the Eq. (4.11) reduces to

$$\mathrm{Re}_3 = 1.956\left(\frac{Gr_m}{\left(\frac{L_t}{D}\right)\left(l_1\left(\frac{\mu_1}{\mu_3}\right)^b + l_3\right)}\right)^{\frac{1}{2.75}} \tag{4.20}$$

4.3 Validation of the steady state equation

The steady state equation derived above has been validated with steady state natural circulation data generated in a uniform diameter rectangular loop [Ref. section 3.1] and also with the data available in the literature.

For each orientation, the steady state data were generated for different heater powers. The range of parameters for the experimental data for each orientation is given in Table-3.1. From the measured temperature difference across the heater (ΔT_h) and the power Q_h, steady state natural circulation mass flow rate W_{ss} is obtained as follows: $W_{ss} = \frac{Q_h}{(\Delta T_h)_{ss} Cp_h}$ where the specific heat Cp_h was calculated based on the average temperature (T_h) of the heater section (taken as the mean of the inlet and outlet temperatures). Knowing the mass flow rate and the loop geometry, the Reynolds numbers and Grashof numbers were calculated using the fluid properties at the loop average temperature. The centre line elevation difference between the heater and cooler used for calculation of modified Grashof number is given in the Table-3.1. Detailed experimental data generated is given in Appendix-3.

4.4 Friction factor correlations considered for laminar, transition and turbulent regions

Natural circulation loops are started up essentially from stagnant conditions. Hence, these loops experience laminar, transition and turbulent flow conditions with progressive increase in power. For example, immediately after the flow initiation at low powers laminar flow is expected to prevail throughout the loop for which friction law is given by f=64/Re. As the power increases the flow increases and the loop enters the transition regime first at the heater outlet, followed by the hot leg and finally the cold leg making the entire loop flow turbulent for which case the friction law is given by $f=0.316/Re^{0.25}$.

The transition from laminar to turbulent flow is reported to occur at Re=2000 for straight pipes. However, in a closed loop with horizontal heater, cooler and several elbows transition is expected to occur at much lower Re values. For example, Creveling et al. (1975) reports that the transition to turbulence occurs at Re=1500. On the other hand, Hallinan and Viskanta reports that the transition occurs at a Re value of 340. In numerical simulations, generally the intersecting point of laminar and turbulent friction correlation is taken as the transition point [Vijayan et al. (1995), Ambrosini and Ferreri (2000)]. The transition zone is generally considered to be between 2000 to 4000 for pipe flows [Ambrosini and Ferreri (2000)].

In natural circulation loops due to the presence of secondary flows, the transition could occur earlier than that in straight pipe. Since transition occurs earlier in natural circulation loops the transition to turbulence is also expected to occur earlier in natural circulation loops. Generally well-established friction law does not exist for the transition zone. Most of the reported correlations are a mathematical extrapolation from laminar to turbulent friction law. In this chapter, therefore it was decided to utilize the steady state data on natural circulation flow in the transition zone to obtain a friction factor correlation. As shown in ***Figure 4.3***, a flow correlation was fitted to the transition region test data. From this correlation, a power law of the form $f=\frac{p}{\mathrm{Re}^{b}}$ was obtained for the transition region using the Eq. (2.3) and Eq. (2.4). The friction law so obtained for the transition zone is given by $f=\frac{1.2063}{\mathrm{Re}^{0.416}}$. The same equation has been compared with a few reported transition zone correlation for forced flow in ***Figure 4.4***. As shown in ***Figure 4.4***, many of the reported transition correlations are close to the proposed friction law.

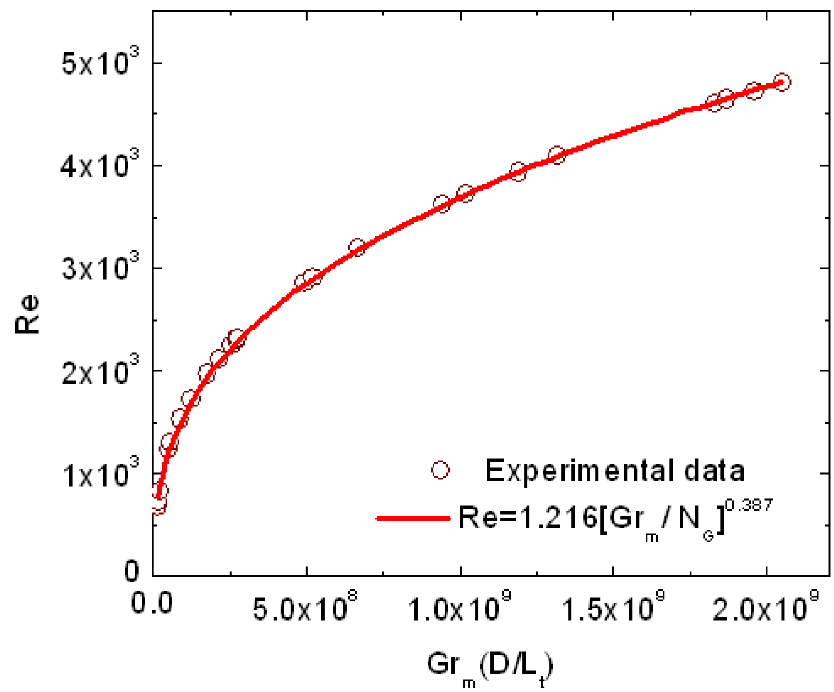

Figure 4.3: Transition region correlation obtained from experimental data

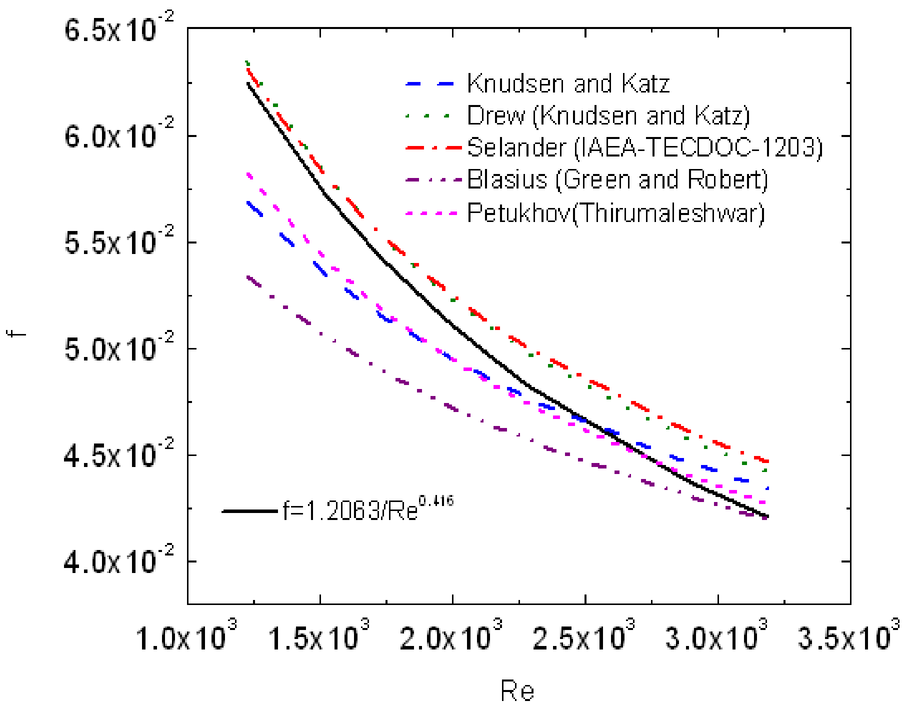

Figure 4.4: Comparison of transition region friction factor correlation with reported correlations

In the present work the change from laminar to transition region and the transition to turbulent region is assumed based on the criterion

$f=\max [f_l, f_{tr}]$ for change from laminar to transition and

$f=\max [f_{tr}, f_{tu}]$ for change from transition to turbulent

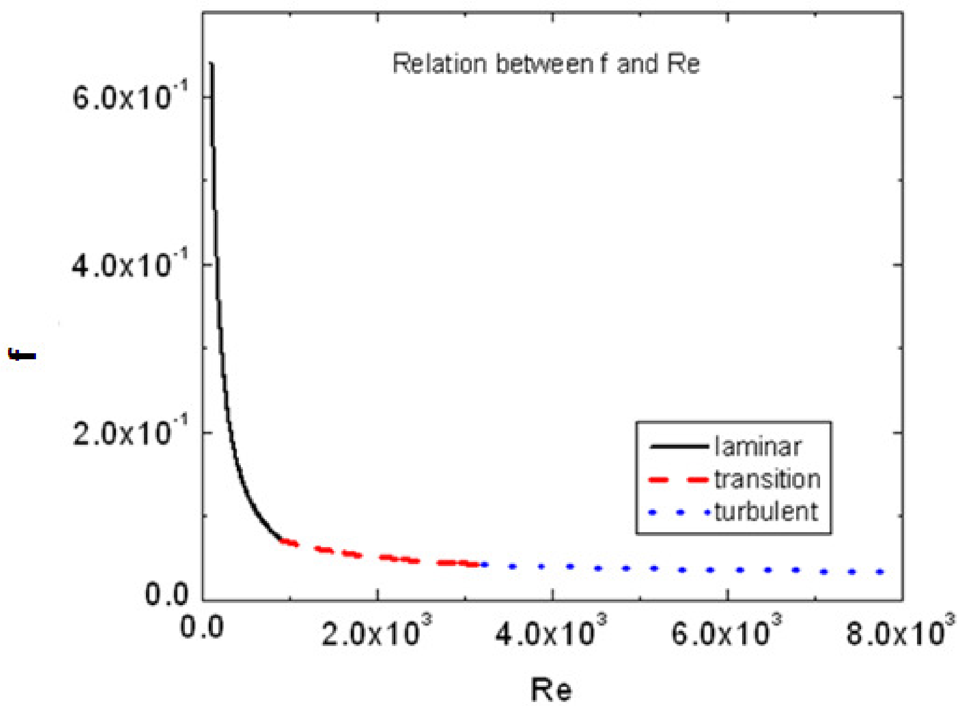

Figure 4.5: Friction coefficient for laminar, transition and turbulent regimes

These criteria actually cause the change from laminar to transition region to occur at Re=898 and change from transition to turbulent region to occur at Re=3196. These are considered appropriate for numerical solution where avoidance of numerical instability while switching friction law is the primary concern. ***Figure 4.5*** shows a plot of f vs. Re for laminar, transition and turbulent flow regimes with the above transition criteria. As expected, there is no discontinuity in the plots of these equations. Similarly, the same friction laws can be used in Eq. (4.11) to obtain the steady state flow equation for fully laminar, fully transition and fully turbulent loop as below.

$$\mathrm{Re} = 0.1768\left[\frac{Gr_m}{N_G}\right]^{0.5} \text{ fully laminar loop} \tag{4.21 a}$$

$$\mathrm{Re} = 1.216\left[\frac{Gr_m}{N_G}\right]^{0.387} \text{ fully transition loop} \tag{4.21 b}$$

$$\mathrm{Re} = 1.956\left[\frac{Gr_m}{N_G}\right]^{0.364} \text{ fully turbulent loop} \tag{4.21 c}$$

Plots of these three equations are given in ***Figure 4.6***. In this figure, the three equations mentioned above have been plotted neglecting property variation so that N_G=L_t/D. As expected smooth transitions has been observed while switching flow regimes in all the three cases. In addition, Eq. (4.12) and Eq. (4.17) has been used for calculating N_G where the three and two region models have been used respectively with variation of viscosity with temperature and plotted in the same figure. Between the plots of Eq. (4.12) and Eq. (4.17), practically no difference is found indicating that a two-region model is adequate. A marginal difference is observed with plots of Eq. (4.21) with maximum deviation of 7%.

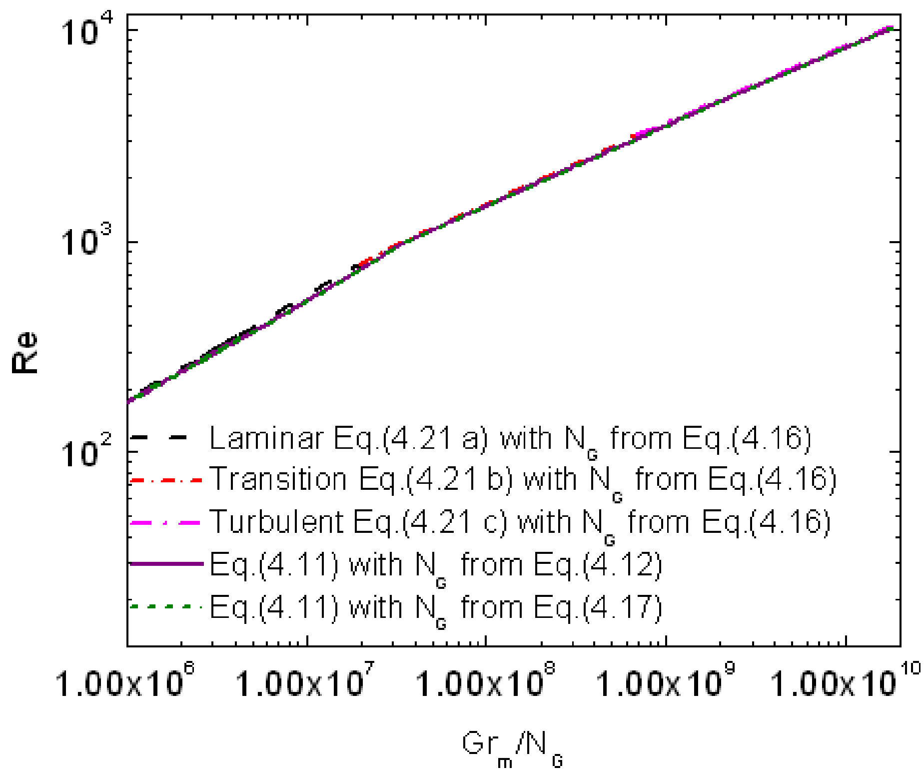

Figure 4.6: Dimensionless flow for laminar, transition and turbulent regimes

4.5. Results and discussion

4.5.1 Comparison with experimental data

Having finalized the friction laws for the laminar, transition and turbulent zone we are in a position to compare the prediction of Eq. (4.21) (where N_G has been estimated by using Eq. (4.17)) with the test data generated in the loop shown in ***Figure 3.1a*** and ***b***.

As mentioned above for a uniform diameter loop, it is possible that the hot leg can be in transition/turbulent flow with the cold leg in laminar /transition flow regime. For using the proposed equation (as given in Eq. (4.21)), Reynolds number at hot leg and cold leg has been calculated (assuming point heat source and point heat sink and the corresponding hot and cold leg lengths are given in Table-4.2) from the steady state data generated in the experiment. Depending upon the value of Reynolds number prevailing in hot and cold legs different friction laws (i.e. $0 < Re \leq 898$ for laminar, $898 \leq Re \leq 3196$ for transition and $Re \geq 3196$ for turbulent) has been used in Eq. (4.21) and the resulting plot is given in ***Figure 4.7*** with the estimated experimental error bar (Using the accuracy in measurement of power and temperature as given in section 3.1, the maximum error in the estimation of mass flow rate by heat balance is estimated as ±5%, ±4%, ±3% and ±4% for HHHC, HHVC, VHHC and VHVC respectively). The steady state equation derived above has been validated with the steady state natural circulation data generated for various orientations of the heater and cooler in the present loop. It has been observed from ***Figure 4.7*** that the calculated Re by using the proposed correlation is showing good agreement with the experimental data. The entire data generated in the present experiments are compared with the present correlation in ***Figure 4.8***.

Table-4.2: Hot and cold leg lengths for the different orientations of the test loop

Orientation	L_1/L_t	L_3/L_t
HHHC	0.5	0.5
HHVC	0.3	0.7
VHHC	0.7	0.3
VHVC	0.5	0.5

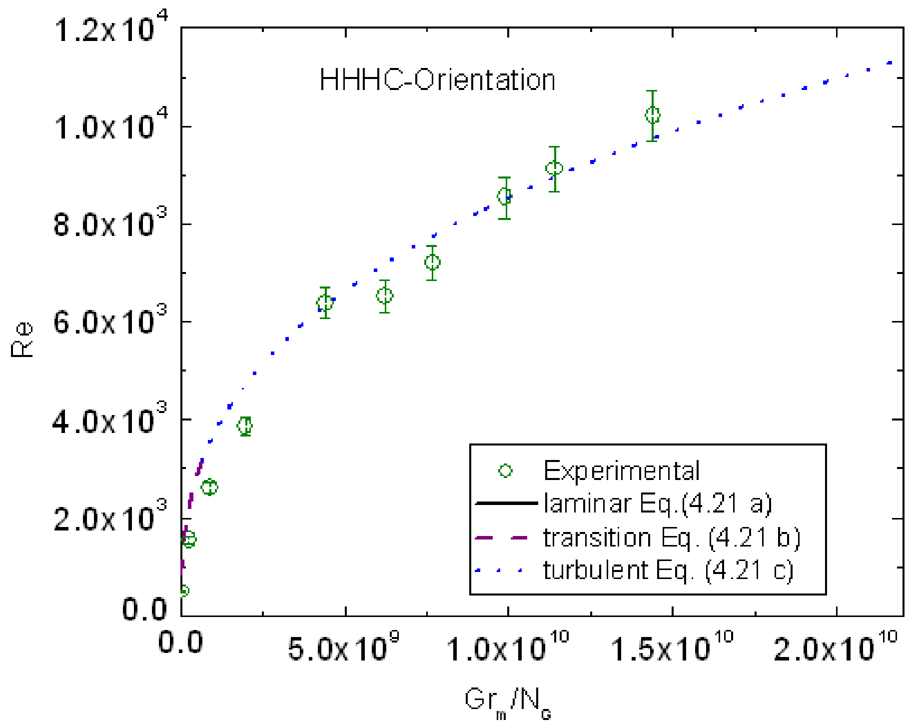

(a) HHHC-Orientation

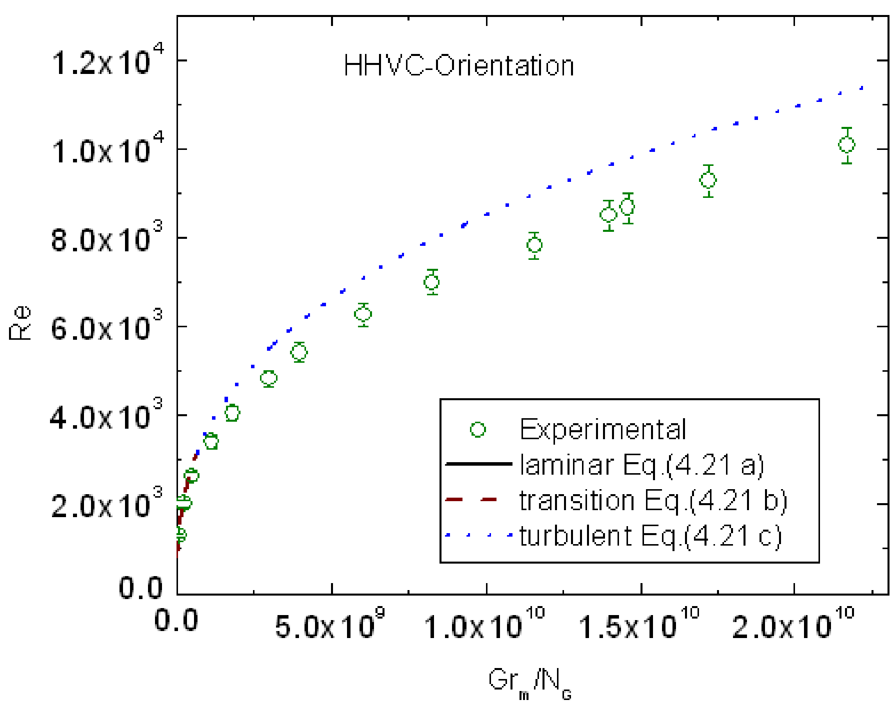

(b) HHVC-Orientation

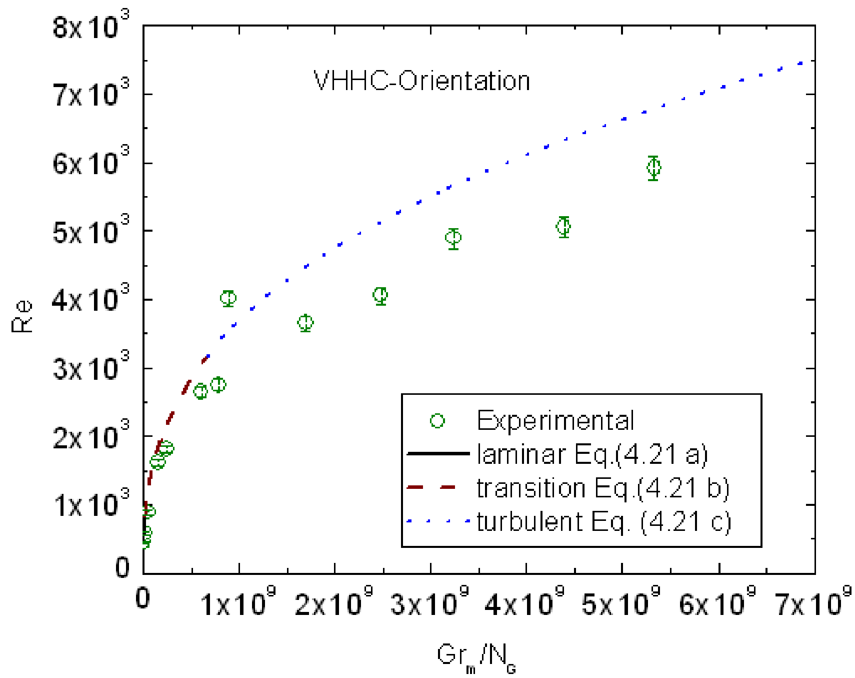

(c) VHHC-Orientation

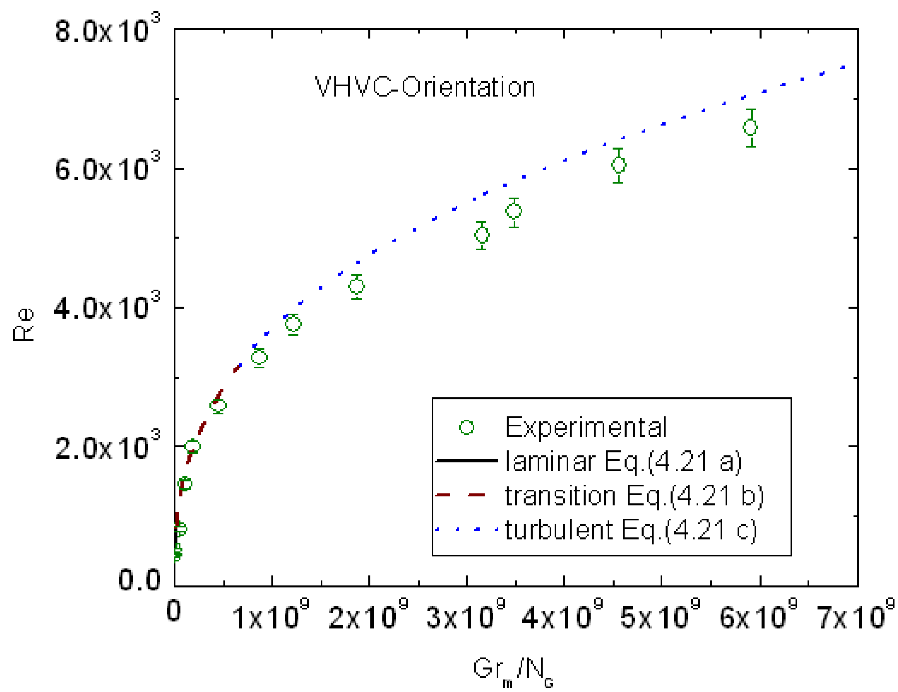

(d) VHVC-Orientation

Figure 4.7: Comparison of test data with proposed equation

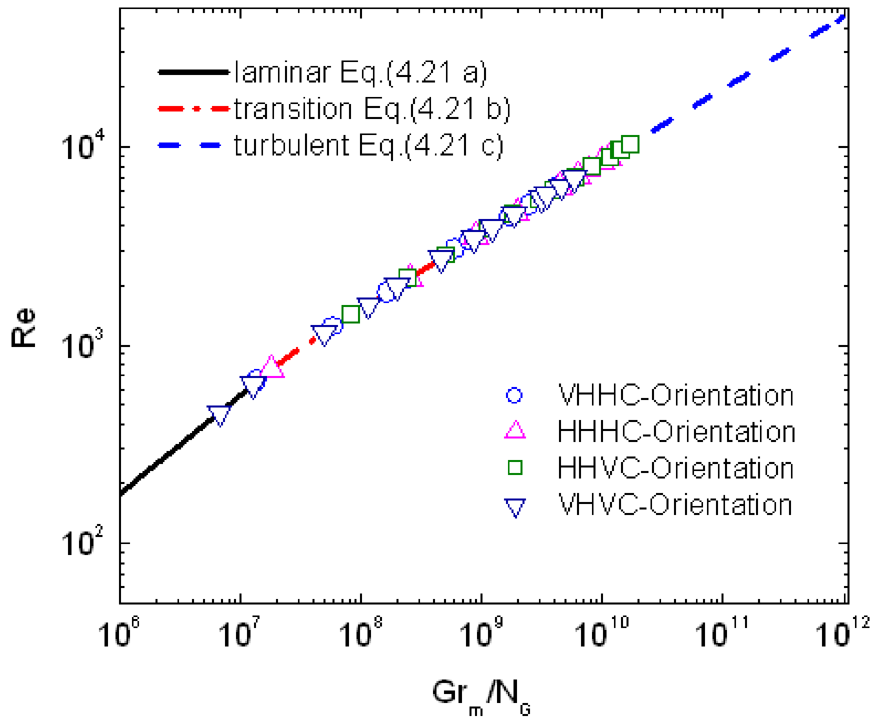

Figure 4.8: Steady state data for all four orientations

4.5.2 Comparison with Literature data

Single-phase natural circulation experiments have been reported by a large number of researchers [Hamilton et al. (1954), Alstad (1955), Bau and Torrance (1981), Huang and Zelaya (1988), Vijayan et al. (2000), Dubey et al. (2004), Bodkha (2009), Misale and Garibaldi (2010)]. However, in many cases, [Bau and Torrance (1981), Misale and Garibaldi (2010)] the data on hot leg and cold leg temperatures are not reported. For the validation of the steady state flow equation presented in this chapter, usable data could be found only in references [Hamilton et al. (1954), Alstad (1955), Huang and Zelaya (1988), Vijayan et al. (2000), Dubey et al. (2004), Bodkha (2009)]. The entire data from literature including the present experimental data where N_G has been calculated using Eq. (4.17) is compared in ***Figure 4.9.***

From the ***Figure 4.9***, it has been observed that the data falling in the transition region is very close to the proposed correlation. As shown in ***Figure 4.6***, the maximum deviation between Eq. (4.21) (single region model with constant properties) and the two or three region models are only 7%. Thus, Eq. (4.21) is adequate for most practical situations. The advantage of Eq. (4.21) is that N_G can be calculated as L_t/D and all the reported data on single-phase natural circulation can be utilized for its validation. ***Figure 4.10*** compares the data available in the literature [Vijayan et al. (2008), Nishihara (1997), Bau and Torrance (1981), Misale et al. (2007), Mousavian et al. (2004), Ho et al. (1997), Holman and Boggs (1960), Misale et al. (1991), Ambrosini et al. (2009)] (where N_G has been calculated using Eq. (4.16)) along with all the data plotted in ***Figure 4.9.***

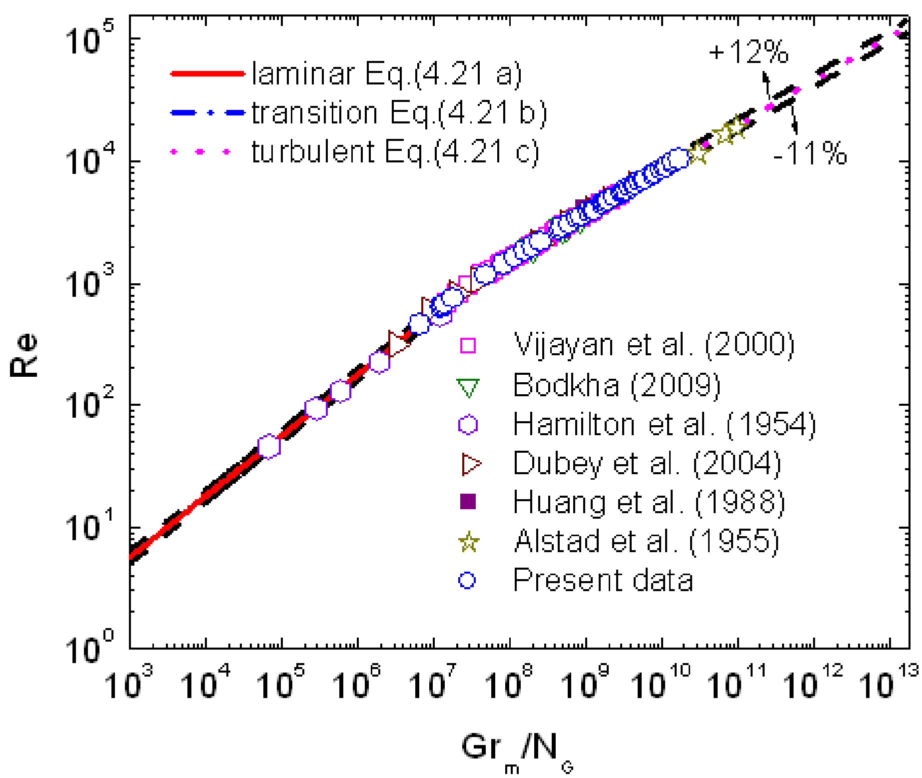

Figure 4.9: Steady state data for uniform diameter loops including present and literature data considering viscosity variation

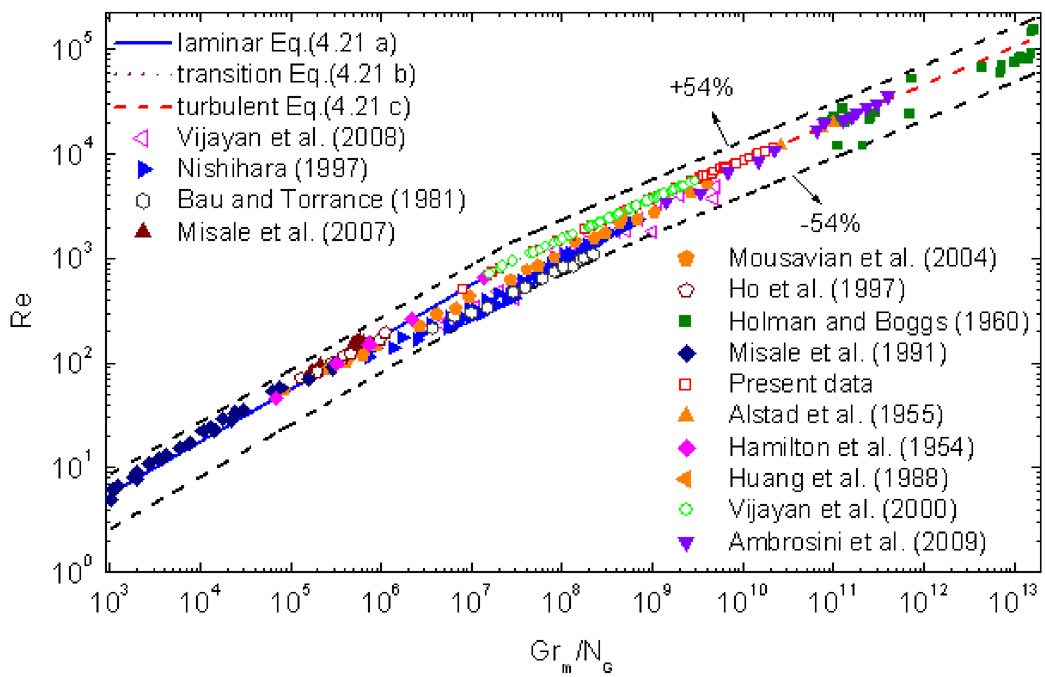

Figure 4.10: Steady state data for uniform diameter loops including present and literature data neglecting viscosity variation

It is observed from ***Figure 4.10*** that by using Eq. (4.21) the agreement with the proposed correlation is reasonable (approximately within ±54%). Considering the variation of viscosity with temperature the prediction accuracy can be significantly improved (within±12%) as shown in ***Figure 4.9***.

4.6 Stability Analysis

Equation (4.11) enables us to calculate the steady state flow in a Natural Circulation Loop (NCL). However, using the steady state flow equation it is difficult to ascertain whether that particular steady state is stable or not. Therefore, linear or non- linear stability analysis is required to perform. As mentioned earlier, since non-linear method involves tedious computations, linear stability analysis provides the best route to generate a stability map. In the linear stability method, for obtaining the characteristic equation for stability parameter, governing equations are perturbed over the steady state and the perturbed governing equations are linearised. Roots of this equation can be obtained using Nyquist criterion. In most of the published literature, the results of the linear stability analysis have been given in dimensionless form. Usually the stability map in dimensionless form is plotted as a function of modified Grashof number, modified Stanton number and L_t/D for a specified geometry of the loop. However, conditions like, when the Grashof number is very high, it becomes difficult to ascertain whether the system remains in single-phase condition. For this reason, a computer code LISA (LInear Stability Analysis) has been developed to carry out the steady state and linear stability analysis of a single-phase natural circulation loop in dimensional form.

The geometry and co-ordinate system considered for the stability analysis is shown in ***Figure 4.11***. In the linear stability method, the steady state flow and temperature are perturbed by an infinitesimal amount as below

$$T = T_{ss} + T' \quad and \quad W = W_{ss} + W' \tag{4.22}$$

where T' and W' are small perturbations over the steady state values. Substituting these in Eq. (4.2), the perturbed momentum equation after linearizing can be written as

$$\frac{dW^{'}}{dt}=\frac{g\rho_0\beta A}{L_t}\oint T^{'}dz+\frac{(2-b)p\mu^{b}W_{ss}^{(1-b)}W^{'}}{2D^{1+b}\rho_0 A^{1-b}} \tag{4.23}$$

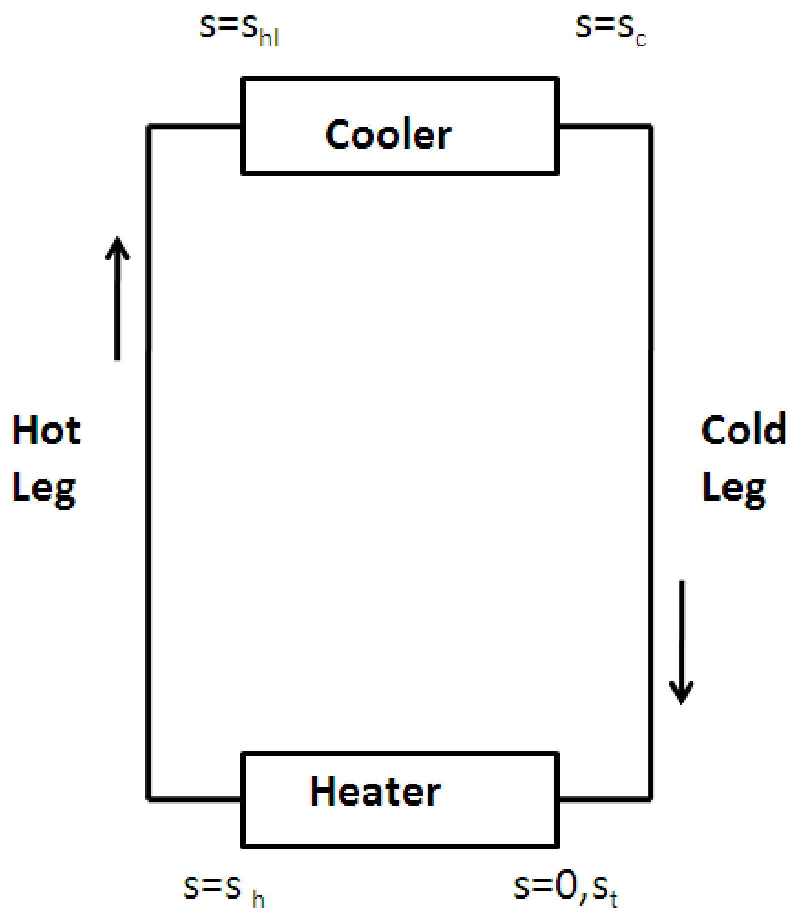

Figure 4.11: Loop geometry and co-ordinates for HHHC orientation

Similarly, the perturbed energy equations for the different segments of the loop can be written as

$$\frac{\partial T^{'}}{\partial t}+\frac{W_{ss}}{\rho_0 A}\frac{\partial T^{'}}{\partial s}+\frac{W^{'}}{\rho_0 A}\left(\frac{q_h P}{W_{ss}Cp}\right)=0 \qquad \text{heater} \quad 0<s\le s_h \tag{4.24}$$

$$\frac{\partial T'}{\partial t}+\frac{W_{ss}}{\rho_0 A}\frac{\partial T'}{\partial s}=0 \qquad \text{pipes } s_h < s \le s_{hl} \quad and \ s_c < s \le s_t \qquad (4.25)$$

$$\frac{\partial T'}{\partial t}+\frac{W_{ss}}{\rho_0 A}\frac{\partial T'}{\partial s}+\frac{UP}{\rho_0 ACp}\left[T'-\frac{W'}{W_{ss}}\left(T_{ss}-T_s\right)\right]=0 \quad \text{cooler } s_{hl} < s \le s_c \qquad (4.26)$$

The small perturbations T′ and W′ can be expressed as

$$T'=\overline{T}(s)\varepsilon e^{\sigma t} \text{ and } W'=\overline{W}\varepsilon e^{\sigma t} \qquad (4.27)$$

So that $\dfrac{\partial T'}{\partial t}=\overline{T}(s)\varepsilon e^{\sigma t}\sigma$ (4.28)

$$\frac{\partial T'}{\partial s}=\frac{\partial \overline{T}(s)}{\partial s}\varepsilon e^{\sigma t} \qquad (4.29)$$

Where ε is a small quantity and σ is the stability parameter, which is a complex number.

Substituting Eq. (4.27-4.29), the momentum equation [i.e. Eq. (4.23)] can be written as

$$F(\sigma) = \sigma\overline{W} - \frac{g\rho_0\beta A}{L_t}\oint\overline{T}(s)dz + \frac{(2-b)p\mu^b W_{ss}^{1-b}\overline{W}}{2D^{1+b}\rho_0 A^{1-b}} = 0 \qquad (4.30)$$

Similarly substituting T′ and W′ in the energy equations and solving the resulting equation, the following equation can be obtained for the heater

$$\overline{T}(s) = \frac{q_h P\overline{W}}{\rho_0 A W_{ss} Cp\sigma}\left[e^{-\frac{\rho_0 As\sigma}{W_{ss}}} - 1\right] + \overline{T_{cl}}e^{-\frac{\rho_0 As\sigma}{W_{ss}}} \qquad (4.31)$$

Where the boundary condition that at s=0, $\overline{T}(s) = \overline{T_{cl}}$, has been used. Similarly, one can obtain the following equation for hot leg

$$\overline{T}(s) = \overline{T_h}\, e^{\frac{\rho_0 A\sigma(s_h - s)}{W_{ss}}} \qquad \text{for } s_h < s \le s_{hl} \qquad (4.32)$$

Where the boundary condition that at s=s$_h$, $\overline{T}(s) = \overline{T_h}$ has been used to eliminate the integration constant.

Similarly, the equation for cold leg is obtained as

$$\overline{T}(s) = \overline{T_c}\, e^{\frac{\rho_0 A \sigma (s_c - s)}{W_{ss}}} \qquad \text{for } s_c < s \le s_t \tag{4.33}$$

Where the boundary condition that at s=s_c, $\overline{T}(s) = \overline{T_c}$ has been used. Equation for the cooler is obtained as

$$\overline{T}(s) = \frac{\overline{W} UP\left[(T_{hl})_{ss} - T_s\right]}{\rho_0 A C_p \sigma}\left[e^{\frac{UP(s_{hl}-s)}{W_{ss}}} - e^{\frac{\rho_0 A (s_{hl}-s)}{W_{ss}}\left(\sigma + \frac{UP}{\rho_0 A C_p}\right)}\right] + \overline{T_{hl}}\, e^{\frac{\rho_0 A (s_{hl}-s)\left(\sigma + \frac{UP}{\rho_0 A C_p}\right)}{W_{ss}}} \tag{4.34}$$

valid for $s_{hl} < s \le s_c$. Where $(T_{hl})_{ss}$ is given by

$$(T_{hl})_{ss} = T_s + \frac{q_h P s_h}{W_{ss} Cp}\left[\frac{1}{1 - e^{\frac{UP(s_{hl} - s_c)}{W_{ss} Cp}}}\right] \tag{4.35}$$

Using these, the integral in the momentum equation can be evaluated as

$$\oint \overline{T}(s)dz = \frac{\dot{W}_{ss}}{\rho_0 A\sigma}\left[\left(\overline{T}_h - \overline{T}_c\right) + \{\overline{T}_c e^{\frac{\rho_0 A\sigma(s_c - s_t)}{\dot{W}_{ss}}} - \overline{T}_h e^{\frac{\rho_0 A\sigma(s_h - s_{hl})}{\dot{W}_{ss}}}\}\right] \tag{4.36}$$

Where $$\overline{T_h} = \overline{T_{cl}}\, e^{-\frac{\rho_0 A\sigma s_h}{W_{ss}}} + \frac{\overline{W} q_h P}{\rho_0 A\sigma Cp W_{ss}}\left[e^{-\frac{\rho_0 A\sigma s_h}{W_{ss}}} - 1\right] \tag{4.37}$$

and

$$\overline{T_c} = \frac{\overline{W} UP\left[(T_{hl})_{ss} - T_s\right]}{\rho_0 A\sigma W_{ss} Cp}\left[e^{\frac{UP(s_{hl}-s_c)}{W_{ss}Cp}} - e^{\frac{\rho_0 A\left(\sigma + \frac{UP}{\rho_0 ACp}\right)(s_{hl}-s_c)}{W_{ss}}}\right] + \overline{T_{cl}}\, e^{\frac{\rho_0 A\left[-\sigma s_c + \frac{UP}{\rho_0 ACp}(s_{hl}-s_c)\right]}{W_{ss}}}$$
$$+ \frac{\overline{W} q_h P}{\rho_0 A\sigma Cp W_{ss}}\left[e^{\frac{\rho_0 A\left\{-\sigma s_c + \frac{UP}{\rho_0 ACp}(s_{hl}-s_c)\right\}}{W_{ss}}} - e^{\frac{\rho_0 A\left\{\sigma(s_h - s_c) + \frac{UP}{\rho_0 ACp}(s_{hl}-s_c)\right\}}{W_{ss}}}\right] \tag{4.38}$$

$$\overline{T_{cl}} = \frac{X + Y}{1 - e^{\frac{\rho_0 A\left\{-\sigma s_t + \frac{UP}{\rho_0 ACp}(s_{hl}-s_c)\right\}}{W_{ss}}}} \tag{4.39}$$

Where

$$X = \frac{\overline{W} UP\left[(T_{hl})_{ss} - T_s\right]}{\rho_0 A\sigma Cp W_{ss}}\left[e^{\frac{\rho_0 A\left\{\sigma(s_c - s_t) + \frac{UP}{\rho_0 ACp}(s_{hl}-s_c)\right\}}{W_{ss}}} - e^{\frac{\rho_0 A\left\{\sigma(s_{hl} - s_t) + \frac{UP}{\rho_0 ACp}(s_{hl}-s_c)\right\}}{W_{ss}}}\right] \tag{4.40}$$

$$Y = \frac{\overline{W} q_h P}{\rho_0 A \sigma Cp W_{ss}} \left[e^{\frac{\rho_0 A \left\{ -\sigma s_t + \frac{UP}{\rho_0 ACp}(s_{hl} - s_c) \right\}}{W_{ss}}} - e^{\frac{\rho_0 A \left\{ \sigma (s_h - s_t) + \frac{UP}{\rho_0 ACp}(s_{hl} - s_c) \right\}}{W_{ss}}} \right] \tag{4.41}$$

for the HHHC orientation. The roots of the characteristic equation [i.e. Eq. (4.30)] were found with the help of Regula-Falsi method. Nyquist plots were also made as shown in ***Figure 4.12*** for a few cases, which confirmed the code predictions.

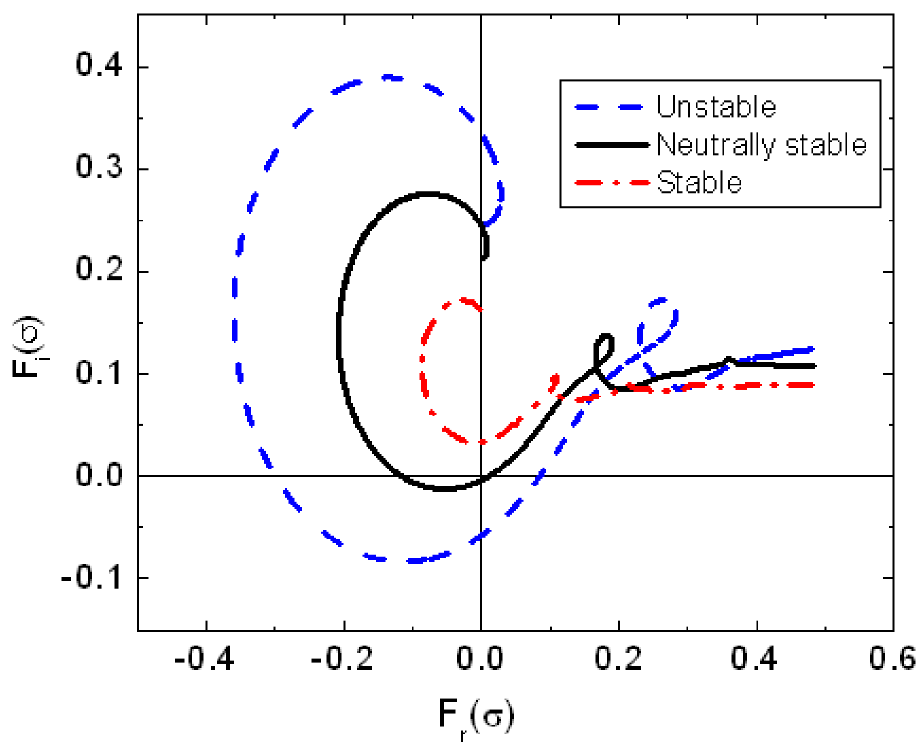

Figure 4.12: Nyquist plot

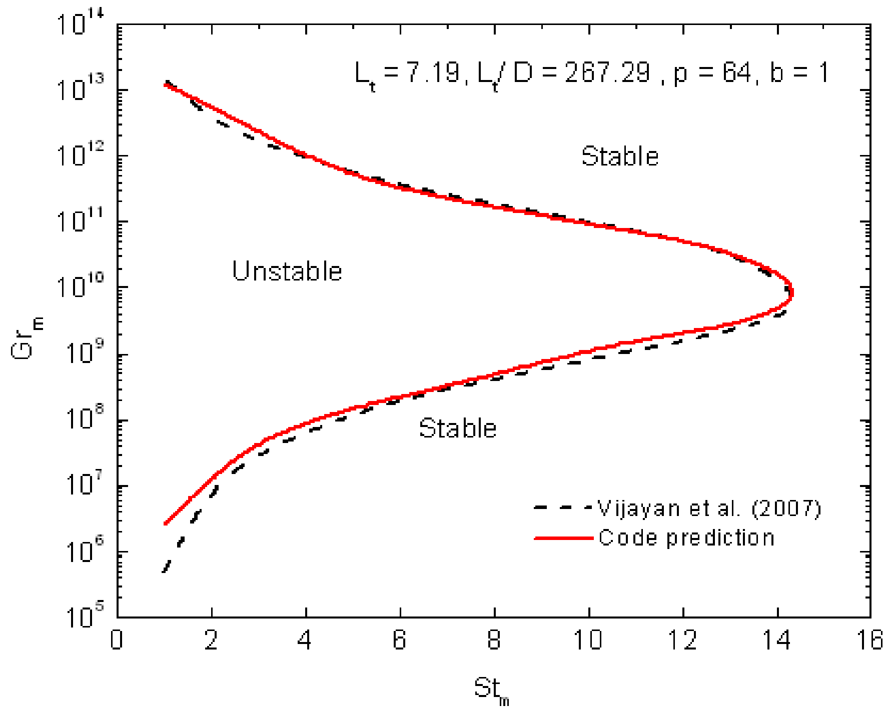

Figure 4.13 a: Stability map for laminar flow (code validation)

The stability map (i.e. the locus of neutrally stable points) predicted for laminar and turbulent flow reported in [Vijayan et al. (2007)] is reproduced in ***Figure 4.13 a*** and **b** using LISA code. As can be seen, LISA code is found to adequately predict the stability threshold. However, for the upper threshold in turbulent flow, the LISA code predicts always unstable operation right up to the critical point. Ambrosini et al. (2004) also predicted using Churchill friction law and friction law suggested by Vijayan et al. and found that the flow is fully unstable in turbulent zone.

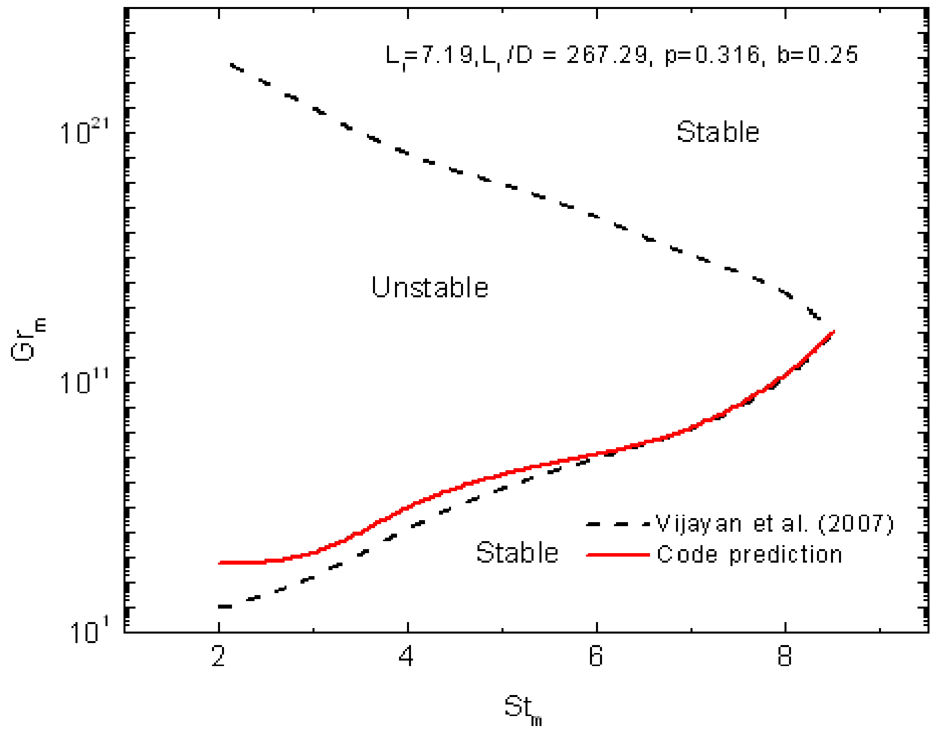

Figure 4.13 b: Stability map for turbulent flow (code validation)

However, in the laminar flow stability map (***Figure 4.13 a***), the flow is not really laminar beyond a Gr_m value of 6.9E+9 (for Re=898). Likewise, in the turbulent flow stability map (***Figure 4.13 b***) the flow is not turbulent below a Gr_m value of 1.8E+11(for Re=3196). Therefore, these stability maps do not represent the true stability map of a single-phase rectangular natural circulation loop.

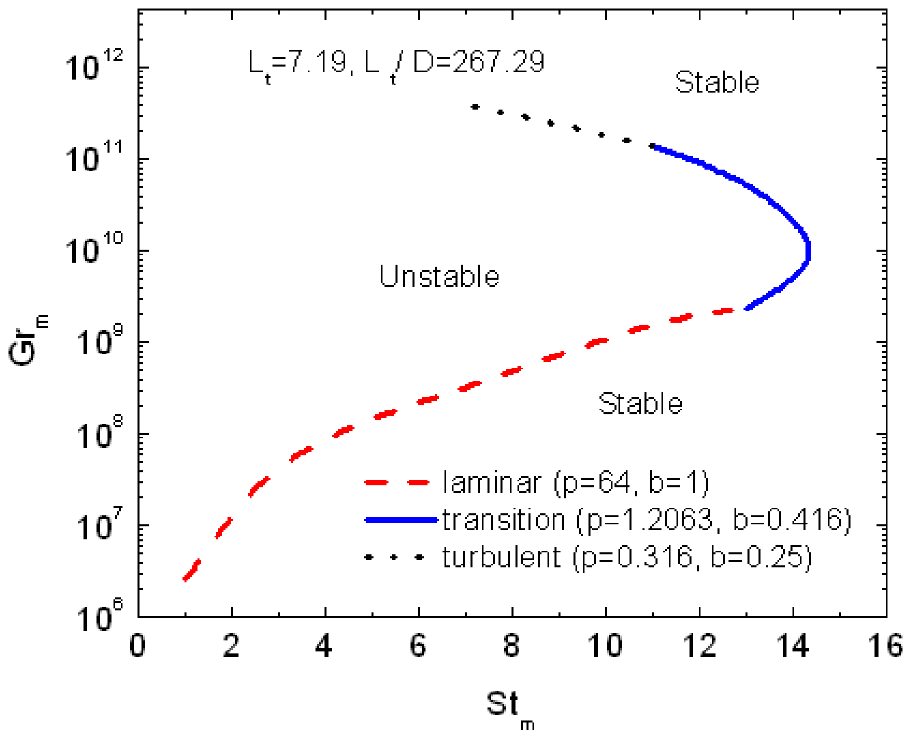

Figure 4.13 c: True stability map for laminar, transition and turbulent flow regimes

In the present work the true stability map is generated which is valid for laminar, transition and turbulent flow regimes (see ***Figure 4.13 c***). In the present analysis, the upper stable zone of the stability map has not been found in the subcritical region for St_m< 7 for turbulent flow.

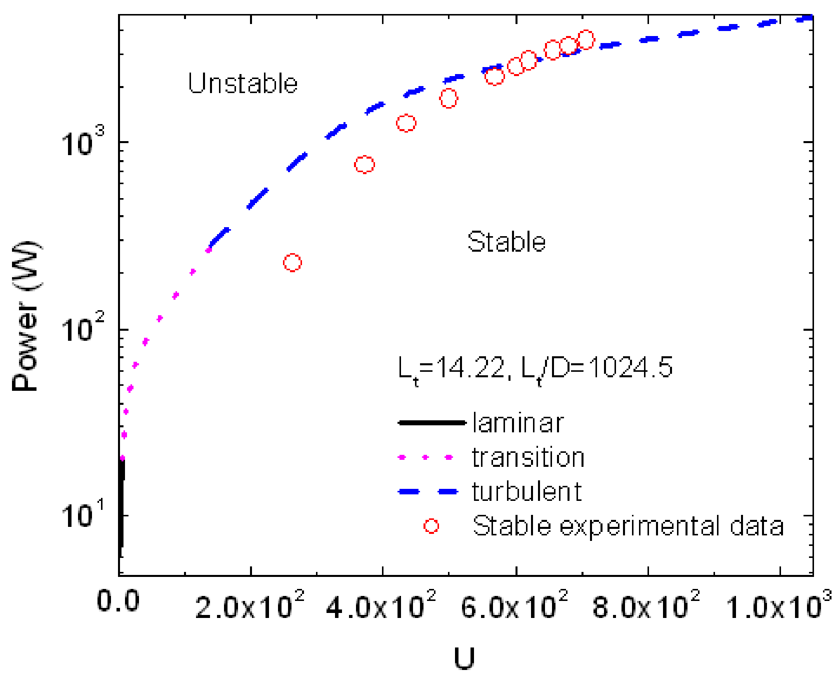

Figure 4.13d: True stability map for present loop (in dimensional form)

Also for the present test loop, a stability map is generated in dimensional form (***Figure 4.13 d***). It has been observed from the ***Figure 4.13 d*** that a few stable experimental data fall in the unstable region. Similar observations are reported by Garibaldi. This can be attributed to the simplifying assumptions made in the linear stability analysis. For example, heat loss, wall effects, local pressure losses and multidimensional effects have not been considered. In this context, it may also be noted that the analysis by Misale et al. (1999) showed that the wall effects play a significant role on stability of single-phase natural circulation.

4.7 Closure

A generalized equation for the steady state flow in single-phase natural circulation loops was derived based on 1-dimensional theory by assuming the loop is partly in laminar and partly in transition or turbulent flow. The derived dimensionless flow equation is applicable for any loop obeying multiple friction laws. The generalized flow equation was tested with the experimental data generated in a uniform diameter rectangular loop for all four orientations such as, Horizontal Heater and Horizontal Cooler (HHHC), Horizontal Heater and Vertical Cooler (HHVC), Vertical Heater and Horizontal Cooler (VHHC) and Vertical Heater and Vertical Cooler (VHVC). From the above, it is observed that the same generalized correlation is applicable for all the four orientations of heater and cooler tested. Data reported in the literature is also showing good agreement with the generalized equation developed.

The stability code LISA based on linear stability analysis methodology has been validated with previously reported stability map for both laminar and turbulent flows. Subsequently a stability map valid for laminar, transition and turbulent regions has been obtained using the LISA code for the same loop. The results showed that there is no stable zone in the subcritical region for $St_m < 7$ for turbulent flow for the loop considered in this study. Also by considering the various effects such as heat loss, wall effects, local pressure losses and multidimensional effects the prediction can be improved.

CHAPTER-5

STEADY STATE FLOW AND STATIC INSTABILITY OF SUPERCRITICAL NATURAL CIRCULATION LOOPS

5.1 Introduction

For thermodynamically supercritical loops, explicit correlation for steady state natural circulation flow is not available. While using the subcritical natural circulation flow equation for supercritical data, it was not able to predict the steady state flow accurately near pseudo critical point. A generalized correlation has been proposed to estimate the steady state flow in supercritical natural circulation loops based on a relationship between dimensionless density and dimensionless enthalpy reported in literature.

Sharp change of fluid properties such as density in the critical region gives rise to instability concerns. The instability could be either density wave type or excursive type (Ledinegg or static instability). Several previous researchers have studied density wave type instability in supercritical natural circulation loops whereas excursive instability is not studied in detail. In the present chapter, therefore, an analysis has been carried out to predict the threshold of excursive instability for both supercritical water and supercritical CO_2.

5.2 Derivation of the generalized flow equation for supercritical fluid

A uniform diameter rectangular loop having horizontal heater and horizontal cooler connected by adiabatic pipes as shown in ***Figure 5.1*** has been considered. In 1-dimensional flow, the only coordinate ‘s’ runs around the loop with origin at the inlet of the heater as shown in ***Figure 5.1***.

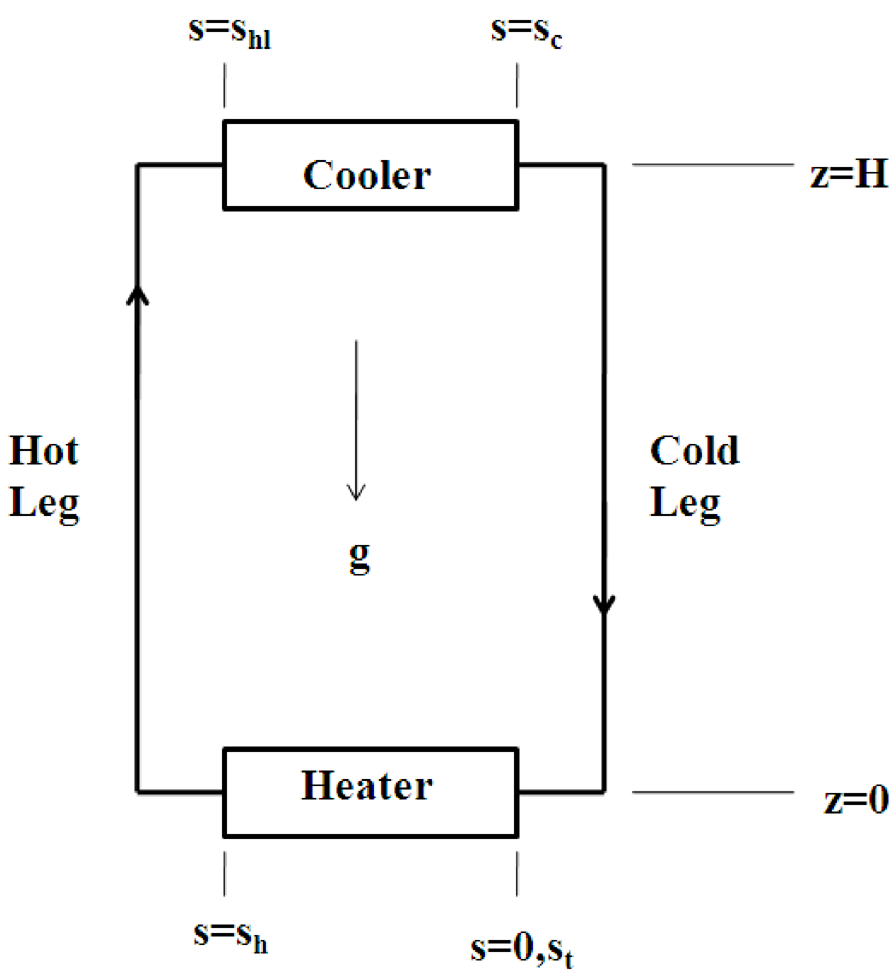

Figure 5.1: Loop geometry and co-ordinates considered for analysis

Assuming 1-dimensional flow with negligible viscous dissipation and axial conduction effects, the governing equations for mass, momentum and energy conservation for a supercritical natural circulation loop in terms of the mass flow rate, W, can be written as

$$\frac{\partial \rho}{\partial t}+\frac{1}{A}\frac{\partial W}{\partial s}=0 \tag{5.1}$$

$$\frac{1}{A}\frac{\partial W}{\partial t}+\frac{1}{A^2}\frac{\partial}{\partial s}\left(\frac{W^2}{\rho}\right)=-\frac{\partial P}{\partial s}-\rho\, g\sin\theta-\frac{fW^2}{2D\rho A^2}-\frac{KW^2}{2\rho A^2 L_t} \tag{5.2}$$

$$\frac{\partial(\rho h)}{\partial t}+\frac{1}{A}\frac{\partial(Wh)}{\partial s}=\begin{cases}\dfrac{q_h P}{A} & \text{(for heater)}\\ 0 & \text{(for pipes)}\\ -\dfrac{q_c P}{A} & \text{(for cooler)}\end{cases} \tag{5.3}$$

In writing the energy equation, a uniform heat flux is assumed for both heater and the cooler. At steady state, the mass conservation equation can be written as

$$\frac{dW}{ds}=0 \tag{5.4}$$

Which means the mass flow rate is independent of the locations in the loop. Integrating the momentum equation around the closed loop yields

$$\frac{L_t}{A}\frac{dW}{dt}+\frac{1}{A^2}\oint d\left(W^2 v\right)=-\oint dP-g\oint \rho dz-\frac{fW^2L_t}{2D\rho A^2}-\frac{KW^2}{2\rho A^2} \tag{5.5}$$

Where z is the elevation and is given by dz=ds sinθ and $v=\frac{1}{\rho}$. Noting that at steady state, the mass flow rate W is a constant, $\oint \partial v=0$ and $\oint \partial p=0$ for a closed loop and we obtain

$$g\oint \rho dz+\frac{fW^2L_t}{2D\rho A^2}+\frac{KW^2}{2\rho A^2}=0 \tag{5.6}$$

The above equation is valid for uniform diameter loops. However, most practical applications of natural circulation such as nuclear reactor loop, solar water heater etc. employ non-uniform diameter loops. Therefore, Eq. (5.6) has been modified to take care of area variations as

$$g\oint \rho dz+\frac{W^2}{2\rho}\sum_{i=1}^{N}\left(\frac{f_iL_i}{D_i}+K_i\right)\frac{1}{A_i^2}=0 \tag{5.7}$$

The steady state energy equation is given by

$$\frac{W}{A}\frac{dh}{ds} = \begin{cases} \dfrac{q_h P_h}{A_h} \\ 0 \\ -\dfrac{q_c P_c}{A_c} \end{cases} \tag{5.8}$$

For uniform diameter loop, $A_h=A_c=A$. It is also possible to absorb the local pressure loss coefficient into an equivalent length L_{ei} such that $K_i = \frac{f_i L_{ei}}{D_i}$. With this, the momentum equation can be written as

$$g\oint \rho dz + \frac{W^2}{2\rho}\sum_{i=1}^{N}\left(\frac{fL_{eff}}{DA^2}\right)_i = 0 \tag{5.9}$$

Ambrosini and Sharabi (2008) found that if dimensionless density ρ* is plotted as a function of dimensionless enthalpy h* for various supercritical fluids, then they collapse into a unique curve as shown in ***Figure 5.2*** where ρ*and h* are defined as

$$\rho^* = \frac{\rho}{\rho_{pc}}; h^* = \beta_{pc}\left(h - h_{pc}\right); \beta_{pc} = \frac{1}{v}\left(\frac{\partial v}{\partial h}\right)_{pc} \tag{5.10}$$

The interesting fact about this relationship is that it is almost independent of the system pressure as shown in ***Figure 5.2*** and applicable for different supercritical fluids. Besides the pseudo critical point (ρ*=1.0 and h*=0) for different fluids correspond to unique points on the ρ* versus h* plot. Only the fluids considered in the present study are plotted in ***Figure 5.2***. However, Ambrosini and Sharabi have considered a few other fluids like ammonia. From ***Figure 5.2***, it is observed that the curves for different fluids superimpose almost exactly from the pseudo critical point all along the supercritical region (lighter fluid region). A slight deviation is shown only in the subcritical region up to h*= -0.7 (heavier fluid region) and this has been reported by Ambrosini and Sharabi (2008).

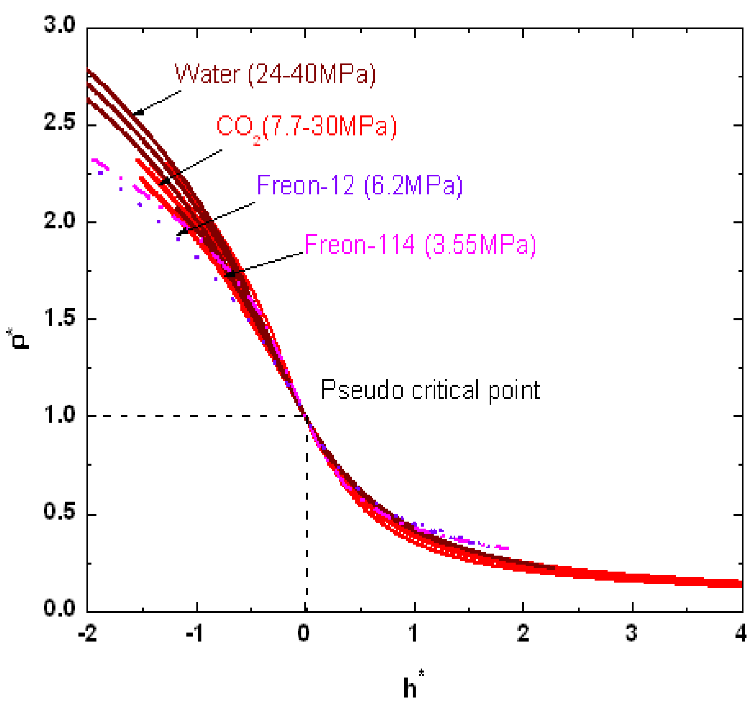

Figure 5.2: Comparison of dimensionless density as function of dimensionless enthalpy for CO_2, Water, Freon-12 and Freon-114

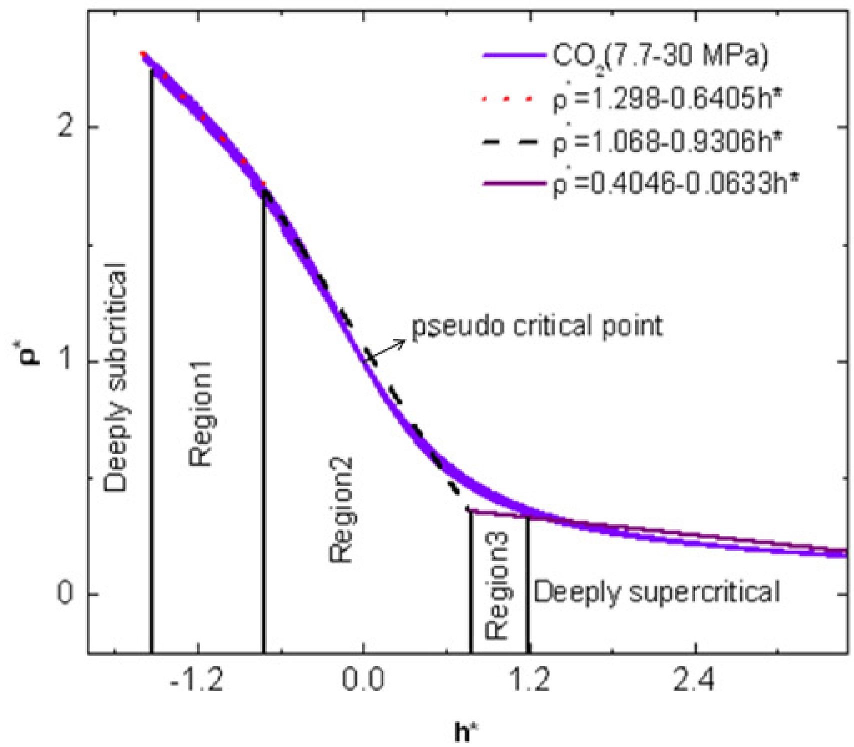

Figure 5.3: Three-region model

The graphical relationship between ρ* and h* provided by Ambrosini and Sharabi can be mathematically fitted into different relationships depending on the accuracy required. For obtaining more accurate prediction in both heavier (subcritical) as well as lighter (supercritical) regions, CO_2 properties alone (***Figure 5.3***) has been considered for finding out the relationship between dimensionless density and dimensionless enthalpy. Also in ***Figure 5.3*** the range of h* considered is quite large compared to the range of h* for the present experimental data.

(a) Sigmoidal relationship

The relationship between ρ^* and h^* can be approximated by a sigmoidal curve. The equation of the sigmoidal curve is given by

$$\rho^* = A + \frac{B}{1 + e^{(1.5181h^* + 0.5689)}} \tag{5.11}$$

Where, A=0.15704 and B=2.4785. It is possible to integrate numerically the momentum equation (Eq. (5.7)) with the above relation to obtain an accurate prediction of steady state flow rate. However, with the sigmoidal relationship an explicit equation for flow rate is difficult to obtain whereas it is possible with linear relation between ρ^* and h^*.

(b) Linear relationship

The simplest relationship between ρ^* and h^* is straight lines. One can use a single, two or three lines to fit the data. A single line for the entire region is a poor fit but offers considerable simplification for calculating natural circulation flow rates. Three lines give a reasonable fit for CO_2 data while the accuracy of two lines is in between one and three line fits. Therefore, three-region model (see ***Figure 5.3***) has been considered for the present analysis.

Linear equation fitted to these three regions is of the form

$$\rho^* = C_1 - C_2 h^* \tag{5.12}$$

Where, the values of the constants C_1 and C_2 for the three regions are

C_1=1.298 and C_2=0.6405 for Region 1 (5.13a)

C_1=1.068 and C_2=0.9306 for Region 2 (5.13b)

C_1=0.4046 and C_2=0.0633 for Region 3 (5 13c)

In the present work, the boundary between region 1 and region 2 and between region 2 and region 3 was defined at h*= -0.7 and at h*=0.76 respectively.

Equation (5.7) can be written in terms of ρ* as

$$g\rho_{pc}\oint \rho^* dz + \frac{W^2}{2\rho}\sum_{i=1}^{N}\left(\frac{fL_{eff}}{DA^2}\right)_i = 0 \tag{5.14}$$

Substituting Eq. (5.12) into Eq. (5.14) and using the definition of h* given by Eq. (5.10), we obtain

$$g\rho_{pc}\beta_{pc}C_2\oint hdz = \frac{W^2}{2\rho_{pc}}\sum_{i=1}^{N}\left(\frac{fL_{eff}}{DA^2}\right)_i \tag{5.15}$$

Where ρ_{pc} is considered as the reference density. For non-dimensionalisation following substitutions are used

$$\omega = \frac{W}{W_{ss}}; \quad \mathcal{H} = \frac{\mathrm{h - h}_r}{\Delta h_{ss}}; \quad S = \frac{s}{H}; \quad Z = \frac{z}{H}; \quad a_i = \frac{A_i}{A_r}; \quad d_i = \frac{D_i}{D_r};$$
$$l_i = \frac{L_i}{L_t}; \quad \left(l_{eff}\right)_i = \frac{\left(L_{eff}\right)_i}{L_t}; \quad A_r = \frac{1}{L_t}\sum_{i=1}^{N} A_i L_i = \frac{V_t}{L_t}; \quad D_r = \frac{1}{L_t}\sum_{i=1}^{N} D_i L_i;$$
$$L_t = \sum_{i=1}^{N} L_i; \quad f_i = \frac{p}{\mathrm{Re}_i^b} = \frac{p\omega^{-b} a_i^b}{\mathrm{Re}_{ss}^b\, d_i^b}; \; h_r = h_{pc} \tag{5.16}$$

For uniform diameter loop A_r=A_i and D_r=D_i, the inside flow area and diameter respectively.

Noting that $\omega = 1$ at steady state, non-dimensional momentum and energy equation can be written as

$$g\rho_{pc}\beta_{pc}C_2 \mathrm{H}\Delta \mathrm{h}_{ss}\oint \mathcal{H}dZ = \frac{pW_{ss}^2}{2\rho_{pc}\,\mathrm{Re}_{ss}^b\, A_r^2} N_G \tag{5.17}$$

$$\text{Where, } \Delta h_{ss} = \frac{Q_h}{W_{ss}} \text{ and } N_G = \frac{L_t}{D_r}\sum_{i=1}^{N}\left(\frac{l_{eff}}{d^{1+b}a^{2-b}}\right)_i \tag{5.18}$$

For uniform diameter loop $N_G = \frac{L_t}{D_r}$ if local pressure losses are negligible.

$$\frac{d\mathcal{H}}{dS} = \begin{cases} \frac{a_h H}{L_t}\frac{V_t}{V_h} & \text{(for heater)} \\ 0 & \text{(for pipes)} \\ -\frac{a_c H}{L_t}\frac{V_t}{V_c} & \text{(for cooler)} \end{cases} \tag{5.19}$$

The steady state solution for the heater can be written as

$$\mathcal{H} = \frac{a_h H}{L_t}\frac{V_t}{V_h} s + \left(\mathcal{H}_{cl}\right)_{ss} \tag{5.20}$$

By setting s=s_h, Eq. (5.20) gives us

$$\left(\mathcal{H}_{hl}\right)_{ss} = 1 + \left(\mathcal{H}_{cl}\right)_{ss} \tag{5.21}$$

Similarly, steady state solution for cooler can be written as

$$\mathcal{H} = \frac{a_c H}{L_t}\frac{V_t}{V_h}\left(s_{hl} - s\right) + \mathcal{H}_{hl} \tag{5.22}$$

Using equations (5.20) - (5.22), the integral in Eq. (5.17) can be calculated as $\oint \mathcal{H} dZ = 1$. The above equation has been derived for a rectangular loop with horizontal heater and horizontal cooler. For other orientations of heater and cooler, the same result can be obtained by taking the centre line elevation difference between the cooler and heater (Δz) instead of the loop height without introducing significant error. Therefore, Eq. (5.17) can be written as

$$g\rho_{pc}\beta_{pc}C_2\Delta z\,\Delta h_{ss} = \frac{pW_{ss}^2}{2\rho_{pc}\,\mathrm{Re}_{ss}^b\,A_r^2}N_G \tag{5.23}$$

Replacing Δh_{ss} in terms of the heater power Q_h and using the definition of Re and N_G, we obtain the mass flow rate as

$$W_{ss} = \left[\frac{2C_2 g\rho_{pc}^2\beta_{pc}D^{1+b}A_r^{2-b}\Delta z Q_h}{pL_t\mu^b}\right]^{\frac{1}{3-b}} \tag{5.24}$$

This equation can be expressed in dimensionless form as

$$\mathrm{Re}_{ss} = C\left[\frac{Gr_m^*}{N_G}\right]^r \tag{5.25}$$

Where,

$$Gr_m^* = \frac{D_r^{\ 3}\rho_{pc}^2 g\beta_{pc}Q_h\Delta z}{A_r\mu^3};\quad \mathrm{Re}_{ss} = \frac{D_r W_{ss}}{A_r\mu};\quad C = \left(\frac{2C_2}{p}\right)^r;\quad r = \frac{1}{(3-b)} \tag{5.26}$$

It may be noted that this equation reduces to that applicable for subcritical single-phase flow by setting C_2=1 and by considering ρ and β at loop average temperature. The above steady state flow rate equation has been tested with data generated with supercritical CO_2 and water in a natural circulation test facility.

5.3 Experiments conducted

5.3.1 Friction factor data

Since the present test facility used commercial pipe, experiments were conducted under forced flow condition to generate friction factor data [Vijayan et al. (2011)]. The data generated and the equation fitted to these data is shown in ***Figure 5.4***. The friction law so obtained is given by $f = 0.12555\,\mathrm{Re}^{-0.15551}$.

Therefore, the steady state subcritical natural circulation flow rate can be obtained from Eq. (5.25) with C_2=1 as

$$\mathrm{Re} = 2.65\left[\frac{Gr_m}{N_G}\right]^{0.352} \qquad (5.27)$$

Similarly using this friction factor relation and the corresponding values of C_2, we can obtain the dimensionless flow equations for the various regions as follows

$$\mathrm{Re} = 2.265\left[\frac{Gr_m^*}{N_G}\right]^{0.352} \quad \text{(Region 1)} \tag{5.28a}$$

$$\mathrm{Re} = 2.583\left[\frac{Gr_m^*}{N_G}\right]^{0.352} \quad \text{(Region 2)} \tag{5.28b}$$

$$\mathrm{Re} = 1.003\left[\frac{Gr_m^*}{N_G}\right]^{0.352} \quad \text{(Region 3)} \tag{5.28c}$$

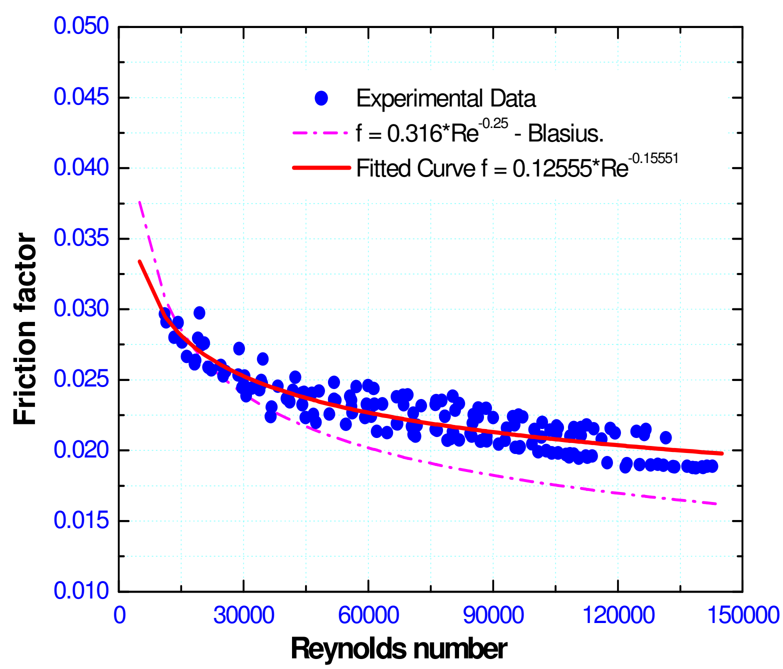

Figure 5.4: Forced flow friction factor data for the tube used for fabrication of the test loop

Similarly, by considering Blasius correlation i.e. $f = 0.316\,\mathrm{Re}^{-0.25}$, the steady state flow rate for subcritical natural circulation can be obtained from Eq. (5.25) with C_2=1 as

$$\mathrm{Re} = 1.956\left[\frac{Gr_m}{N_G}\right]^{0.364} \tag{5.29}$$

Using this friction factor relation and the corresponding values of C_2, we can obtain the dimensionless flow equations for the various regions as follows

$$\mathrm{Re} = 1.664\left[\frac{Gr_m^*}{N_G}\right]^{0.364} \text{ (Region 1)} \tag{5.30a}$$

$$\mathrm{Re} = 1.907\left[\frac{Gr_m^*}{N_G}\right]^{0.364} \text{ (Region 2)} \tag{5.30b}$$

$$\mathrm{Re} = 0.717\left[\frac{Gr_m^*}{N_G}\right]^{0.364} \text{ (Region 3)} \tag{5.30c}$$

5.3.2 Natural circulation data

For comparing the proposed flow correlation with the existing subcritical flow correlation, experiments were conducted in the near critical and supercritical regions of CO_2 and water [Ref. Chapter 3].

For each orientation, the steady state data were generated for different heater powers. The range of parameters for the experimental data for CO_2 and water at supercritical pressure is given in Table-3.2 and Table-3.3 respectively. From the measured heater power and enthalpy rise across the heater, the mass flow rate was estimated by heat balance. The centre line elevation difference between the heater and cooler used for calculation of modified Grashof number is also given in the table. Detailed experimental data generated is given in Appendix-4 and Appendix-5.

5.3.2.1 Deeply subcritical natural circulation data

Steady state natural circulation data for water under subcritical condition and also limited water and CO_2 data for supercritical pressure with temperature far less than critical point, fall under this category. The range of parameters for water and CO_2 at deeply subcritical condition is given in Table-5.1. Detailed experimental data fall under this category is given in Appendix-6. These data are compared with the subcritical flow correlation reported in [Vijayan (2002)] and is found to be in good agreement as shown in ***Figure 5.5***.

Table-5.1: Range of parameters for the test data (deeply subcritical condition)

Orientation	**Centre line elevation difference between cooler and heater, m**	**Range of parameters for the data**						
		Pressure (MPa)	**Power, W**		**Re**		**Gr_m**	
			Min.	**Max.**	**Min.**	**Max.**	**Min.**	**Max.**
HHHC (water)	4.10	3.0-15.0	500.0	7000.0	2.1E+03	5.6E+04	2.68E+11	2.37E+15
HHVC (water)	2.75	3.0	1497.8	3522.5	4.1E+03	1.0E+04	1.91E+12	2.3E+13
VHHC (water)	2.70	3.0	2266.7	3067.2	4.1E+03	5.9E+03	2.7E+12	5.9E+12
VHVC (water)	1.35	3.0	2039.7	2996.0	4.3E+03	6.6E+03	2.02E+12	6.4E+12
HHHC(super-critical water)	4.10	22.5-22.7	3500.0	5000.0	2.9E+04	4.4E+04	2.7E+14	9.4E+14
HHHC(super-critical CO_2)	4.10	8.4-9.1	50.0	107.0	1.4E+04	2.5E+04	5.7E+13	2.4E+14

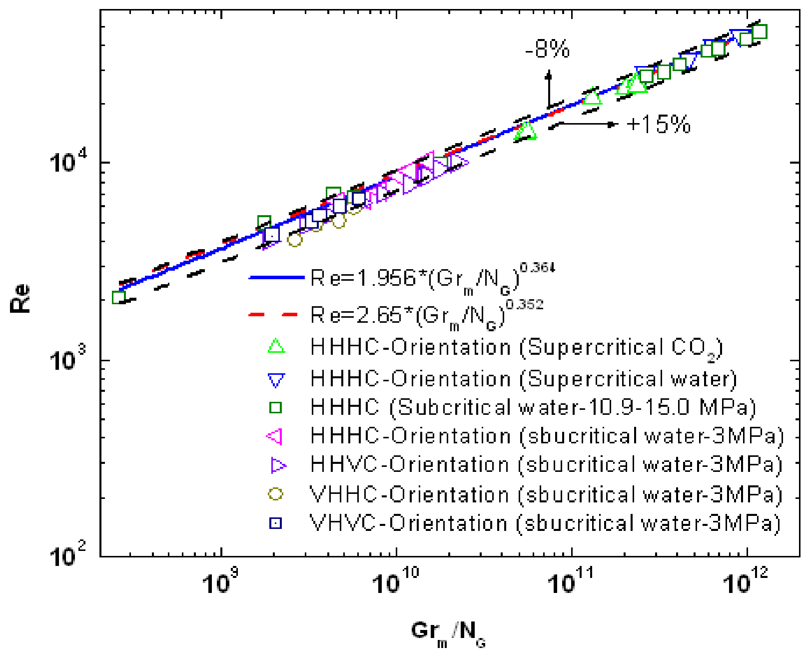

Figure 5.5: Steady state natural circulation flow

5.3.2.2 Natural circulation data with supercritical CO_2 and water

The range of parameters of all steady state natural circulation data for CO_2 and water given in Table-3.2 and Table- 3.3 fall in this category. These data are first categorized into various regions and compared with correlations applicable to these regions below.

i) Region 1 ($-1.53 < h^* < -0.7$)

These data are compared with subcritical flow correlation in ***Figure 5.6 a***. In this case, the supercritical pressure data with heater outlet temperature less than 0.7Tpc has been considered.

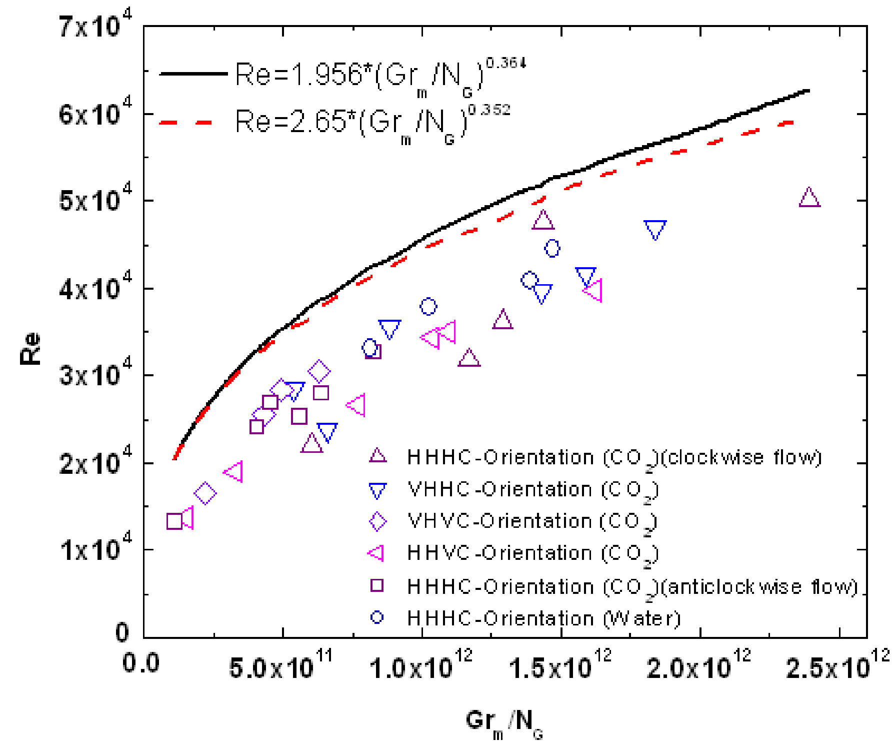

(a) Region 1

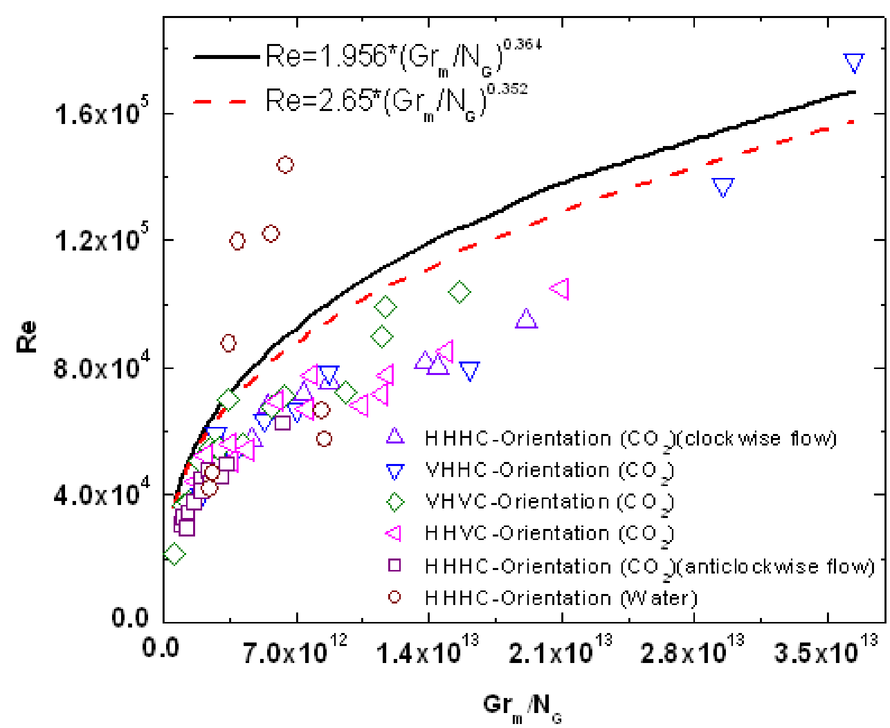

(b) Region2 ($0.7T_{pc} \leq T \leq 1.3T_{pc}$)

ii) Region 2 (-0.7<h*<0.76)

These data are compared with subcritical flow correlation in ***Figure 5.6 b***. In this case, the heater outlet temperature is in between 0.7Tpc to 1.3Tpc.

iii) Region 3 (0.76 < h*<1.2)

In this case, the heater outlet temperature is beyond 1.3Tpc. Such data are also compared with subcritical flow correlation in ***Figure 5.6 c***.

Except for the data in deeply subcritical region ***(Figure 5.5)***, all other data showed poor agreement with the subcritical flow correlation.

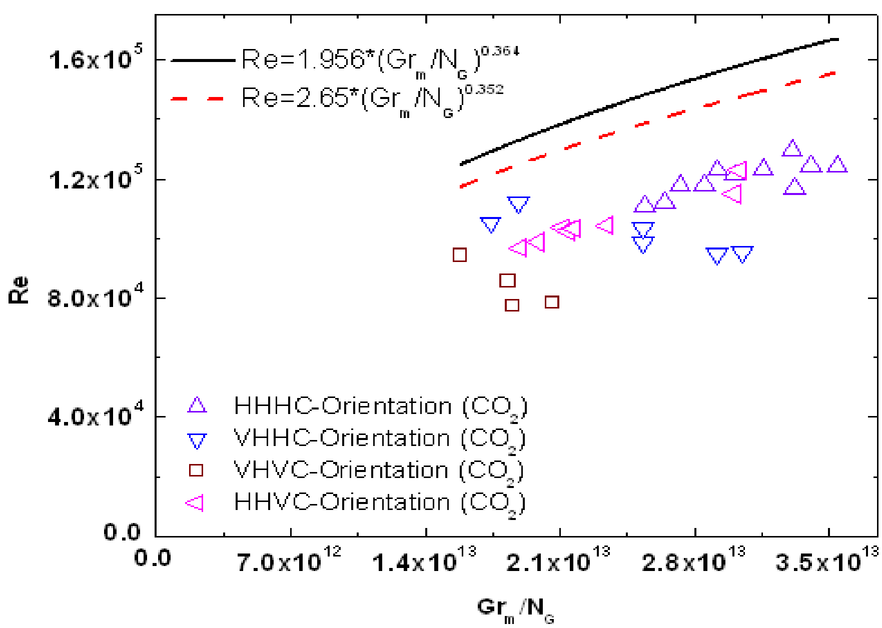

(c) Region 3

Figure 5.6: Comparison of subcritical correlation for supercritical pressure data

5.3.2.3 Deeply supercritical natural circulation data with water

Limited number of supercritical pressure water data fall under this category. Table-5.2 shows the range of parameter for deeply supercritical water data. These data [Ref.Appendix-7] are compared with subcritical flow correlation in ***Figure 5.7***. It has been observed from ***Figure 5.7*** that the present experimental water data falling in the deeply supercritical region is in reasonable agreement (±%10) with the subcritical correlation as compared to the data falling near the pseudo critical region (i.e. Region 1, 2 and 3) (Ref. ***Figure 5.6***). This can be attributed to the fact that at deeply subcritical (***Figure 5.5***) and deeply supercritical (***Figure 5.7***) region, variation in property of fluid is not significant. Therefore, in these regions subcritical correlation is applicable. However, near the pseudo critical region where property variation is more, deviation from subcritical correlation has been observed.

Table-5.2: Range of parameters for steady state natural circulation data with water (deeply supercritical condition)

Variables		**Range**
Orientation		HHHC (Clockwise flow)
Pressure		22.9-23.6MPa
Power		6.0-8.0 kW
Re	Min.	7.76E+04
	Max.	8.54E+04
Gr_m	Min.	4.12E+15
	Max.	5.06E+15

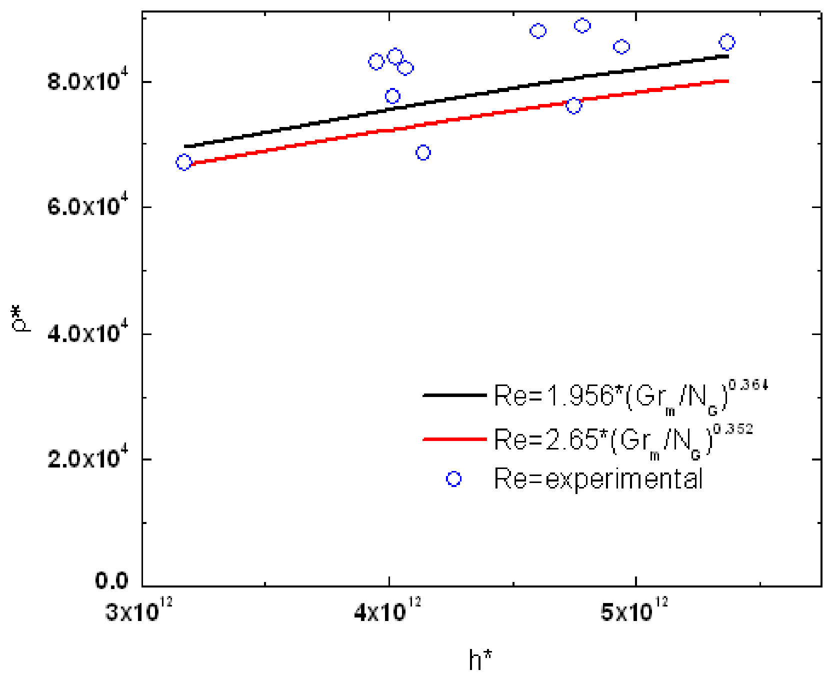

Figure 5.7: Deeply supercritical data

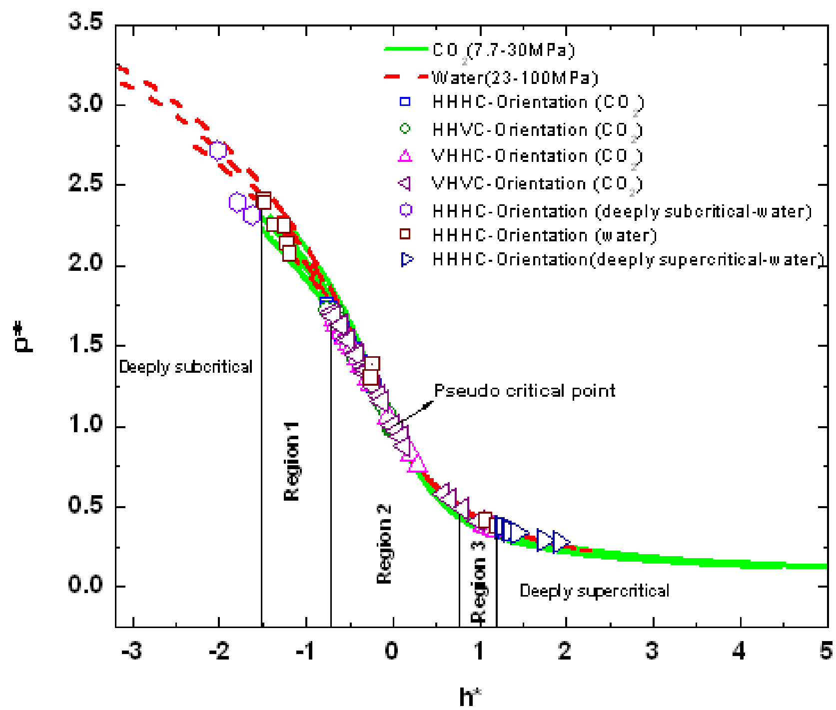

Figure 5.8: Experimental data on dimensionless density and dimensionless enthalpy plot (CO_2 and water data)

In order to find the region where subcritical correlation is applicable, present experimental data i.e. supercritical CO_2 and water has been plotted in dimensionless density and enthalpy as shown in ***Figure 5.8***.

From the figure, the boundary between region 1 and deeply subcritical and that between region 3 and deeply supercritical has been observed at h*= -1.53 and at h*=1.2 respectively.

5.4 Comparison with the present data

The steady state equation derived above for supercritical condition has been validated with the steady state natural circulation data generated for different orientations of the heater and the cooler in the present loop. Supercritical natural circulation data from ***Figure 5.6*** are re-plotted in ***Figure 5.9*** for CO_2 and water. It has been observed from ***Figure 5.9*** that the Re calculated for different regions using the present correlation is showing good agreement with the present experimental data as compared to subcritical flow correlation given in ***Figure 5.6***.

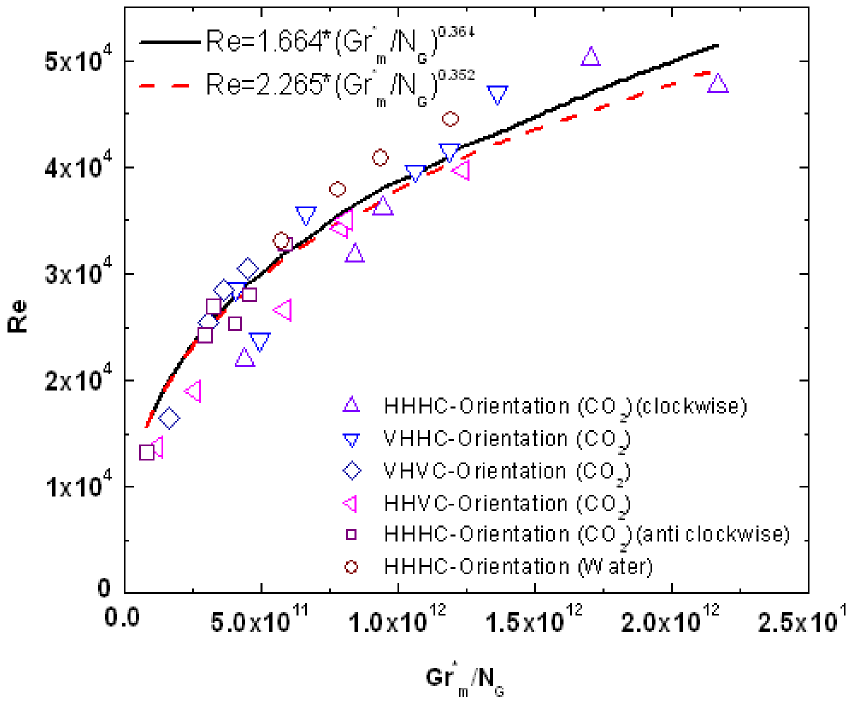

(a) Region 1 (-1.53< h* < -0.7)

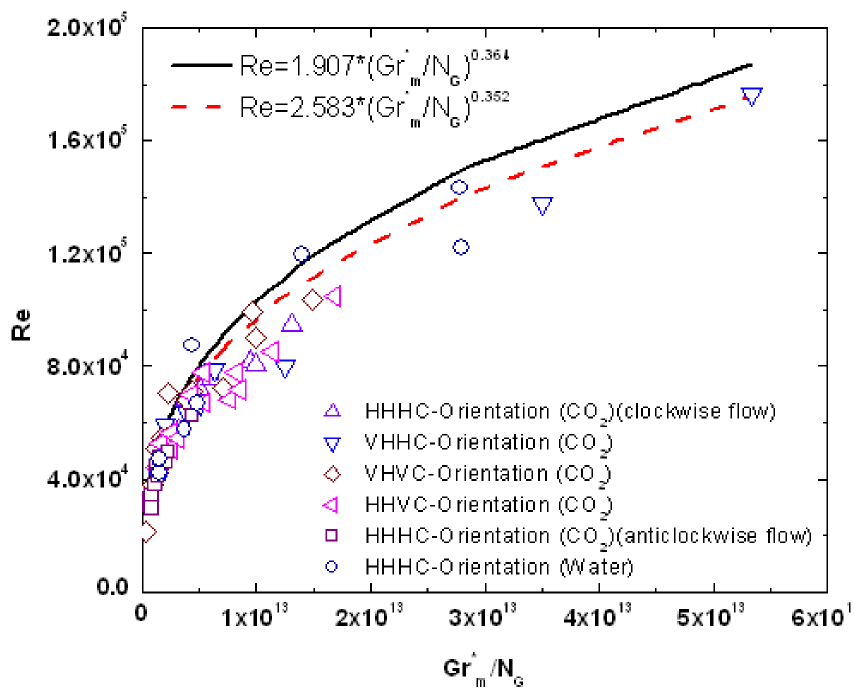

(b) Region 2 (-0.7< h* < 0.76)

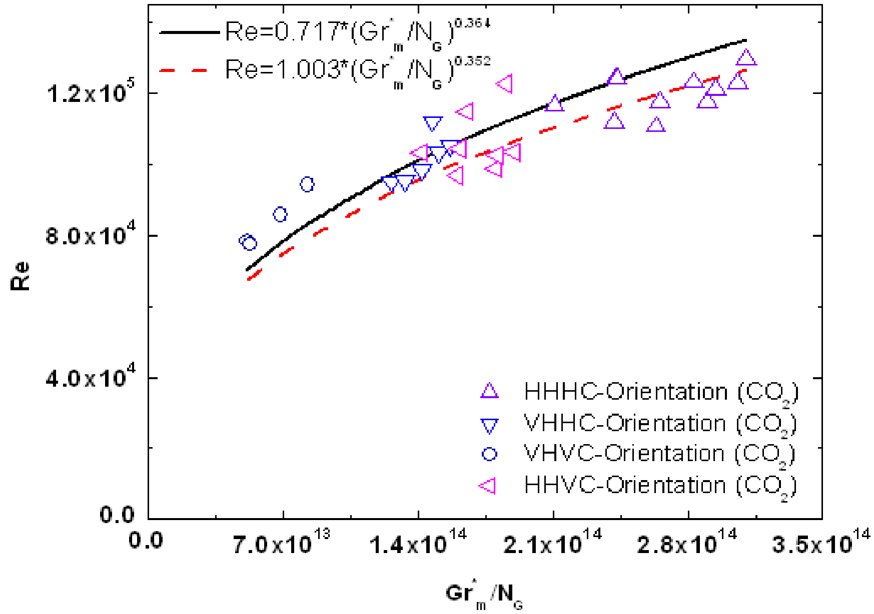

(c) Region 3 (0.76<h* <1.2)

Figure 5.9: Comparison of proposed correlation with supercritical pressure (CO_2 and water) data

5.5 Comparisons with literature data

In literature, very few papers report experimental data on supercritical natural circulation [Holman and Boggs (1960), Harden (1963), Lomperski and Cho (2004), Yoshikawa et al. (2005)] for validation of the steady state flow correlation presented in this chapter. For validation of the proposed correlation, usable data could be found in [Holman and Boggs (1960), Harden (1963), Lomperski and Cho (2004)]. Yoshikawa et al. (2005) studied the performance of a somewhat complex supercritical CO_2 loop and the complete geometrical details were not available and hence could not be considered.

Table-5.3: Geometric details of different supercritical loops

Author		Pressure, MPa	Fluid used	Circulation Length, m	Diameter, m	Height, m	Source and sink orientation	N_G
Lomperski et al.[2004]		8.0	CO_2	15.3	0.0121	2.0	HHHC	1488.6
Holman and Boggs [1960]		6.2	Freon-12	5.55	0.0109	0.9398	VHVC	509.2
Harden [1963]	**Loop1**	3.55	Freon-114	8.53	0.0236	1.22	VHVC	361.6
	Loop2	3.3	Freon-114	11.58	0.0236	2.84	VHVC	490.3
Present CO_2 loop	**Loop1**	8.6	CO_2	14.22	0.01388	4.10	HHHC	1024.5
	Loop2	8.5-9.0	CO_2	14.22	0.01388	2.75	HHVC	1024.5
	Loop3	8.7-9.1	CO_2	14.22	0.01388	2.70	VHHC	1024.5
	Loop4	8.5-8.7	CO_2	14.22	0.01388	1.35	VHVC	1024.5
Present H_2O loop		22.5-24.1	Water	14.22	0.01388	4.10	HHHC	1024.5

Table-5.3 shows the geometric details of the remaining loops. In addition, the reported experimental data is for three different fluids. ***Figure 5.10*** shows the comparison between the Lomperski and Cho (2004) data with the proposed correlation. Data reported in this paper is falling in region 2. It has been observed from ***Figure 5.10*** that the present correlation is in reasonable agreement with the reported data [90% of the experimental data falls within ±10%].

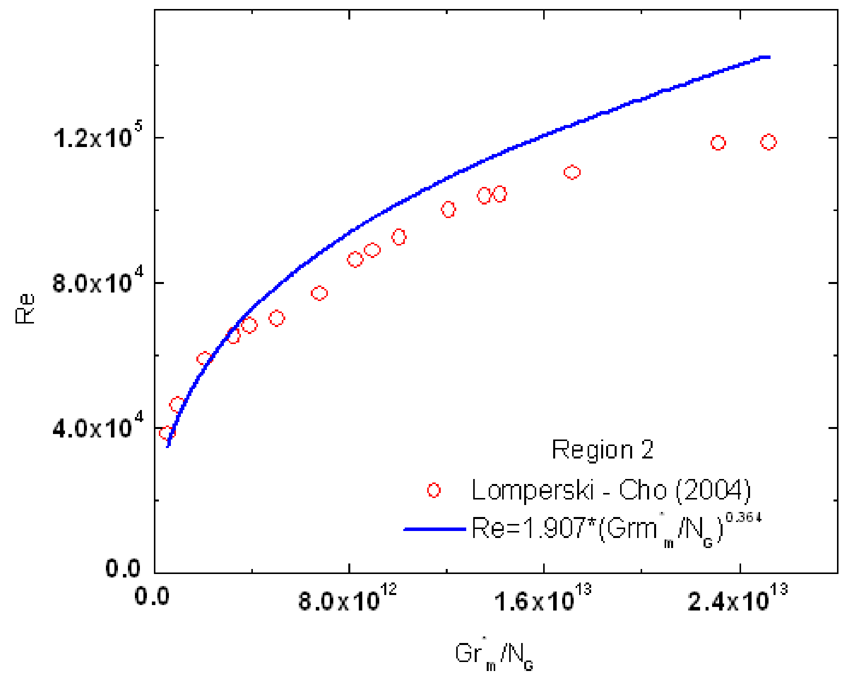

Fig.5.10: Comparison of supercritical data of Lomperski and Cho (2004) with supercritical flow correlation

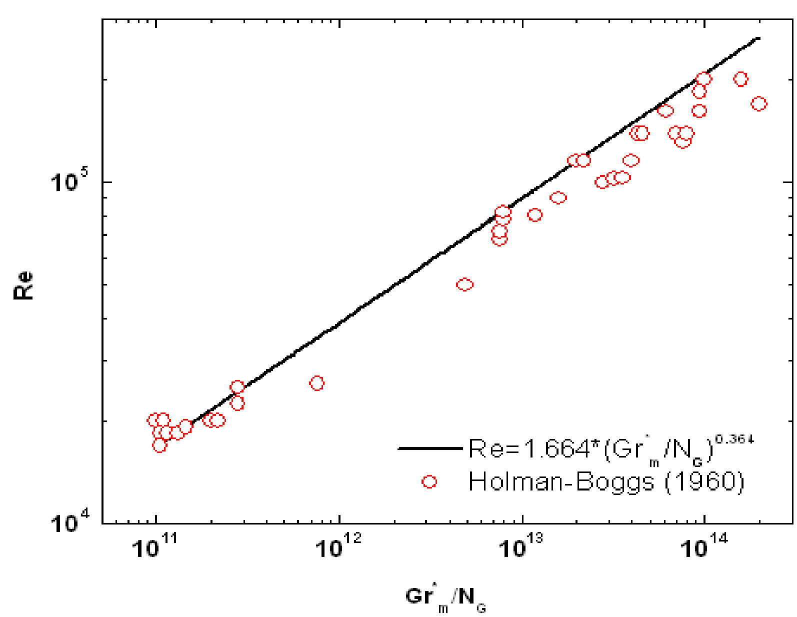

(a) Region 1

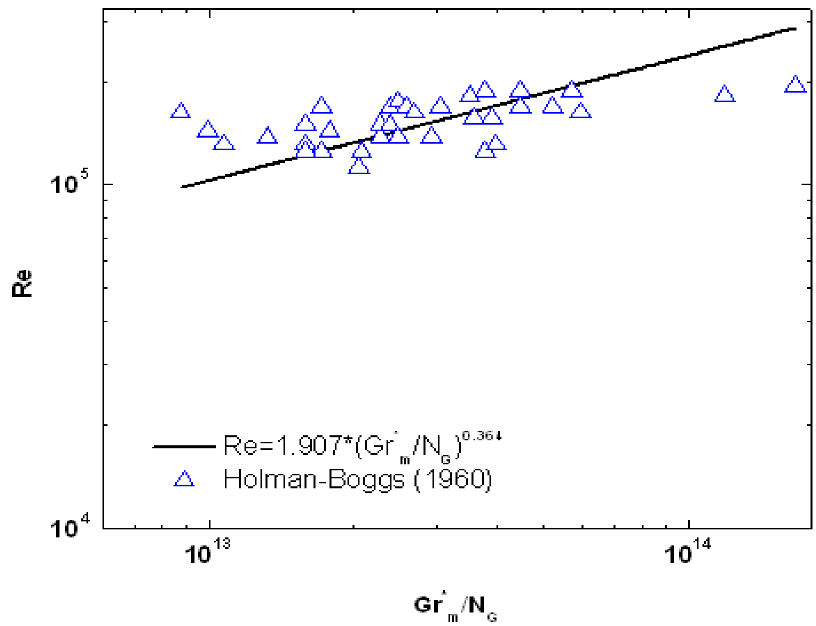

Figure 5.11: Comparison of Holman and Boggs data (1960) with proposed correlation

The proposed correlation (for region 1 and region 2) is compared with Holman and Boggs (1960) data for supercritical Freon-12 in ***Figure 5.11 a*** and ***b*** respectively. It is observed that the proposed correlation is in reasonable agreement with the reported data [90% of the experimental data falls within ±20% for region 1 and ±25% for region 2]. Data reported in Harden (1963) for Freon-114 also fall in the regions 1 and 2. Hence, the reported data for Freon-114 is compared with the proposed correlation in ***Figure 5.12 a*** and ***b*** respectively. The proposed correlation is in reasonable agreement with the reported data [90% of the experimental data falls within ±5% for region 1 and ±10% for region 2]. It has been observed that most of the data reported in the literature for different fluid falls either in the region 1 or in region 2.

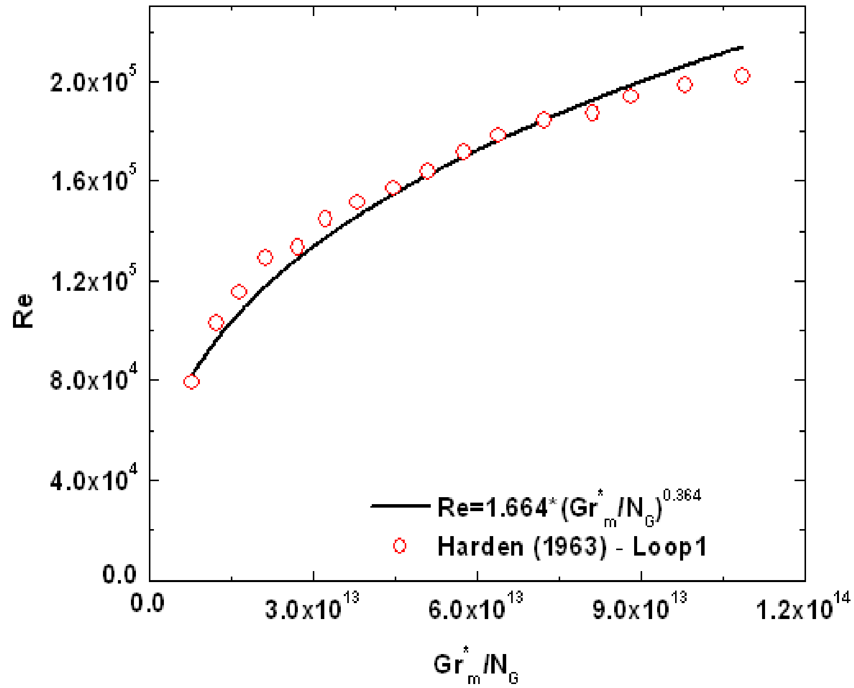

(a) Region1

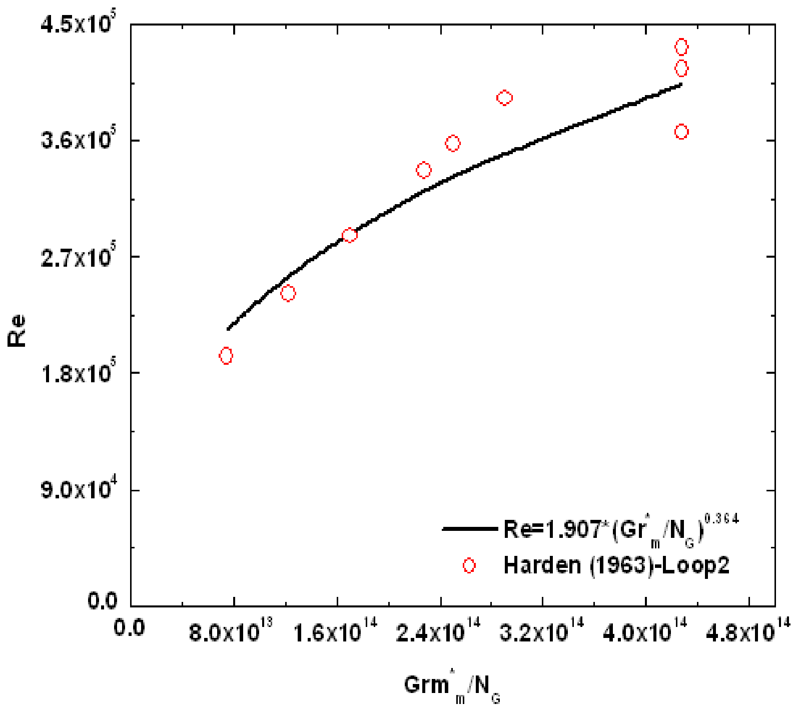

(b) Region2

Fig.5.12: Comparison of supercritical data of Freon-114 (Harden, 1963) with supercritical flow correlation

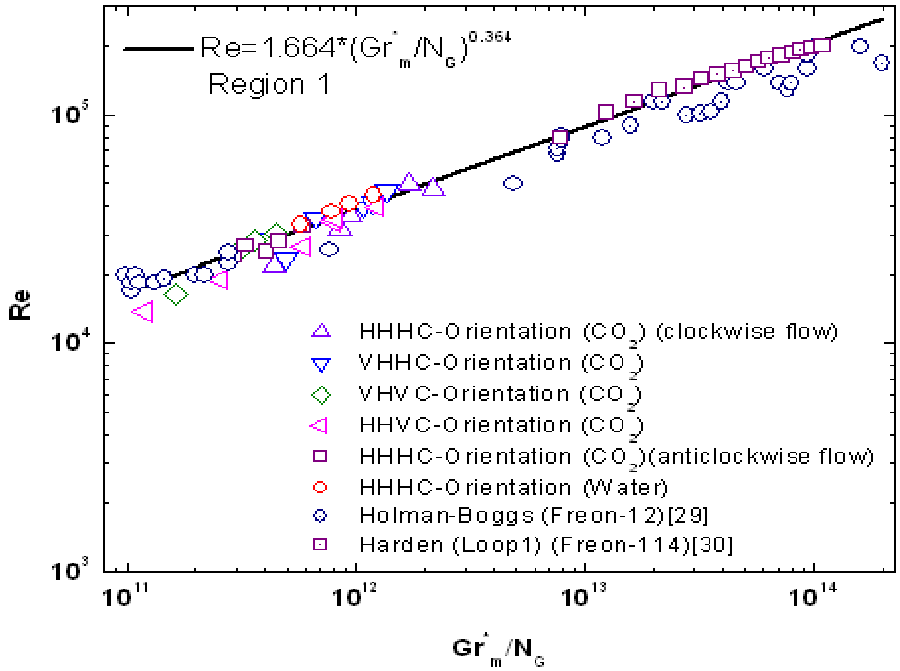

(a) Region 1

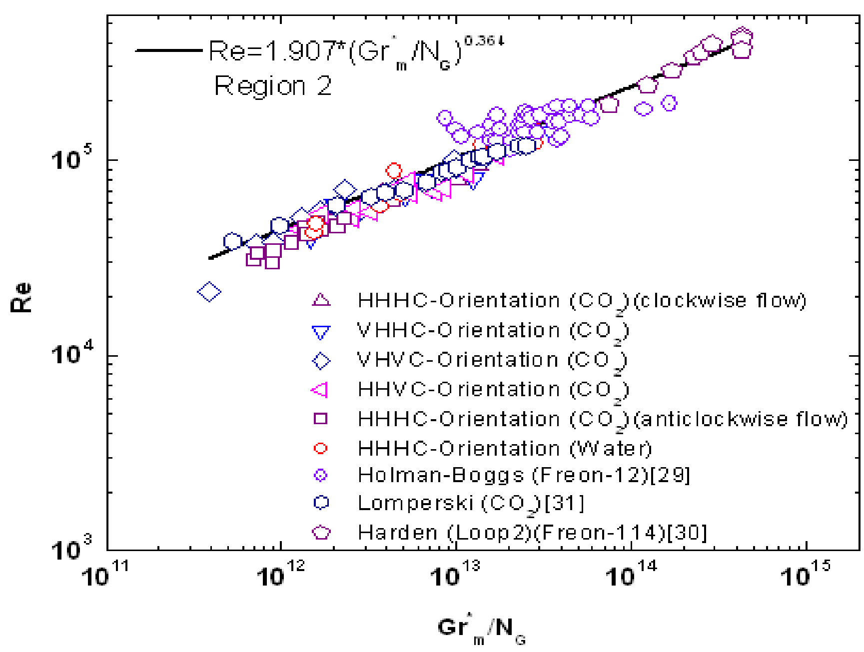

(b) Region 2

Figure 5.13: Steady state natural circulation data for different supercritical fluids

Figure 5.13 a and ***b*** compares the data available in the literature [Holman and Boggs (1960), Harden (1963), Lomperski and Cho (2004)] along with the present CO_2 and water data (in region 1 and region 2) respectively.

5.6 Prediction of static instability for supercritical fluid

Steep change of fluid properties in the pseudo critical region like density gives rise to concerns of flow instabilities for supercritical fluids. Literature review revealed that the flow and pressure oscillations might occur for supercritical fluids under certain operating conditions. These oscillations were observed in systems with forced flow as well as natural circulation. The occurrence of such instabilities is undesirable for reliable operation of the system. Furthermore, in nuclear reactors flow and pressure oscillations may induce undesirable power oscillations. Consequently, there is considerable interest to investigate the conditions leading to these oscillations [Zuber (1966)].

Supercritical systems are also subject to static instability (also known as Ledinegg instability). In case of Ledinegg instability, if the flow change by a small amount, another steady state is not possible in the vicinity of the original steady state [Boure et al. (1973)] leading to a flow excursion. The cause of the phenomena lies in the steady state laws. Hence, the threshold of the instability can be predicted using steady state laws. A static instability can lead either to a different steady state condition or to a periodic behavior. The occurrence of multiple steady state solutions is the fundamental cause of this instability. The stability criterion for the Ledinegg type instability is given by d(ΔP)/dG < 0 i.e. negative slope in static system characteristic [Boure et al. (1973)]. In ***Figure 5.14***, point 'b' satisfies this criterion.

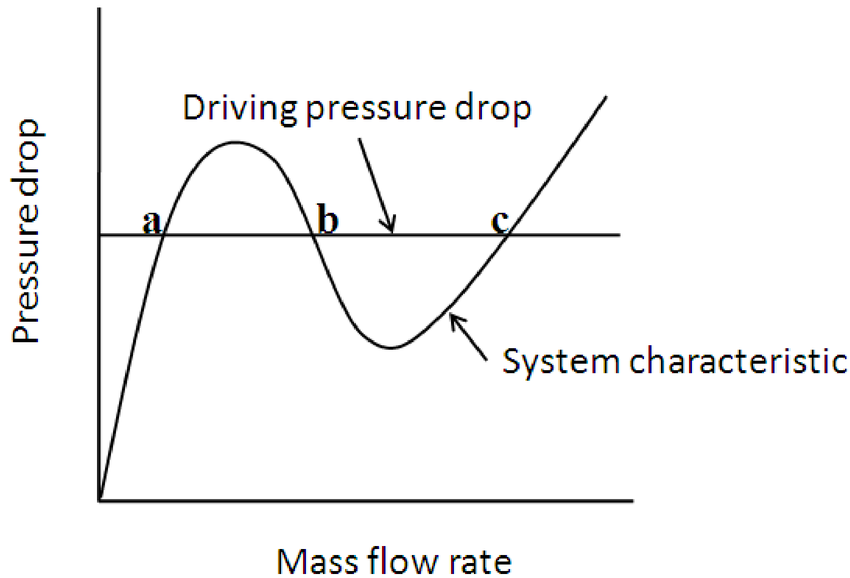

Figure 5.14 Static instability in a natural circulation system

5.6.1 Analytical model

The threshold of excursive instability can be obtained by steady state conservation equation from Eq. (5.2) noting that $\oint \partial v = 0$, the steady state momentum equation for uniform diameter loop can be written as

$$\frac{fW^2 L_t}{2D\rho_0 A^2} + \frac{KW^2}{2\rho_0 A^2} + g\oint \rho dz = 0 \tag{5.31}$$

From the above equation friction pressure drop term for the entire loop [ref. ***Figure 5.1***] can be written in terms of different sections of the loop such as cold leg, heater, hot leg and cooler as

$$\frac{fW^2 L_t}{2D\rho_0 A^2} = \frac{W^2 f_{cl} L_{cl}}{2\rho_{cl} A^2 D} + \frac{W^2}{2A^2 D}\left[\sum_{i=1}^{N} \frac{f_i L_i}{\rho_i}\right]_h + \frac{W^2 f_{hl} L_{hl}}{2\rho_{hl} A^2 D} + \frac{W^2}{2A^2 D}\left[\sum_{i=1}^{N} \frac{f_i L_i}{\rho_i}\right]_c \quad (5.32)$$

Local pressure drop and gravity term for the entire loop can also be expressed in the similar manner. Substituting friction pressure drop term, local pressure drop term and gravity term for the entire loop in Eq. (5.31) and after rearranging, we obtain

$$gH\rho_{cl} = gH\rho_{hl} + \frac{W^2}{2DA^2}\left[\frac{f_{cl} L_{cl}}{\rho_{cl}} + \left(\sum_{i=1}^{N} \frac{f_i L_i}{\rho_i}\right)_h + \frac{f_{hl} L_{hl}}{\rho_{hl}} + \left(\sum_{i=1}^{N} \frac{f_i L_i}{\rho_i}\right)_c\right] + \frac{W^2}{A^2}\left(\frac{K_{cl}}{\rho_{cl}} + \frac{K_{hl}}{\rho_{hl}}\right) \quad (5.33)$$

The left hand side of the Eq. (5.33) represents the gravitational pressure drop in the cold leg, which is driving the flow in the loop. The first term on the right hand side represents the gravitational pressure loss in hot leg, the second term represents the distributed friction pressure loss over the entire loop and the third term represents the local pressure loss over the entire loop. Thus, the entire right hand side represents the system characteristic and the left hand side the driving head [Todreas and Kazimi (1990)].

5.6.2 Static instability analysis with supercritical water

To identify the occurrence of static instability, the system characteristic and the driving pressure have been plotted against the mass flow rate in ***Figure 5.15*** for different power. As the driving head is practically independent of the mass flow rate, it depicts a horizontal line. The system characteristic has been plotted for different powers. The lower and upper threshold of instability has been identified as shown in ***Figure 5.15 a*** and ***b*** respectively for water.

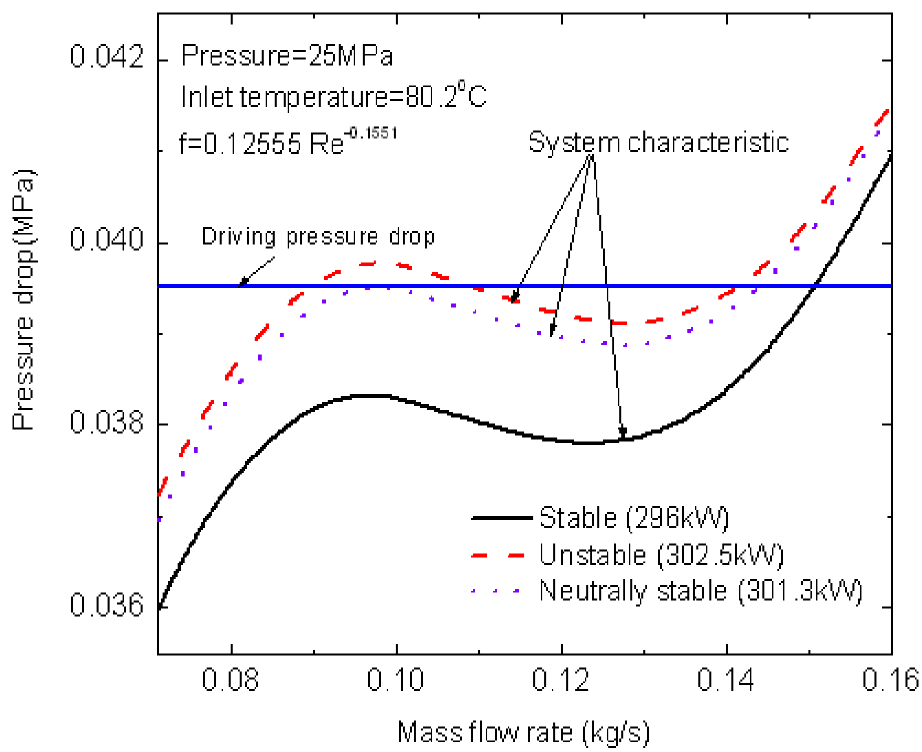

(a) Lower threshold

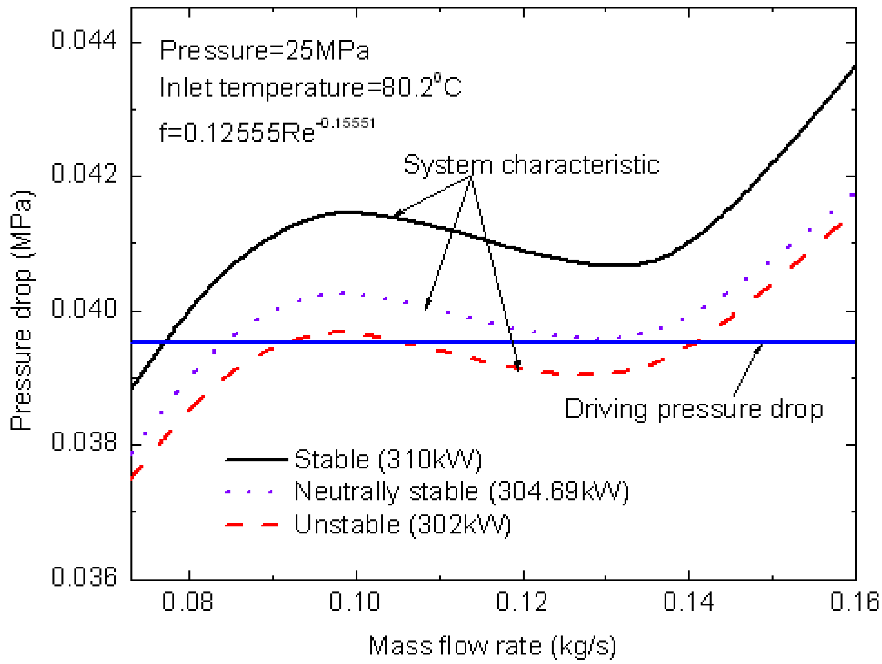

(b) Upper threshold

Figure 5.15 Threshold of Ledinegg or excursive instability

It is observed from the ***Figure 5.15a*** that for power less than 301.3kW there is only one steady state flow rate satisfying the Eq. (5.33) and is stable. However, at power 302.5kW there are three steady state flow rate satisfying the Eq. (5.33) and makes the system unstable. In case of water at supercritical pressure condition, excursive instability is observed only at high value of sub-pseudo critical number (N_{subpc}) (i.e. up to 2.9) in the present analysis. In this context, it may also be noted that the analysis done by Ambrosini (2007) also showed that the excursive behavior is observed only at sufficiently large value of sub-pseudo-critical number. However, with water when $N_{subpc} < 2.9$ static instability has not been observed.

Figure 5.16 shows stability map at different pressures in the present loop. It is observed from ***Figure 5.16*** that unstable zone decreases with rise in pressure. It may be noted that for all cases, the predicted threshold value of power is far higher than the experimental conditions with water in the present loop.

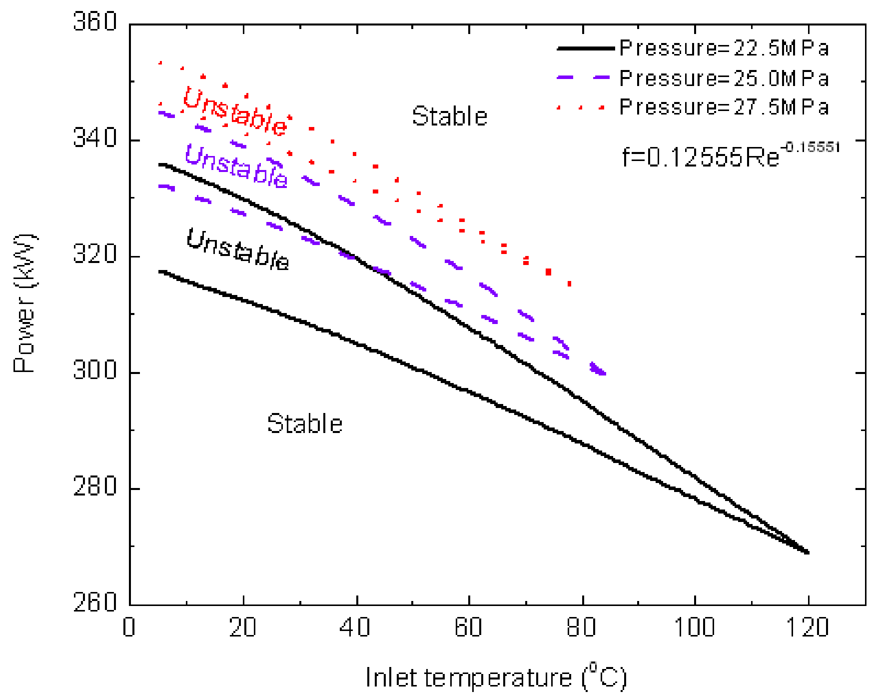

Figure 5.16: Stability map

5.6.3 Static instability analysis with supercritical CO_2

Figure 5.17 shows the variation of driving pressure drop and system characteristic with the mass flow rate. With CO_2 analysis has been carried out for a wide range of pressure from 7.4 to 30 MPa. However, multiple steady state solutions have not been observed for the present loop.

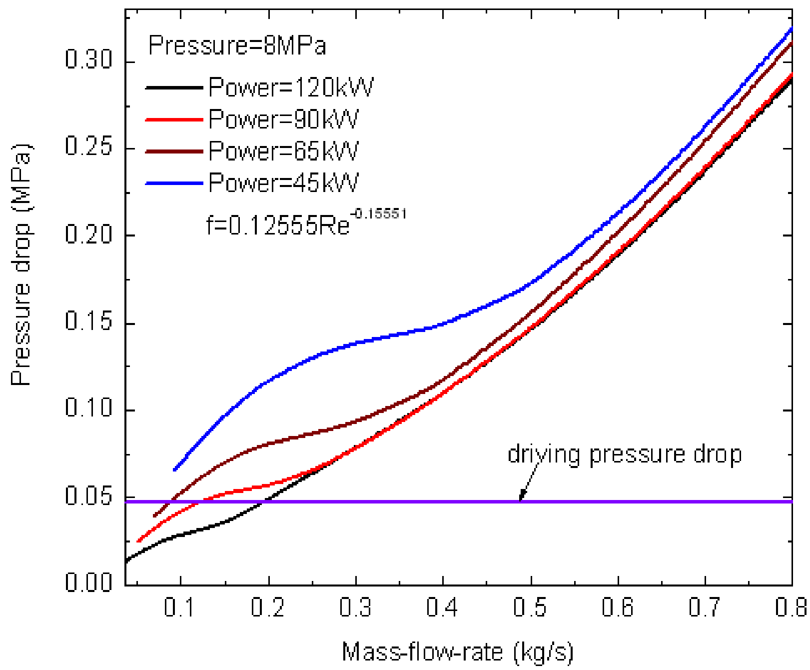

Figure 5.17: Pressure drop vs. mass flow rate for CO_2 at supercritical pressure

5.7 Closure

The dimensionless relationship proposed by Ambrosini and Sharabi is found useful to the present study. Ambrosini and Sharabi had already applied their dimensionless relationship between ρ* and h* for various fluids like water, CO_2 and ammonia. This relationship is tested in addition for Freon-12 and Freon-114 in the present study. As proposed by them the data for Freon-12 and Freon-114 is found to collapse on a unique curve like that for other fluids.

A generalized correlation for the steady state flow applicable to supercritical natural circulation loops was derived. Due to sharp change of fluid properties such as density at supercritical pressure, Boussinesq approximation is not valid. Present analysis makes use of dimensionless relationship between the density and the enthalpy of supercritical fluids proposed by Ambrosini and Sharabi to develop a new model for density variation in supercritical fluid. This relationship is reasonably general and it is valid for several fluids and therefore enables us to generate a generalized flow correlation valid for different fluids at supercritical pressure. This generalized flow correlation was tested with the experimental data generated with supercritical CO_2 in a uniform diameter rectangular loop for all four orientations of heater and cooler. Subsequently the correlation was tested with supercritical water data generated for HHHC orientation. It is observed that the same generalized correlation is applicable for the supercritical CO_2 and water data. Further, the data reported in literature for CO_2, Freon-12 and Freon-114 has also been compared with the proposed correlations showing reasonable agreement with the proposed correlation. It is observed that the same generalized correlation is applicable for all supercritical fluids for which data were available.

The threshold of excursive instability has been judged by checking for the occurrence of multiple steady state solutions. Static instability is observed in the present natural circulation loop with supercritical water whereas instability is not observed with supercritical CO_2. The effect of pressure is found to reduce the unstable region. At higher pressures, instability is observed with very low inlet temperature.

CHAPTER-6

CONCLUSIONS AND RECOMMENDATION FOR FUTURE WORK

Detailed investigations have been carried out to obtain a more valuable insight into natural circulation phenomena involving subcritical and supercritical fluid conditions and the findings are presented in this thesis.

6.1 Natural circulation analysis at subcritical pressure condition

To compare the thermal hydraulic performance of different natural circulation loops dimensionless equations independent of loop geometry are desirable. The available dimensionless equation for steady state flow in both uniform and non-uniform diameter loops is applicable only when the flow in the loop is under fully laminar or fully turbulent flow condition. However, the equation is not applicable if the flow in the loop follows two different friction laws.

In chapter 4, a generalized equation for the steady state flow in single-phase natural circulation loops is derived based on 1-dimensional theory by assuming the loop to be in partly laminar and partly in transition or turbulent flow. Unlike the available dimensionless equation, the derived dimensionless flow equation is applicable for any loop obeying multiple friction laws. For the first time the generalized flow equation valid for all the three regions i.e. laminar, transition and turbulent has been obtained.

The generalized flow equation was tested with the experimental data generated in a uniform diameter rectangular loop for all four orientations such as, Horizontal Heater and Horizontal Cooler (HHHC), Horizontal Heater and Vertical Cooler (HHVC), Vertical Heater and Horizontal Cooler (VHHC) and Vertical Heater and Vertical Cooler (VHVC). From the present analysis, it is observed that the same generalized correlation is applicable for all the four orientations of heater and cooler tested. Data reported in the literature is also showing good agreement with the generalized equation developed.

The stability code LISA based on linear stability analysis methodology has been developed and validated with previously reported stability map for both laminar and turbulent flows. Subsequently a stability map valid for laminar, transition and turbulent regions has been obtained using the LISA code for the same loop. The results showed that there is no stable zone in the subcritical region for $St_m < 7$ for turbulent flow for the loop geometry considered in this study. Also by considering the various effects such as heat loss, wall effects, local pressure losses and multidimensional effects the prediction can be improved.

6.2 Natural circulation analysis at supercritical pressure condition

Supercritical fluids undergo large change in density, specific heat and other thermodynamic and thermo physical properties without the formation of interfaces and separate phases. It is observed that, the traditional 1-dimensional formulations used for subcritical natural circulation analysis with constant fluid properties and

Boussinesq approximation is not valid for supercritical fluids where density change is quite sharp in the neighborhood of the critical region.

In chapter 5, new studies are being conducted to generate the performance of natural circulation loops with supercritical fluids. Analysis makes use of dimensionless relationship between the density and the enthalpy of supercritical fluids proposed by Ambrosini and Sharabi to develop a new model for density variation in supercritical fluids. This relationship is reasonably general and it is valid for several fluids and therefore enables us to generate a generalized flow correlation valid for different fluids at supercritical pressure. This generalized flow correlation was tested with the experimental data generated with supercritical CO_2 in a uniform diameter rectangular loop for all four orientations of heater and cooler. Subsequently the correlation was tested with supercritical water data generated for HHHC orientation. It is observed that the same generalized correlation is applicable for the supercritical CO_2 and H_2O data. Further, the data reported in literature for CO_2, Freon-12 and Freon-114 has also been compared with the proposed correlations showing reasonable agreement with the proposed correlation. It is observed that the same generalized correlation is applicable for all supercritical fluids for which data were available.

Furthermore, in nuclear reactor, flow and pressure oscillations may induce undesirable power excursion. Consequently, there is considerable interest to investigate the conditions leading to the initiation of these oscillations. At supercritical pressure, a flow system with heat addition could undergo flow excursion. The flow excursion instability involves a sudden change in the flow rate to a lower value. In chapter 5, static instability in a closed loop natural circulation system at supercritical condition has been investigated for supercritical water and CO_2. Static instability is predicted for the present natural circulation loop with supercritical water whereas static instability is not predicted for the same loop with supercritical CO_2. The effect of pressure is found to reduce the unstable region. At higher pressures, instability is observed with very low inlet temperature.

6.3 Summary

- A generalized flow equation for single-phase natural circulation loop under subcritical pressure condition was derived based on 1-D theory by assuming the loop is partly in laminar and partly in transition or turbulent flow for the first time.
- Proposed generalized flow correlation was validated with the in-house experimental data as well as with published data available in the literature.
- The stability code LISA (LInear Stability Analysis) based on linear stability analysis methodology has been developed.
- A stability map valid for laminar, transition and turbulent regions has been obtained using the LISA code.
- A generalized correlation for the steady state flow applicable to supercritical natural circulation loops was derived using the relationship between dimensionless density and dimensionless enthalpy proposed by Ambrosini and Sharabi.

- It is observed that the same generalized correlation is applicable for all supercritical fluids for which data were available.
- Proposed generalized flow correlation under supercritical condition was validated with the in-house experimental data as well as with published data available in the literature.
- The threshold of excursive instability has been judged by checking for the occurrence of multiple steady state solutions.
- Static instability is observed in the present natural circulation loop with supercritical water.
- Static instability is not observed with supercritical CO_2 in the present natural circulation loop.
- The effect of pressure is found to reduce the unstable region.

6.4 Recommendations for future work

Computational modeling could be used to resolve the issue of multiple friction laws. However, such computations often involve 3-dimensional CFD models. Full 3-dimensional CFD simulations of complex geometry natural circulation systems are going to be a major challenge. The viable approach is to use coupled 1-dimensional and multidimensional CFD where the 1-dimensional model is used for the majority of the components and multidimensional CFD is used to generate the friction and heat transfer correlations for the components of interest. For example, the adiabatic pipes can be easily modeled by 1-dimensional approach whereas the horizontal heater and cooler section can be modeled by 3-dimensional CFD. Even for benchmarking of such codes simple models like the one proposed in chapter 4 would be useful.

1-dimensional lumped parameter methods are adequate for safety evaluations and gives conservative results, however 3-dimensional computations will reduce unnecessary conservatism and bring more accurate and valuable insight in certain cases. However, 3-dimensional numerical analysis requires huge resources in terms of time and computational power. For example, consider the reactor system, which consist of a large number of components such as reactor core, containment, steam drum, primary and secondary system etc. Simulation of the entire reactor system in 3-dimension is not always desirable for all the components of the reactor system. Therefore, it is possible to assume that in certain components of a reactor system 3-dimensional effect is less significant (such as flows within a coolant pipe) as compared to some other components (such as upper and lower plena, down comer and core of a reactor vessel etc). Therefore, a coupled 1-dimensional/2-dimensional or 3-dimensional simulation for supercritical natural circulation loops will be more effective compared to a full 3-dimensional simulation.

Presently there are not enough experimental data available to validate the proposed generalized correlation under supercritical pressure condition. Therefore, more experimental studies should be carried out to support the proposed correlation. In the present analysis at supercritical condition, linear relationship between dimensionless density and dimensionless enthalpy has been considered for finding out simple explicit steady state flow equation. However, it is also possible to obtain a better correlation for steady state flow under supercritical condition simply by considering better approximation between dimensionless density and dimensionless enthalpy.

In the present analysis static instability is investigated for the present natural circulation loop with supercritical water and CO_2. However, density wave instability is not studied for the supercritical fluids. Therefore, it is possible to study density wave instability for the present loop.

Appendix-1: Evaluation of overall heat transfer coefficient from test data

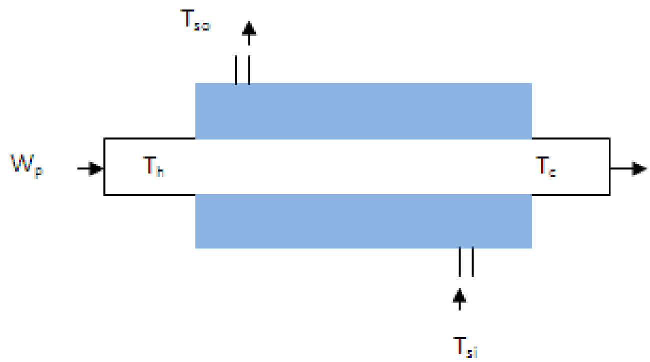

Figure A1: Evaluation of overall heat transfer coefficient

With the measured terminal temperatures, the Log Mean Temperature Difference (LMTD) is calculated [Ref. Figure: A1] as

$$LMTD = \frac{(T_h - T_{so}) - (T_c - T_{si})}{\ln\left(\frac{T_h - T_{so}}{T_c - T_{si}}\right)}$$

The heat removed by the cooler is estimated as $Q_c = W_p (C_p)_p (T_h - T_c)$, where the primary side flow rate (W_p) is estimated from heat balance using the measured heater power and temperature rise across the heater. Then the overall heat transfer coefficient is estimated as $U_i = \frac{Q_c}{A_i LMTD}$, where A_i is the heat transfer area in the cooler $(= \pi D_i L_c)$

Appendix -2: Derivation of conservation equations for 1-dimensional flow

Assumptions: (i) Fully developed flow through the pipe

(ii) Fluid is incompressible

A.2.1 Derivation of continuity equation

Rate of mass in - Rate of mass out =Rate of increase of mass

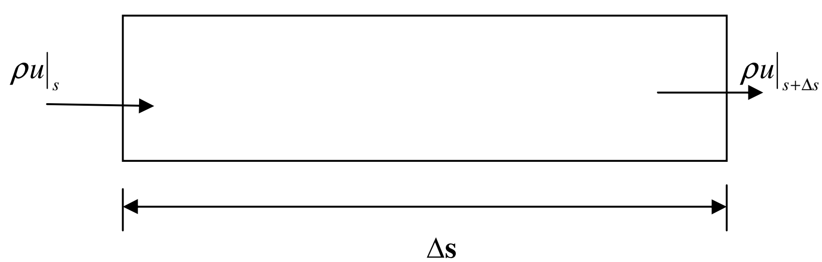

Figure A2: Elemental control volume used in the derivation of the general 1-dimensional continuity equation

$$\rho u|_s - \rho u|_{s+\Delta s} = \frac{\partial}{\partial t}(\rho \Delta s) \tag{1}$$

$$\frac{\partial \rho}{\partial t} + \frac{\partial}{\partial s}(\rho u) = 0 \tag{2}$$

We can write the above equation in terms of mass flow rate as

$$\frac{\partial \rho}{\partial t}+\frac{1}{A}\frac{\partial W}{\partial s}=0 \tag{3}$$

For incompressible flow, $\rho =$ constant

Therefore, $\frac{\partial W}{\partial s}=0$ (4)

or, W=constant

A.2.2 Derivation of momentum equation

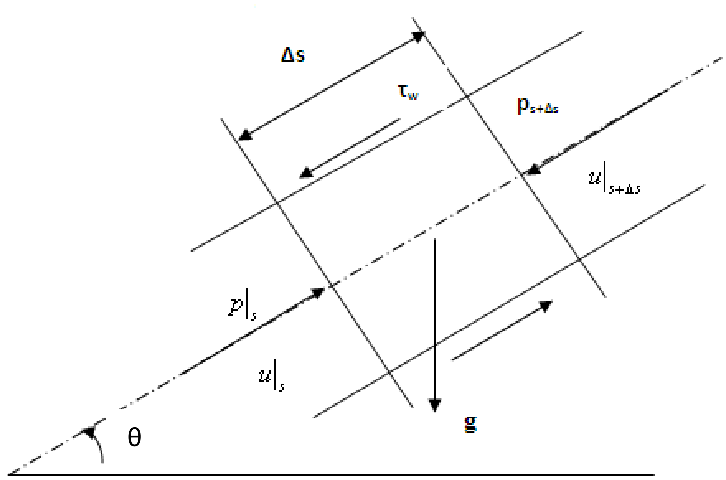

Figure A3: Elemental control volume used in the derivation of the general 1-dimensional momentum equation

For derivation of 1-dimensional momentum equation, an elemental control volume of length Δs has been considered as shown in ***Figure.A3.*** The inclination of the control volume with respect to the horizontal is given by the angle θ.

Sum of the applied forces = Rate of change of momentum

$$A\,p\big|_{s} - A\,p\big|_{s+\Delta s} + W\,u\big|_{s} - W\,u\big|_{s+\Delta s} - \tau_w \pi D \Delta s - \rho A \Delta s g \sin\theta = A\Delta s \rho \frac{\partial u}{\partial t} \tag{5}$$

$$-A\frac{\partial p}{\partial s}\Delta s - (\rho A u)\frac{\partial u}{\partial s}\Delta s - \tau_w \pi D \Delta s - \rho A \Delta s g \sin\theta = A\Delta s \rho \frac{\partial u}{\partial t} \tag{6}$$

Dividing throughout by AΔs, we can write the above equation as

$$-\frac{\partial p}{\partial s} - \frac{\partial\left(\rho u^2\right)}{\partial s} - \frac{\tau_w \pi D}{A} - \rho g \sin\theta = \rho \frac{\partial u}{\partial t} \tag{7}$$

Wall shear stress is given by $$\tau_w = \frac{f\rho u^2}{8} \tag{8}$$

Where, f is the Darcy-Weisbach friction factor. Substituting for wall shear stress in Eq. (7), we get

$$-\frac{\partial p}{\partial s} - \frac{\partial\left(\rho u^2\right)}{\partial s} - f\,\frac{\rho u^2}{8}\frac{\pi D}{A} - \rho g \sin\theta = \rho \frac{\partial u}{\partial t} \tag{9}$$

$$-\frac{\partial p}{\partial s}-\frac{\partial}{\partial s}\left(\rho\frac{W^2}{\rho^2A^2}\right)-f\frac{\rho}{8}\left(\frac{W}{\rho A}\right)^2\frac{P}{A}-\rho g\sin\theta=\rho\frac{\partial u}{\partial t} \quad (10)$$

$$\rho\frac{\partial}{\partial t}\left(\frac{W}{\rho A}\right)+\frac{\partial}{\partial s}\left(\frac{W^2}{\rho A^2}\right)=-\frac{\partial p}{\partial s}-\rho g\sin\theta-\frac{fW^2P}{8\rho A^3} \quad (11)$$

$$\frac{\partial}{\partial t}\left(\frac{W}{A}\right)+\frac{\partial}{\partial s}\left(\frac{W^2}{\rho A^2}\right)=-\frac{\partial p}{\partial s}-\rho g\sin\theta-\frac{fW^2}{2\rho D_hA^2} \quad (12)$$

Where $D_h=\frac{4A}{P}$ (13)

Eq. (12) can be written as

$$\frac{1}{A}\frac{\partial}{\partial t}W+\frac{1}{A^2}\frac{\partial}{\partial s}\left(\frac{W^2}{\rho}\right)=-\frac{\partial p}{\partial s}-\rho g\sin\theta-\frac{fW^2}{2\rho D_hA^2} \quad (14)$$

Integrating over the closed loop

$$\frac{L_t}{A}\frac{\partial W}{\partial t}+\frac{W^2}{A^2}\oint\partial v=-\oint\partial p-g\oint\rho dz-\frac{fW^2L_t}{2\rho D_hA^2} \quad (15)$$

Where dz=sinθds and for closed loop $\oint\partial v=0$ and $\oint\partial p=0$. The above equation can be written as $\frac{L_t}{A}\frac{dW}{dt}=-g\oint\rho dz-\frac{fW^2L_t}{2\rho D_hA^2}$ (16)

The friction head loss is only the part of the total head loss which must be overcome in pipe lines and other fluid flow circuits. Other losses may occur due to the presence of valves, elbows and any other fittings that involve a change in direction of flow or in the area of the flow passage. By considering the local pressure loss Eq. (16) can be written as

$$\frac{L_t}{A}\frac{dW}{dt} = -g\oint \rho dz - \frac{fW^2 L_t}{2\rho D_h A^2} - \frac{KW^2}{2\rho A^2} \tag{17}$$

A.2.3 Derivation of energy equation

Assumptions: Viscous dissipation and axial conduction effects are negligible.

(a) For heater

Assumptions: The heater is assumed to be supplied with a constant heat flux.

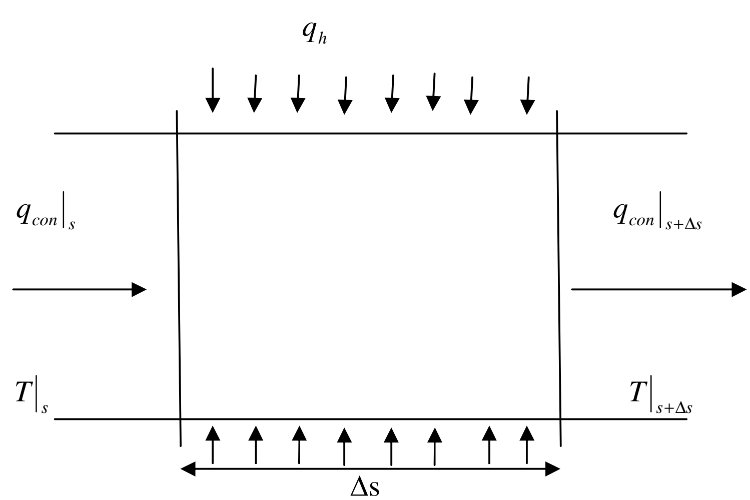

Figure A4: Elemental control volume used in the derivation of the general 1-dimensional energy equation for heater

$$WCpT\big|_{s} - WCpT\big|_{s+\Delta s} + q_{con}\big|_{s} A - q_{con}\big|_{s+\Delta s} A + q_h \pi D_i \Delta s = A\Delta s \rho \, Cp \frac{\partial T}{\partial t} \tag{18}$$

$$WCp\left(-\frac{\partial T}{\partial s}\Delta s\right) + A\left(-\frac{\partial q_{con}}{\partial s}\Delta s\right) + q_h \pi D_i \Delta s = A\Delta s \rho \, Cp \frac{\partial T}{\partial t} \tag{19}$$

Dividing throughout by AρΔsCp

$$\frac{\partial T}{\partial t} + \frac{W}{A\rho}\frac{\partial T}{\partial s} + \frac{1}{\rho \, Cp}\frac{\partial q_{con}}{\partial s} = \frac{q_h \pi D_i}{A\rho \, Cp} \tag{20}$$

We can write Eq. (20) as

$$\frac{\partial T}{\partial t} + \frac{W}{A\rho}\frac{\partial T}{\partial s} + \frac{1}{\rho \, Cp}\frac{\partial q_{con}}{\partial s} = \frac{q_h P}{A\rho \, Cp} \tag{21}$$

Where $q = -k\frac{\partial T}{\partial s}$ .Neglecting conduction part we can write the above equation as

$$\frac{\partial T}{\partial t} + \frac{W}{A\rho}\frac{\partial T}{\partial s} = \frac{q_h P}{A\rho \, Cp} \tag{22}$$

(b) For cooler

Assumptions: The cooler is assumed with constant rate of cooling water flow in the secondary side at a constant temperature, Ts.

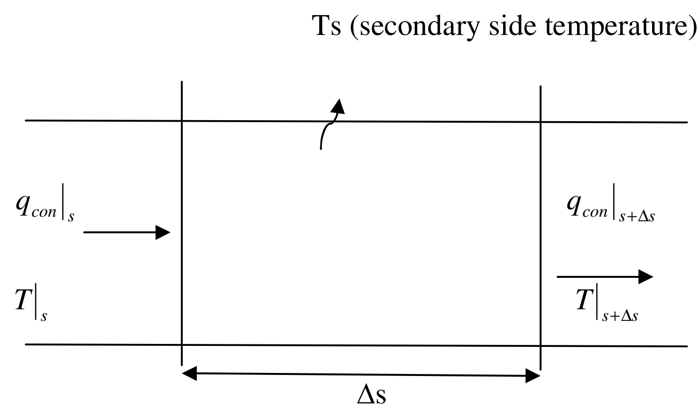

Figure A5: Elemental control volume used in the derivation of the general 1-dimensional energy equation for cooler

$$WCpT\big|_s - WCpT\big|_{s+\Delta s} + q_{con}\big|_s A - q_{con}\big|_{s+\Delta s} A - U(T - T_s)\pi D_i \Delta s = A\Delta s\rho\, Cp\frac{\partial T}{\partial t} \quad (23)$$

$$WCp\left(-\frac{\partial T}{\partial s}\Delta s\right) + A\left(-\frac{\partial q_{con}}{\partial s}\Delta s\right) - U(T - T_s)\pi D_i \Delta s = A\Delta s\rho\, Cp\frac{\partial T}{\partial t} \quad (24)$$

Dividing throughout by AρΔsCp

$$\frac{\partial T}{\partial t} + \frac{W}{A\rho}\frac{\partial T}{\partial s} + \frac{1}{\rho Cp}\frac{\partial q_{con}}{\partial s} = -\frac{U(T - T_s)\pi D_i}{A\rho\, Cp} \quad (25)$$

We can write Eq. (25) as

$$\frac{\partial T}{\partial t}+\frac{W}{A\rho}\frac{\partial T}{\partial s}+\frac{1}{\rho Cp}\frac{\partial q_{con}}{\partial s}=-\frac{U(T-T_s)P}{A\rho Cp} \tag{26}$$

Where $q=-k\frac{\partial T}{\partial s}$ .Neglecting conduction part we can write the above equation as

$$\frac{\partial T}{\partial t}+\frac{W}{A\rho}\frac{\partial T}{\partial s}=-\frac{U(T-T_s)P}{A\rho Cp} \tag{27}$$

(c) For pipes

Assumptions: Adiabatic condition is assumed in the flow pipes.

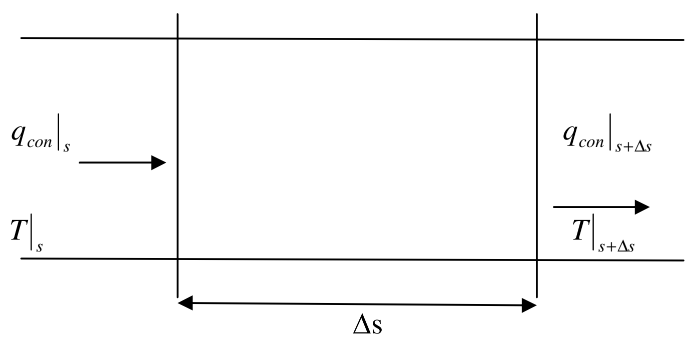

Figure A6: Elemental control volume used in the derivation of the general 1-dimensional energy equation for adiabatic pipes

$$WCpT|_s-WCpT|_{s+\Delta s}+q_{con}|_s A-q_{con}|_{s+\Delta s} A=A\Delta s\rho Cp\frac{\partial T}{\partial t} \tag{28}$$

$$WCp\left(-\frac{\partial T}{\partial s}\Delta s\right)+A\left(-\frac{\partial q_{con}}{\partial s}\Delta s\right)=A\Delta s\rho Cp\frac{\partial T}{\partial t} \tag{29}$$

Dividing throughout by AρΔsCp

$$\frac{\partial T}{\partial t}+\frac{W}{A\rho}\frac{\partial T}{\partial s}+\frac{1}{\rho Cp}\frac{\partial q_{con}}{\partial s}=0 \tag{30}$$

Where $q=-k\frac{\partial T}{\partial s}$ .Neglecting conduction part we can write the above equation as

$$\frac{\partial T}{\partial t}+\frac{W}{A\rho}\frac{\partial T}{\partial s}=0 \tag{31}$$

Appendix-3: Steady state experimental data generated for various orientations of the heater and cooler for subcritical pressure conditions

Table: A.3.1 Steady state data for HHHC orientation

Power, W	T_{mean}	T_{hi}	T_{ho}	W_{ss}	Gr_m	$Gr_m(D/L_t)$	Re
225.4	29.6	24.4	34.8	0.005175	2.11E+10	1.82E+07	4.82E+02
759.0	46.1	38.3	53.9	0.011665	2.81E+11	2.59E+08	1.53E+03
1251.0	59.0	49.2	68.8	0.015245	1.05E+12	9.04E+08	2.61E+03
1716.6	68.3	56.9	79.6	0.018168	2.10E+12	1.97E+09	3.86E+03
2233.6	77.7	64.9	90.5	0.020918	4.72E+12	4.41E+09	6.38E+03
2540.8	82.1	68.5	95.6	0.022374	6.66E+12	6.23E+09	6.52E+03
2734.2	85.9	71.8	99.9	0.023202	8.20E+12	7.68E+09	7.20E+03
3096.5	89.6	74.6	104.5	0.024673	1.06E+13	9.89E+09	8.54E+03
3253.4	93.1	77.7	108.5	0.025189	1.22E+13	1.14E+10	9.12E+03
3507.1	96.1	80.3	111.9	0.026320	1.55E+13	1.44E+10	1.02E+04

Table: A.3.2 Steady state data for HHVC orientation

Power, W	T_{mean}	T_{hi}	T_{ho}	W_{ss}	Gr_m	$Gr_m(D/L_t)$	Re
504.4	42.9	36.1	49.7	0.008856	9.06E+10	8.42E+07	1.29E+03
749.5	52.5	45.6	61.3	0.011433	2.63E+11	2.48E+08	2.01E+03
999.8	60.1	51.2	69.0	0.013442	5.34E+11	5.03E+08	2.64E+03
1263.4	70.4	60.3	80.4	0.015061	1.22E+12	1.14E+09	3.41E+03
1497.8	75.3	64.6	86.0	0.016717	1.91E+12	1.82E+09	4.06E+03
1775.5	82.9	71.3	94.5	0.018256	3.13E+12	2.99E+09	4.84E+03
2000.3	87.8	75.4	100.1	0.019300	4.17E+12	3.98E+09	5.43E+03
2265.4	94.8	81.7	107.9	0.020574	6.33E+12	6.04E+09	6.27E+03
2521.8	99.6	85.8	113.3	0.021832	8.66E+12	8.27E+09	7.00E+03
2790.3	105.4	90.9	119.8	0.022906	1.22E+13	1.16E+10	7.84E+03
3035.6	109.5	94.5	124.5	0.023977	1.47E+13	1.40E+10	8.53E+03
3051.6	110.6	95.6	125.6	0.024136	1.53E+13	1.46E+10	8.68E+03
3275.9	114.8	99.2	130.3	0.024919	1.80E+13	1.72E+10	9.29E+03
3522.5	118.9	103.0	134.8	0.026085	2.27E+13	2.17E+10	1.01E+04

Table: A.3.3 Steady state data for VHHC orientation

Power, W	T_{mean}	T_{hi}	T_{ho}	W_{ss}	Gr_m	$Gr_m(D/L_t)$	Re
244.9	32.3	26.3	38.2	0.004937	1.72E+10	1.40E+07	5.81E+02
265.1	32.5	24.4	40.6	0.003915	1.75E+10	1.32E+07	4.51E+02
501.2	38.5	29.5	47.5	0.006670	5.84E+10	5.89E+07	8.84E+02
746.5	47.4	38.7	56.1	0.010279	1.82E+11	1.63E+08	1.61E+03
1004.4	50.9	39.9	61.9	0.010964	2.84E+11	2.49E+08	1.81E+03
1232.3	60.4	49.6	71.1	0.013683	6.81E+11	6.06E+08	2.65E+03
1546.9	63.2	49.7	76.6	0.013791	9.33E+11	7.93E+08	2.75E+03
1749.3	59.9	49.8	69.9	0.020732	9.67E+11	8.95E+08	4.01E+03
2042.4	71.2	56.2	86.1	0.016318	1.87E+12	1.70E+09	3.65E+03
2266.7	75.8	59.8	91.7	0.016944	2.73E+12	2.48E+09	4.06E+03
2564.9	78.9	63.2	94.7	0.019426	3.57E+12	3.24E+09	4.89E+03
2797.9	83.8	66.3	101.3	0.019072	4.85E+12	4.39E+09	5.06E+03
3067.2	86.3	69.3	103.2	0.021530	5.87E+12	5.33E+09	5.91E+03

Table: A.3.4 Steady state data for VHVC orientation

Power, W	T_{mean}	T_{hi}	T_{ho}	W_{ss}	Gr_m	$Gr_m(D/L_t)$	Re
249.5	35.9	27.9	44.0	0.003704	1.54E+10	1.27E+07	5.01E+02
250.6	29.9	21.8	37.9	0.00372	8.25E+09	6.70E+06	4.28E+02
509.9	44.1	32.6	55.5	0.005325	4.99E+10	5.02E+07	8.05E+02
735.4	50.7	40.3	61.0	0.008511	1.28E+11	1.16E+08	1.45E+03
1000.3	55.4	44.3	66.5	0.010766	2.20E+11	1.98E+08	1.99E+03
1253.6	65.9	53.5	78.4	0.012042	5.08E+11	4.61E+08	2.58E+03
1556.9	74.7	60.9	88.4	0.0135	9.70E+11	8.75E+08	3.27E+03
1752.3	80.7	66.1	95.3	0.014321	1.36E+12	1.23E+09	3.75E+03
2039.7	85.9	70.2	101.7	0.015437	2.02E+12	1.87E+09	4.29E+03
2342.01	96.4	79.2	113.6	0.016171	3.40E+12	3.16E+09	5.03E+03
2498.7	96.6	79.2	114.0	0.017075	3.74E+12	3.48E+09	5.37E+03
2756.3	103.5	85.3	121.6	0.018023	4.90E+12	4.56E+09	6.04E+03
2996.0	107.0	88.2	125.8	0.018870	6.35E+12	5.91E+09	6.58E+03

Appendix-4: Steady state experimental data for supercritical CO_2

Table: A.4.1 HHHC orientation (supercritical CO_2)

Power, W	T_{hi}	T_{ho}	T_{mean}	Re	Gr_m	$Gr_m(D/L_t)$
203.7	18.2	21.4	19.8	2.20E+04	6.23E+14	6.05E+11
288.2	22.1	25.3	23.7	3.18E+04	1.2E+15	1.17E+12
387.9	18.2	22.2	20.2	3.62E+04	1.33E+15	1.29E+12
504.7	25.8	28.9	27.4	5.63E+04	3.02E+15	2.93E+12
504.8	22.9	26.7	24.8	5.01E+04	2.47E+15	2.4E+12
590.5	23.5	28.1	25.8	4.77E+04	1.48E+15	1.44E+12
702.9	26.3	30.7	28.5	5.74E+04	4.79E+15	4.65E+12
785.3	26.9	30.9	28.9	6.78E+04	5.63E+15	5.47E+12
907.9	29.9	33.7	31.8	7.55E+04	9.04E+15	8.77E+12
977.5	27.2	32.1	29.7	7.21E+04	7.61E+15	7.39E+12
1103.0	32.2	35.7	33.9	8.03E+04	1.49E+16	1.45E+13
1184.1	31.1	35.2	33.2	8.15E+04	1.42E+16	1.38E+13
1406.2	32.2	35.9	34.1	9.45E+04	1.97E+16	1.91E+13
1691.8	47.6	72.8	60.2	1.17E+05	3.42E+16	3.32E+13
1904.0	48.9	77.9	63.4	1.24E+05	3.51E+16	3.4E+13
1908.6	53.2	89.7	71.5	1.12E+05	2.72E+16	2.64E+13
1916.0	48.1	76.5	62.3	1.24E+05	3.65E+16	3.54E+13
2077.1	52.9	91.1	72.0	1.18E+05	2.94E+16	2.85E+13
2090.6	54.8	97.3	76.1	1.11E+05	2.62E+16	2.54E+13
2197.7	51.8	89.9	70.9	1.23E+05	3.25E+16	3.16E+13
2287.1	54.9	99.3	77.1	1.18E+05	2.81E+16	2.72E+13
2293.2	52.9	94.8	73.9	1.21E+05	3.1E+16	3.01E+13
2391.7	54.3	98.7	76.5	1.23E+05	3.01E+16	2.92E+13

Table: A.4.2 HHVC orientation (supercritical CO_2)

Power, W	T_{hi}	T_{ho}	T_{mean}	Re	Gr_m	$Gr_m(D/L_t)$
101.5	17.7	19.9	18.8	1.38E+04	1.6E+14	1.55E+11
189.7	16.2	19.7	17.9	1.89E+04	3.37E+14	3.27E+11
300.0	20.7	24.8	22.8	2.66E+04	7.92E+14	7.69E+11
395.9	20.5	25.1	22.8	3.43E+04	1.07E+15	1.04E+12
491.5	18.2	23.6	20.9	3.51E+04	1.13E+15	1.1E+12
499.6	24.0	28.1	26.1	4.41E+04	1.84E+15	1.78E+12
587.9	20.2	25.9	23.1	3.97E+04	1.67E+15	1.62E+12
590.3	25.2	29.3	27.3	5.26E+04	2.32E+15	2.25E+12
700.4	27.4	32.0	29.7	5.08E+04	3.73E+15	3.62E+12
806.5	25.8	31.0	28.4	5.63E+04	3.61E+15	3.51E+12
820.1	28.0	33.1	30.6	5.43E+04	4.52E+15	4.39E+12
900.6	32.4	35.4	33.9	7.78E+04	8.04E+15	7.8E+12
987.2	31.3	35.5	33.4	6.70E+04	7.79E+15	7.56E+12
1000.1	29.1	33.8	31.5	6.97E+04	6.18E+15	6E+12
1099.2	33.5	36.6	35.1	7.78E+04	1.21E+16	1.18E+13
1100.1	33.6	37.1	35.4	7.18E+04	1.19E+16	1.15E+13
1199.3	31.9	36.5	34.2	6.83E+04	1.07E+16	1.04E+13
1216.9	34.7	37.6	36.2	8.53E+04	1.54E+16	1.49E+13
1405.6	36.3	38.8	37.6	1.05E+05	2.16E+16	2.1E+13
1698.0	46.8	75.6	61.2	1.03E+05	2.23E+16	2.17E+13
1890.9	49.3	88.9	69.1	9.69E+04	1.95E+16	1.89E+13
1894.7	47.0	79.3	63.2	1.05E+05	2.41E+16	2.34E+13
1990.9	44.5	70.8	57.7	1.15E+05	3.09E+16	3E+13
2090.6	48.9	89.7	69.3	1.03E+05	2.21E+16	2.14E+13
2095.4	50.1	93.9	72.0	9.89E+04	2.05E+16	1.99E+13
2186.7	49.6	93.1	71.4	1.04E+05	2.18E+16	2.12E+13
2200.5	44.8	73.4	59.1	1.23E+05	3.12E+16	3.03E+13

Table: A.4.3 VHHC orientation (supercritical CO_2)

Power, W	T_{hi}	T_{ho}	T_{mean}	Re	Gr_m	$Gr_m(D/L_t)$
248.9	20.6	23.6	22.1	2.86E+04	5.55E+14	5.38E+11
249.9	23.4	27.0	25.2	2.38E+04	6.79E+14	6.59E+11
353.5	21.7	25.3	23.5	3.57E+04	9.09E+14	8.82E+11
450.6	24.5	28.7	26.6	3.97E+04	1.48E+15	1.43E+12
499.9	26.9	31.5	29.2	4.02E+04	2.04E+15	1.98E+12
549.7	24.8	29.2	27.0	4.71E+04	1.89E+15	1.84E+12
549.9	22.5	27.5	25.0	4.16E+04	1.64E+15	1.59E+12
747.8	25.6	30.4	28.0	5.92E+04	2.86E+15	2.78E+12
756.7	28.7	33.7	31.2	5.29E+04	3.82E+15	3.71E+12
951.7	29.8	34.9	32.4	6.37E+04	5.49E+15	5.32E+12
1044.7	31.5	36.5	34.0	6.67E+04	7.26E+15	7.05E+12
1156.2	32.7	37.1	34.9	7.87E+04	8.99E+15	8.73E+12
1350.9	35.9	39.9	37.9	7.99E+04	1.66E+16	1.61E+13
1450.4	40.2	42.7	41.5	1.38E+05	3.04E+16	2.95E+13
1652.9	41.1	44.4	42.8	1.77E+05	3.75E+16	3.64E+13
1697.5	45.8	76.5	61.2	1.12E+05	1.93E+16	1.88E+13
1706.6	44.2	65.2	54.7	9.52E+04	2.98E+16	2.91E+13
1789.4	43.9	65.8	54.9	9.56E+04	3.12E+16	3.05E+13
1793.2	46.9	82.1	64.5	1.05E+05	1.78E+16	1.74E+13
1917.2	48.1	79.3	63.7	9.86E+04	2.59E+16	2.53E+13
2012.0	48.9	81.5	65.2	1.04E+05	2.6E+16	2.53E+13

Table: A.4.4 VHVC orientation (supercritical CO_2)

Power, W	T_{hi}	T_{ho}	T_{mean}	Re	Gr_m	$Gr_m(D/L_t)$
205.8	19.4	23.6	21.5	1.65E+04	2.29E+14	2.22E+11
290.4	23.1	27.0	25.1	2.55E+04	4.44E+14	4.31E+11
293.3	25.9	30.1	28.0	2.14E+04	5.68E+14	5.52E+11
405.6	19.1	24.5	21.8	2.85E+04	5.11E+14	4.96E+11
421.2	21.9	27.0	24.5	3.06E+04	6.46E+14	6.27E+11
497.4	28.4	32.6	30.5	3.79E+04	1.32E+15	1.28E+12
499.3	25.9	30.4	28.2	3.69E+04	1.05E+15	1.02E+12
690.4	30.9	34.6	32.8	5.46E+04	2.5E+15	2.43E+12
691.1	28.4	32.9	30.7	5.07E+04	1.93E+15	1.87E+12
808.9	28.7	34.3	31.5	4.48E+04	2.51E+15	2.44E+12
907.6	31.2	34.9	33.1	7.03E+04	3.49E+15	3.38E+12
995.3	28.9	34.6	31.8	5.46E+04	2.98E+15	2.89E+12
1017.6	31.2	35.9	33.6	5.59E+04	4.27E+15	4.14E+12
1205.6	33.2	36.9	35.1	7.09E+04	6.52E+15	6.32E+12
1207.8	32.4	36.6	34.5	6.77E+04	5.9E+15	5.73E+12
1303.7	36.3	38.5	37.4	9.00E+04	1.19E+16	1.15E+13
1401.1	34.6	37.9	36.3	7.24E+04	9.87E+15	9.58E+12
1411.7	35.9	38.2	37.1	9.92E+04	1.21E+16	1.17E+13
1600.7	36.6	39.1	37.9	1.04E+05	1.61E+16	1.56E+13
1700.0	38.1	51.4	44.8	7.75E+04	1.91E+16	1.86E+13
1803.7	37.6	49.1	43.4	7.85E+04	2.12E+16	2.06E+13
1899.5	39.4	57.9	48.7	8.57E+04	1.88E+16	1.83E+13
1999.6	41.3	66.7	54.0	9.43E+04	1.62E+16	1.58E+13

Appendix-5: Steady state experimental data generated for supercritical water

Table: A.5.1 HHHC orientation (supercritical water)

Power, W	T_{hi}	T_{ho}	T_{mean}	Re	Gr_m	$Gr_m(D/L_t)$
4500	264.9	292.4	278.7	3.31E+04	8.33E+14	8.13E+11
5000	275.7	300.8	288.3	3.79E+04	1.05E+15	1.03E+12
5500	295.3	319.1	307.2	4.45E+04	1.51E+15	1.47E+12
5500	289.7	315.6	302.7	4.08E+04	1.42E+15	1.39E+12
6000	324.4	348.0	336.2	4.70E+04	2.67E+15	2.6E+12
6100	319.5	346.6	333.1	4.21E+04	2.54E+15	2.47E+12
6500	341.4	354.5	347.9	8.75E+04	3.56E+15	3.46E+12
7000	396.5	422.5	409.5	1.19E+05	4.04E+15	3.92E+12
7000	367.8	376.4	372.1	6.66E+04	8.58E+15	8.32E+12
7000	369.6	379.7	374.7	5.75E+04	8.74E+15	8.48E+12
7500	386.3	401.3	393.8	1.43E+05	6.66E+15	6.47E+12
8000	389.8	411.2	400.5	1.22E+05	5.84E+15	5.67E+12

Appendix-6: Steady state experimental data (Deeply subcritical condition)

Table: A.6.1 Steady state data for HHHC orientation

[Water at subcritical pressure (3.0-15.0MPa)]

Power, W	T_{hi}	T_{ho}	T_{mean}	Re	Gr_m	$Gr_m(D/L_t)$
500.0	46.0	55.9	50.9	2.06E+03	2.68E+11	2.61E+08
1000.0	69.8	81.6	75.7	4.92E+03	1.8E+12	1.76E+09
1400.0	87.1	102.4	94.8	6.65E+03	5.86E+12	5.72E+09
1500.0	81.5	96.4	88.9	6.87E+03	4.5E+12	4.39E+09
2000.0	107.7	126.0	116.9	9.83E+03	1.84E+13	1.8E+10
2233.6	64.9	90.5	77.7	6.37E+03	4.72E+12	4.61E+09
2540.8	68.5	95.6	82.1	6.53E+03	6.66E+12	6.5E+09
2734.2	71.8	99.9	85.9	7.21E+03	8.2E+12	8.01E+09
3096.5	74.6	104.5	89.6	8.57E+03	1.06E+13	1.03E+10
3253.4	77.7	108.5	93.1	9.17E+03	1.22E+13	1.19E+10
3507.1	80.3	111.9	96.1	1.03E+04	1.55E+13	1.51E+10
4000.0	195.5	218.0	206.8	2.76E+04	2.76E+14	2.7E+11
4500.0	196.9	221.2	209.1	2.89E+04	3.48E+14	3.4E+11
4500.0	214.3	237.9	226.1	3.17E+04	4.28E+14	4.17E+11
5000.0	231.2	254.8	243.0	3.69E+04	6.26E+14	6.11E+11
5500.0	231.1	256.4	243.8	3.79E+04	7.11E+14	6.94E+11
5500.0	250.6	274.6	262.6	4.17E+04	9.44E+14	9.21E+11
6000.0	250.8	276.5	263.7	4.25E+04	1.03E+15	1.01E+12
6000.0	261.9	285.9	273.9	4.65E+04	1.23E+15	1.2E+12
7000.0	294.2	317.3	305.8	5.61E+04	2.37E+15	2.31E+12

Table: A.6.2 Steady state data for HHVC orientation

[Water at subcritical pressure (3.0MPa)]

Power, W	T_{hi}	T_{ho}	T_{mean}	Re	Gr_m	$Gr_m(D/L_t)$
1497.8	64.6	86.0	75.3	4.05E+03	1.91E+12	1.82E+09
1775.5	71.3	94.5	82.9	4.84E+03	3.13E+12	2.99E+09
2000.3	75.4	100.1	87.8	5.43E+03	4.17E+12	3.98E+09
2265.4	81.7	107.9	94.8	6.27E+03	6.33E+12	6.04E+09
2521.8	85.8	113.3	99.6	7.00E+03	8.66E+12	8.27E+09
2790.3	90.9	119.8	105.4	7.84E+03	1.22E+13	1.16E+10
3035.6	94.5	124.5	109.5	8.53E+03	1.47E+13	1.40E+10
3051.6	95.6	125.6	110.6	8.68E+03	1.53E+13	1.46E+10
3275.9	99.2	130.3	114.8	9.29E+03	1.80E+13	1.72E+10
3522.5	103.0	134.8	118.9	1.01E+04	2.27E+13	2.17E+10

Table: A.6.3 Steady state data for VHHC orientation

[Water at subcritical pressure (3.0MPa)]

Power, W	T_{hi}	T_{ho}	T_{mean}	Re	Gr_m	$Gr_m(D/L_t)$
2266.7	59.8	91.7	75.8	4.06E+03	2.73E+12	2.48E+09
2564.9	63.2	94.7	78.9	4.89E+03	3.57E+12	3.24E+09
2797.9	66.3	101.3	83.8	5.06E+03	4.85E+12	4.39E+09
3067.2	69.3	103.2	86.3	5.91E+03	5.87E+12	5.33E+09

Table: A.6.4 Steady state data for VHVC orientation

[Water at subcritical pressure (3.0MPa)]

Power, W	T_{hi}	T_{ho}	T_{mean}	Re	Gr_m	$Gr_m(D/L_t)$
2039.7	70.2	101.7	85.9	4.29E+03	2.02E+12	1.87E+09
2342.0	79.2	113.6	96.4	5.03E+03	3.4E+12	3.16E+09
2498.7	79.2	114.0	96.6	5.37E+03	3.74E+12	3.48E+09
2756.3	85.3	121.6	103.5	6.04E+03	4.9E+12	4.56E+09
2996.0	88.2	125.8	107.0	6.58E+03	6.35E+12	5.91E+09

Table: A.6.5 Steady state data for HHHC orientation (supercritical water)

Power, W	T_{hi}	T_{ho}	T_{mean}	Re	Gr_m	$Gr_m(D/L_t)$
3500	208.2	227.7	217.9	2.89E+04	2.71E+14	2.65E+11
4000	236.2	256.9	246.6	3.39E+04	4.77E+14	4.66E+11
4500	254.7	275.2	264.9	3.98E+04	6.69E+14	6.53E+11
5000	269.4	290.6	280.0	4.44E+04	9.42E+14	9.19E+11

Table: A.6.6 Steady state data for HHHC orientation (supercritical CO_2)

Power, W	**T_{hi}**	**T_{ho}**	**T_{mean}**	**Re**	**Gr_m**	**$Gr_m(D/L_t)$**
50.1	18.0	18.5	18.3	1.43E+04	5.72E+13	5.59E+10
50. 8	15.7	16.3	16.0	1.42E+04	5.52E+13	5.38E+10
76.0	17.7	18.5	18.1	2.14E+04	1.34E+14	1.31E+11
101.5	16.8	18.0	17.4	2.43E+04	2.07E+14	2.02E+11
106.9	16.8	18.0	17.4	2.59E+04	2.41E+14	2.36E+11
106.9	17.0	18.3	17.7	2.48E+04	2.43E+14	2.38E+11

Appendix-7: Steady state experimental data (Deeply supercritical condition)

Table: A.7.1 Steady state data for HHHC orientation (supercritical water)

Power, W	T_{hi}	T_{ho}	T_{mean}	Re	Gr_m	$Gr_m(D/L_t)$
6000	388.8	417.3	403.1	7.76E+04	4.12E+15	4.02E+12
6500	390.2	421.2	405.7	8.39E+04	4.13E+15	4.03E+12
6500	391.0	416.0	403.5	8.87E+04	4.87E+15	4.75E+12
7000	394.1	445.8	419.9	6.69E+04	3.25E+15	3.17E+12
7000	392.7	429.0	410.9	8.31E+04	4.05E+15	3.95E+12
7000	386.0	426.8	406.4	6.86E+04	4.24E+15	4.14E+12
7500	386.0	415.6	400.8	8.61E+04	5.5E+15	5.37E+12
7500	392.3	432.4	412.4	8.21E+04	4.17E+15	4.07E+12
8000	388.8	425.4	407.1	8.54E+04	5.06E+15	4.94E+12

APPENDIX -8
List of own publications

(i) Swapnalee B.T., Vijayan P.K., 2011, A generalized flow equation for single-phase natural circulation loops obeying multiple friction laws, International Journal of Heat and Mass Transfer 54, 2618-2629.

(ii) B.T.Swapnalee, P.K.Vijayan, M. Sharma, D.S. Pilkhwal, 2012, Steady state flow and static instability of supercritical natural circulation loops, Nuclear Engineering and Design, 245, 99-112.

(iii) Swapnalee B.T., P.K.Vijayan, 2010, Simulation of single-phase natural circulation instability in a rectangular loop using CFD code PHOENICS, Proceedings of the 37th National and 4th International Conference on Fluid Mechanics and Fluid Power, IIT Madras, Chennai, India.

(iv) B.T.Swapnalee, P.K.Vijayan, M. Sharma, D.S. Pilkhwal, D. Saha, R.K. Sinha, 2011, Steady state performance of subcritical and supercritical pressure natural circulation in the same test facility, Proceedings of 19th International Conference on Nuclear Engineering (ICONE19), Chiba, Japan.

(v) P.K.Vijayan, B.T.Swapnalee, M. Sharma, D.S. Pilkhwal, D. Saha, R.K. Sinha, 2011, Experimental investigations on the steady state and stability behavior of supercritical pressure natural circulation, 14th International Topical Meeting on Nuclear Reactor Thermal Hydraulics (NURETH-14), Toronto, Ontario, Canada.

(vi) Swapnalee B.T., P.K.Vijayan, 2010, Simulation of single-phase natural circulation instability in a rectangular loop using CFD code PHOENICS, Poster presentation on 20th National and 9th International ISHMT-ASME Heat and Mass Transfer Conference, Mumbai, India.

REFERENCES

Alstad, C. D., Isbin, H. S., Amundson, N. R., 1955, *Transient behavior of single phase natural circulation loop systems, A. I. Ch. E. Journal, 1(4) , 417-425.*

Ambrosini, W., Forgione, N., Ferreri, J. C., Bucci, M., 2004, *The effect of wall friction in single-phase natural circulation stability at the transition between laminar and turbulent flow, Annals of Nuclear Energy 31, 1833-1865.*

Ambrosini. W., Ferreri, J. C., 2000, *Stability analysis of single-phase thermosyphon loops by finite difference methods, Nuclear Engineering and Design, 201, 11-23.*

Ambrosini, W., Forgione, N., Ferreri, J.C., Bucci, M., 2004, *The effect of wall friction in single-phase natural circulation stability at the transition between laminar and turbulent flow, Annals of Nuclear Energy 31, 1833-1865.*

Ambrosini, W., Forgione, N., Oriolo, F., Semeraro, E., Tarantino, M., 2009, *Experimental Study on natural circulation and air- injection enhanced circulation with different fluids, Journal of Engineering for Gas Turbine and Power 131, 032902-(1-7).*

Ambrosini, W., 2007, *On the analogies in the dynamic behavior of heated channels with boiling and supercritical fluids, Nuclear Engineering and Design, 237, 1164-1174.*

Ambrosini, W., Sharabi, M., 2008, *Dimensionless parameters in stability analysis of heated channels with fluids at supercritical pressures, Nuclear Engineering and Design, 238, 1917-1929.*

Bau, H. H., Torrance, K.E., 1981, *On the stability and flow reversal of an asymmetrically heated open convection loop*, J. Fluid Mechanics 106, 417-433.

Bau, H. H., Torrance, K. E., 1981, *Transient and steady state behavior of an open, symmetrically heated, free convection loop, International Journal of Heat and Mass Transfer 24 (4), 597-609.*

Bodkha, K., *Study on stabilization of single-phase natural circulation system using mechanical gadgets, M. Tech. thesis, Homi Bhabha National Institute, Mumbai, India, 2009.*

Boure J.A., Bergles, A.E. and Tong L.S., 1973, *Review of two phase flow instability, Nuclear Engineering and Design, 25, 165-192.*

Chatoorgoon, V., 2001, *Stability of supercritical fluid flow in a single channel natural convection loop, International journal of heat and mass transfer, 44, 1963-1972.*

Creveling, H. F., De Paz. J. F., Baladi, J. Y., Schoenhals, R.J., 1975, *Stability characteristic of a single-phase free convection loop, J. Fluid Mechanics, 67, 65-84.*

Driscoll, M.J., Hejzlar, P., 2004, *300MWe Supercritical CO_2 plant layout and design, Report No: MIT-GFR-014, MIT Nuclear Engineering Department, June.*

Dubey, P., Rao, G. S. S. P., Pilkhawal, D. S., Vijayan, P. K., Saha, D." *Analysis of experimental data on two-phase natural circulation from the flow pattern transition instability studies facility at Apsara reactor", BARC/2004/E/031, Bhabha Atomic Research Centre, Mumbai, India, 2004.*

Dulera, A. Basak, R. K. Sinha, 2005, *Options for design of 600MWth Indian high temperature reactor for hydrogen production, INSAC-2005, BARC, Mumbai, November-15.*

Garibaldi, P., *Single phase natural circulation loops: Effects of geometry and heat sink temperature on dynamic behavior and stability, Ph. D. thesis.*

Generation IV International Forum (GIF), 2002. *A technology roadmap for the Generation IV Nuclear Energy Systems, GIF-002-00.*

Green, D. W., Robert H. Perry, *Perry's Chemical engineer's handbook", Mc Graw-Hill, 8th edition (2007), pp. 6.1-6.56.*

Greif, R., 1988, *Natural circulation loops, Journal of Heat Transfer.110, 1243-1258.*

Hallinan, K. P., Viskanta, R., *Heat transfer from a rod bundle under natural circulation conditions, NUREG/CR-4556.*

Hamilton, D. C., Lynch, F. E., Palmer, L. D., *The nature of flow of ordinary fluids in a thermal convection harp, ORNL-1624, March-16, 1954.*

Harden, D.G., *Transient behavior of a Natural-Circulation Loop operating near the thermodynamic critical point, ANL-6710 (May 1963).*

Ho, C. J., Chiou, S. P., Hu, C.S., 1997, *Heat transfer characteristic of a rectangular natural circulation loop containing water near its density extreme, International Journal of Heat and Mass Transfer 40 (15), 3553-3558.*

Holman, J. P, Boggs, J. H., 1960, *Heat transfer to Freon 12 near the critical state in a natural circulation loop, Journal of Heat Transfer 82, 221-226.*

Huang, B. J., Zelaya, R., 1988, *Heat transfer behavior of a rectangular Thermosyphon loop, Journal of Heat Transfer, 110, 487-493.*

International Atomic Energy Agency, *Thermo hydraulic relationships for advanced water-cooled reactors, IAEA-TECDOC-1203, April (2001), pp.118-119.*

International Atomic Energy Agency, *Design Features to Achieve Defence in Depth in Small and Medium Sized Reactors, IAEA Nuclear Energy Series, No.NP-T-2.2, Annex IX, Vienna (2009), pp.228-245.*

Jain R., Corradini M.L., 2006, *A linear stability analysis for natural circulation loops under supercritical conditions, Nuclear Technology 155, 312-323.*

Japikse**,** 1973*, Advances in thermosyphon technology. In: Irvine, T.F. Jr, Hartnett, J.P. (Eds.) Advances in Heat Transfer, vol.9.Academic Press, New York, pp.1-111.*

Knudsen J. G., Katz, D. L., *Fluid Dynamics and Heat Transfer, International Student Edition, McGraw-hill book Company, New York St. Louis San Francisco, Tokyo,1958, pp.146-212.*

Kostin, V. I., Samoilov, O. B., Vavilkin, V. N. , Panov, Yu. K. , Kurachenkov, A. V., Bolshukhin, M.A., Alekeev, V. I. , Shmelev, I. V., Baranaev, Yu. D., Pekanov, A. A., *Small floating nuclear power plants with ABV reactors for electric power generation, heat production and seawater desalination, Fifteenth Annual Conference of the Indian Nuclear Society, INSAC-2004, November 15-17, Mumbai, India.*

Lomperski, S., Cho, D., 2004, *Stability of a natural circulation loop with a fluid heated through the thermo dynamic pseudo critical point, proceedings of ICAPP'04, Pittsburgh, PA USA, June 13-17.*

Manish S., Vijayan P.K. Pilkhwal D.S, Saha D, Sinha R.K., 2010, *Linear and nonlinear stability analysis of a supercritical natural circulation loop, Journal of Engineering for Gas Turbines and Power, Vol.132/102904-(1-9)(October).*

MAZZI, R., 2005, *CAREM: An innovative integrated PWR, 18th International Conference on Structural Mechanics in Reactor Technology (SMiRT-18), Beijing, China, August 7-12, SMiRT18-S01-2.*

Mertol, A., Greif, R., 1985, *A review of natural circulation loops. In: Kakac, S.,Aung, W. Viskanta R. (Eds), Natural Convection: Fundamentals and Applications. Hemisphere, New York, pp.1022-1071.*

Misale, M., Tagaliafico, L., Tanda, G., 1991, *Experiments in a free convection rectangular loop, in Proceedings of the 4th International Symposium on transport Phenomena in Heat and Mass Transfer, pp.203-211, Sydney, Australia, July.*

Misale, M., Ruffino P., Frogheri M., 1999, *The influence of the wall thermal capacity and axial conduction over a single-phase natural circulation loop: 2D numerical study, Eurotherm seminar no.63, Single and two-phase natural circulation, 177-186.*

Misale, M., Garibaldi, P., Passos, J. C., G.G.de Bitencourt, 2007, *Experimental Thermal and Fluid Science 31 (8), 1111-1120.*

Misale, M., Garibaldi, P., 2010, *Dynamic behavior of a rectangular Single Phase Natural Circulation Loop: Influence of Loop inclination, Proceedings of 20th National and 9th International ISHMT-ASME Heat and Mass Transfer Conference, 4-6 January, Mumbai, India.*

Modro, S. M., Fisher, J., Weaver, K., Babka, P. Reyes, J., Groome, J. , Wilson, G., 2002, *Generation-IV Multi-Application Small Light Water Reactor (MASLWR), Proceedings of ICONE-10, Tenth International Conference on nuclear energy, April 14-18, Arlington, Virginia, USA.*

Mousavian, S. K., Misale, M., Auria, F. D', Salehi, M. A., 2004, *Transient and stability analysis in single-phase natural circulation, Annals of Nuclear Energy 31 (10), 1177-1198.*

Nishihara, T., 1997, *Oscillatory instability of a single-phase natural circulation loop, in proceedings of the 8th International Topical Meeting on Nuclear Reactor Thermal-Hydraulics (NURETH'97), pp.839-847, Kyoto, Japan, September-October.*

Pioro, I. L. and Duffey R.B., *Heat transfer and hydraulic resistance at supercritical pressures in power engineering applications, ASME press, Three Park Avenue, New York, 2007.*

Pioro, Igor L., Romney, B. Duffey, 2005, *Experimental heat transfer in supercritical water flowing inside channels (survey), Nuclear Engineering and Design, 235, 2407-2430.*

Pioro, Igor L., Khartabil, Hussam F., Duffey, Romney B., 2004, *Heat transfer to supercritical fluids flowing in channels-empirical correlations (survey), Nuclear Engineering and Design, 230, 69-91.*

Reiss, T., Feher, S., Sz. Czifrus, 2008, *Coupled neutronics and thermal hydraulics calculations with burn-up for HPLWRs, Progress in nuclear energy, 50, 52-61.*

Sienicki, James J., Bruce W. Spencer, 2002, *Power optimization in the STAR-LM modular convection reactor system, Proceedings of ICONE 10, Tenth International Conference on Nuclear Engineering, Arlington, Virginia, USA, April 14-18.*

Silin, V. A., Voznesensky, V. A., Afrov, A. M.,1993, *The light water reactor with natural circulation of the coolant at super critical pressure B-500 SKDI, Nuclear Engineering and Design, 144 , 327-336.*

Smith, C. F., Halsey, W. G., Brown, N. W., Sienicki, J. J., Moisseytsev, A., Wade, D. C. ,2008, *SSTAR: The US-lead-cooled fast reactor (LFR), Journal of Nuclear Materials 376 , 255-259.*

Swapnalee B.T., Vijayan P.K., 2011, *A generalized flow equation for single-phase natural circulation loops obeying multiple friction laws, International Journal of Heat and Mass Transfer 54, 2618-2629.*

Thirumaleshwar, M., *Fundamentals of Heat and mass transfer, Pearson Education, 2006, pp.454-455.*

Todreas, N.E and Kazimi, M.S., 1990, *Nuclear Systems II, Elements of Thermal Hydraulic Design*, Hemisphere Publications, New York, USA.

Tom, S.K.S., Hauptmann, E.G., 1979, *The feasibility of cooling heavy water reactors with supercritical fluids, Nuclear Engineering and Design 53,187-196.*

Torgerson, D.F., Basma, A., Shalaby, Pang, S., 2006, *CANDU technology for generation III+ and IV reactors, Nuclear Engineering and Design, 236, 1565-1572.*

Vijayan, P. K., Austregesilo, H., 1994, *Scaling laws for single-phase natural circulation loops, Nuclear Engineering and Design 152, 331-347.*

Vijayan, P. K., Austregesilo, H., Teschendorff, V., 1995, *Simulation of the unstable behavior of single phase natural circulation with repetitive flow reversals in a rectangular loop using computer code ATHLET, Nuclear Engineering and Design,155,623-641.*

Vijayan, P. K.,2002, *Experimental observations on the general trends of the steady state and stability behavior of single phase natural circulation loops, Nuclear Engineering and Design, 215 , 139-152.*

Vijayan, P. K., Bade, M. H., Saha, D., Sinha, R. K., Venkat Raj, V., *A Generalized correlation for the steady state flow in Single state Natural circulation Loops, BARC/2000/E/021.*

Vijayan, P.K., Sharma, M., Saha, D., 2007, *Steady state and stability characteristics of single phase natural circulation in a rectangular loop with different heater and cooler orientation, Experimental Thermal and Fluid Science 31, 925-945.*

Vijayan, P.K., Nayak, A. K., Saha, D., Gartia, M.R., *Effect of loop diameter on the steady state and stability behavior of single phase and two phase natural* *circulation loops, Science and technology of nuclear installations, volume 2008, article ID: 672704,17 pages, doi:10.1155/2008/672704.*

Vijayan P. K., Sharma M., Pilkhwal D.S. and Saha D., *Steady state and stability characteristics of a supercritical pressure natural circulation loop (SPNCL) with CO_2, Annual progress report of the work done under IAEA research contract no. 14344/R2 as part of the IAEA CRP on heat transfer behavior and thermo-hydraulics code testing for SCWRs, 2010.*

Vijayan, P.K., Thakuria, S. B., Sharma, M., Pilkhwal, D.S., Saha, D., Sinha, R.K., 2011, *Experimental investigations on the steady state and stability behavior of supercritical pressure natural circulation, NURETH-331, accepted for the 14th International Topical Meeting on Nuclear Reactor Thermal Hydraulics (NURETH-14), Toronto, Ontario, Canada, September 25-29.*

Welander, P., 1967, *On the oscillatory instability of a differentially heated fluid loop, J. Fluid Mechanics, 29, 17-30.*

Yi, T.T, Koshizuka S., Oka Y., 2004, *A linear stability analysis of supercritical water reactors (I) thermal hydraulic stability, Journal of nuclear Science and Technology, 41, 1166-1175.*

Yoshikawa S., Smith Jr R.L., Inomata H., Matsumura Y., Arai K.,2005, *Performance of a natural circulation system for supercritical fluids, J. of Supercritical fluids 36,70-80.*

Zhao, J., Saha, P., Kazimi, M.S., *Stability of supercritical water-cooled reactor during steady state and sliding pressure startup conditions, NURETH-11, Avignon, France, Oct.2-6,2005.*

Zuber, N., *An analysis of thermally induced flow oscillations in the near critical and supercritical thermodynamic region, Final report, NAS8-11422, May 25, 1966.*

Zvirin, Y. A,1981, *A review of natural circulation loops in pressurized water reactors and other systems, Nuclear Engineering and Design, 67, 203-225.*